

BOLU ABANT İZZET BAYSAL UNIVERSITY
THE GRADUATE SCHOOL OF NATURAL AND APPLIED
SCIENCES
DEPARTMENT OF CHEMISTRY



COMPUTATIONAL INVESTIGATION OF ELECTRONIC
AND OPTICAL PROPERTIES OF METAL NANO-
CLUSTERS SUPPORTED ON N-DOPED BILAYER
GRAPHENE STRUCTURES

DOCTOR OF PHILOSOPHY

ÖZLEM ÜNLÜ

BOLU, MARCH 2019

APPROVAL OF THE THESIS

Computational Investigation of Electronic and Optical Properties of Metal Nano-Clusters Supported on N-Doped Bilayer Graphene Structures submitted by **Özlem ÜNLÜ** and defended before the below named jury in partial fulfillment of the requirements for the degree of **Doctor of Philosophy** in **Department of Chemistry, The Graduate School of Natural and Applied Sciences of Bolu Abant İzzet Baysal University** in **29.03.2019** by

Examining Committee Members

Signature

Supervisor
Prof. Dr. İzzet MORKAN
Bolu Abant İzzet Baysal University



.....

Member
Assoc. Prof. Dr. Bahadır ALTINTAŞ
Bolu Abant İzzet Baysal University



.....

Member
Assoc. Prof. Dr. Mecit AKSU
Düzce University



.....

Member
Assist. Prof. Dr. Erhan BUDAK
Bolu Abant İzzet Baysal University



.....

Member
Assist. Prof. Dr. Aliye KAHYAOĞLU
Düzce University



.....

Prof. Dr. Ömer ÖZYURT



Director of Graduate School of Natural and Applied Sciences

To my son, Attila Ozan



DECLARATION

I hereby declare that all information in this document has been obtained and presented in accordance with academic rules and ethical conduct. I also declare that, as required by these rules and conduct, I have fully cited and referenced all material and results that are not original to this work.

Özlem ÜNLÜ



ABSTRACT

COMPUTATIONAL INVESTIGATION OF ELECTRONIC AND OPTICAL PROPERTIES OF METAL NANO-CLUSTERS SUPPORTED ON N-DOPED BILAYER GRAPHENE STRUCTURES

PHD THESIS
ÖZLEM ÜNLÜ

BOLU ABANT IZZET BAYSAL UNIVERSITY GRADUATE SCHOOL OF NATURAL AND APPLIED SCIENCES
DEPARTMENT OF CHEMISTRY
(SUPERVISOR: PROF. DR. IZZET MORKAN)

BOLU, MARCH 2019

Graphene has attracted great interest in the last few years owing to its extraordinary properties with potential applications like nanoelectronics, batteries, and hydrogen storage. To investigate electronic and optical behaviours of some rare metal nanoclusters supported between bilayer graphene sheets, *ab initio* first principle Density Functional Theory (DFT) calculations were performed on Tungsten, Rhenium and Osmium nanoclusters and metal oxides of these transition metal structures supported between graphene layers. All of the $\bar{\Gamma}$ and \bar{A}_1 points of the Brillouin zone were considered. The band structures and density of states (DOS) were calculated for the metal and metal oxide inserted bilayer graphene structures. The effect of nitrogen doping on the electronic and optical properties of bilayer graphene structures was also investigated. The results show that the electronic and optical properties of metal inserted bilayer graphene structures are affected by the type of dopant and metal as a result of charge transfer. Nitrogen doped graphene systems showed change in local density as a result of charge transfer due to its extra one electron. Intercalation of transition metal atoms lead to narrowing the band gap with an increase in conductor character. The data presented with this study can be used for further catalytic studies and guide the experimental studies.

KEYWORDS: Density Functional Theory, Electronic properties, Optical properties, Bilayer graphene systems, GGA.

ÖZET

**AZOT KATKILI ÇİFT KATMANLI GRAFEN İLE DESTEKLENMİŞ
METAL NANOKÜMELERİNİN ELEKTRONİK VE OPTİK
ÖZELLİKLERİNİN HESAPLAMALI İNCELENMESİ
DOKTORA TEZİ
ÖZLEM ÜNLÜ
BOLU ABANT İZZET BAYSAL ÜNİVERSİTESİ
FEN BİLİMLERİ ENSTİTÜSÜ
KİMYA ANABİLİM DALI
(TEZ DANIŞMANI: PROF. DR. İZZET MORKAN)**

BOLU, MART - 2019

Grafen sıradışı özelliklere sahip olmasının yanı sıra nano-elektronikler, sensörler, kompozitler, piller, süper kapasitörler ve hidrojen depolama gibi uygulamalarda kullanılabilme potansiyeli ile son yıllarda yoğun ilgi görmektedir. Çift katmanlı grafen yapıları arasına interkale edilmiş Renyum, Tungsten ve Osmiyum metal nanokümelere ve bu metallerin oksitlerinin elektronik ve optik özellikleri temel set denklemi kullanılarak *ab-initio* temel-set Yoğunluk Fonksiyon Teoremi (DFT) ile hesaplanarak incelenmiştir. Tüm grafen yapılarının DFT hesaplamaları *ab-initio* pseudo-potansiyel yaklaşımı ile geliştirilmiş gradyent yaklaşımına (GGA) dayanarak BPW91 temel set denklemi kullanılarak hesaplanmıştır. Sonrasında optimizasyonu yapılmış geçiş metali ile desteklenmiş çift katmanlı grafen yapıları azot ile katkılanarak değişen elektronik ve optik davranışları incelenmiştir. Yapılan analizler sonucunda metal katılmış çift katmanlı grafen yapılarının elektronik ve optik özelliklerinin yük transferi nedeniyle metalin ve katkılayıcının türüne bağlı olduğu görülmüştür. Grafen sistemlerinin azot ile katkılanması içerdiği fazladan bir elektron sebebi ile lokal elektron yoğunluğunda değişime sebep olmaktadır. Geçiş metallerinin grafen sistemlerinin arasına interkale edilmesi, bant boşluğunun azalmasına ve dolayısıyla iletkenlik özelliğinin artmasına sebep olmuştur. Bu çalışmada hesaplanan veriler, gelecekte katalitik hesaplamalara ve deneysel çalışmalara rehberlik niteliği taşımaktadır.

ANAHTAR KELİMELER: Yoğunluk Fonksiyon Teorisi, Elektronik özellikler, Optik özellikler, Çift katmanlı grafen sistemleri, GGA.

TABLE OF CONTENTS

	<u>Page</u>
ABSTRACT	v
ÖZET	vi
TABLE OF CONTENTS	vii
LIST OF FIGURES	ix
LIST OF TABLES	xi
LIST OF ABBREVIATIONS AND SYMBOLS	xiii
1. INTRODUCTION	1
1.1 Carbon Nanomaterials	3
1.2 Atomic structure of Graphene	5
1.3 Electronic structure of Graphene.....	7
1.3.1 Electronic properties of Monolayer Graphene.....	8
1.3.2 Electronic properties of Graphite.....	13
1.3.3 Electronic properties of Bilayer Graphene	19
1.4 Optical Properties of Graphene Structures	22
1.4.1 Optical conductance of graphene structures	22
1.4.2 Refractive Index.....	24
1.4.3 Optical properties of bilayer graphene.....	26
1.5 Tailoring the graphene-based structures.....	27
1.5.1 Nitrogen Doping	28
1.5.2 Metal Intercalation	29
2. AIM AND SCOPE OF THE STUDY	33
3. MATERIALS AND METHODS	35
3.1 Density Functional Theory	35
3.1.1 The Hohenberg-Kohn theorems.....	36
3.1.2 Kohn-Sham Equation.....	37
3.2 Quantumwise ATK-VNL Nanolab and its related functional theory.....	38
4. RESULTS AND DISCUSSIONS	46
4.1 Geometry Optimizations	46
4.2 Molecular Dynamic Analysis	49
4.3 Band Structure Analysis	54
4.4 Electron Density	60
4.5 Electron Difference Density	63
4.6 Electron Localizaiton Functions.....	65
4.7 Molecular Energy Analysis	65
4.8 Optical Properties	67
5. CONCLUSIONS AND RECOMMENDATIONS	74
6. REFERENCES	75
7. APPENDICES	79

Appendix A.1	79
Appendix A.2	101
Appendix A.3	107
Appendix A.4	113
8. CURRICULUM VITAE	125



LIST OF FIGURES

	<u>Page</u>
Figure 1.1. Optical image of monolayer graphene.....	2
Figure 1.2. Steps in Mechanical exfoliation method on a substrate.....	2
Figure 1.3. Papers and patents in graphene research between 2004 and 2018.	2
Figure 1.4. Top research areas of graphene used studies	3
Figure 1.5. Possible hybridizations of carbon.	4
Figure 1.6. Allotropes of carbon.	5
Figure 1.7. Graphene, basic building block for graphitic materials.....	6
Figure 1.8. The σ and π bonding in graphene.	7
Figure 1.9. Lattice structure of graphene	7
Figure 1.10. Graphene (a) The honeycomb structure, (b) The Brouillin zone.....	9
Figure 1.11. The reciprocal lattice of graphene..	12
Figure 1.12. The “Dirac cone” dispersion of the quasiparticles in graphene.....	13
Figure 1.13. Graphite (a) AB- (b) ABC- (c) Unit cell (d) The Brillouin zone.....	15
Figure 1.14. Graphite (a) The lattice structure (b) The Brillouin zone.	16
Figure 1.15. Lattice structure of the graphene bilayer.	19
Figure 1.16. Dispersions in the bilayer graphene.....	21
Figure 1.17. Tunable Fano resonance in back-gated bilayer graphene.	27
Figure 1.19. Calculated band structures.	29
Figure 1.20. Three adsorption sites on the graphene surfaces..	30
Figure 1.21. The sandwich like graphene-Cr-graphene structure	31
Figure 1.22. The effect of transition metal atoms on defective BLG.....	32
Figure 3.1. Workflow chart of the study	44
Figure 4.1. Optimized geometries of graphene structures.	47
Figure 4.2. Angular distribution analysis.	50
Figure 4.3. The radial distribution analysis.....	51
Figure 4.4. Coordination number distribution analysis.....	52
Figure 4.5. Mass density profile analysis.....	53
Figure 4.6. Neutron scattering factor analysis.....	54
Figure 4.7. Band structures of graphene, BLG, WBLG, ReBLG and OsBLG.....	56
Figure 4.8. Band structures of nitrogen doped metal bilayer graphene	57
Figure 4.9. Band structres of metal oxides inserted bilayer graphene structures..	58
Figure 4.10. Brillouin zones.....	59
Figure 4.11. Electron density scheme of BLG	60
Figure 4.12. Electron density schemes of ReBLG.....	61
Figure 4.13. Electron density schemes of ReNBLG.	62
Figure 4.14. Electron density schemes of OsOBLG.	62
Figure 4.15. Summarization of Bader charges of the structures	63
Figure 4.16. Electron difference density schemes.....	64
Figure 4.17. ELF models.....	65
Figure 4.18. Molecular energy spectrum analysis.....	66
Figure 4.19. Energy-absorption spectra	67
Figure 4.20. Energy-absorption spectra.	68
Figure 4.21. Energy-absorption spectra	68
Figure 4.22. Energy-Dielectric constant spectra	69

Figure 4.23. Energy-Dielectric constant spectra	69
Figure 4.24. Energy-Dielectric constant spectra	70
Figure 4.25. Energy-optical conductivity spectra	70
Figure 4.26. Energy-optical conductivity spectra	71
Figure 4.27. Energy-optical conductivity spectra	71
Figure 4.28. Absorption-wavelength spectra	72
Figure 4.29. Absorption-wavelength spectra.	72
Figure 4.30. Absorption-wavelength spectra.	73
Figure 7.1. Angular distribution of graphene.....	101
Figure 7.2. Angular distribution of BLG	101
Figure 7.3. Angular distribution of WBLG.....	102
Figure 7.4. Angular distribution of ReBLG	102
Figure 7.5. Angular distribution of OsBLG	103
Figure 7.6. Angular distribution of WNBLG.....	103
Figure 7.7. Angular distribution of ReNBLG	104
Figure 7.8. Angular distribution of OsNBLG	104
Figure 7.9. Angular distribution of WOBLG.....	105
Figure 7.10. Angular distribution of ReOBLG	105
Figure 7.11. Angular distribution of OsOBLG	106
Figure 7.12. Radial distribution of graphene.....	107
Figure 7.13. Radial distribution of BLG	107
Figure 7.14. Radial distribution of WBLG	108
Figure 7.15. Radial distribution of ReBLG.....	108
Figure 7.16. Radial distribution of OSBLG	109
Figure 7.17. Radial distribution of WNBLG.....	109
Figure 7.18. Radial distribution of ReNBLG.....	110
Figure 7.19. Radial distribution of OsNBLG.....	110
Figure 7.20. Radial distribution of ReOBLG.....	111
Figure 7.21. Radial distribution of WOBLG.....	111
Figure 7.22. Radial distribution of OsOBLG.....	112

LIST OF TABLES

	<u>Page</u>
Table 1.1. Typical values of Slonczewski-Weiss-McClure parameters.....	18
Table 4.1 Bond lengths and distances between layers.	48
Table 4.2. The total energies	48
Table 4.3. Chemical potential energies	60
Table 4.4. Molecular energy spectra	67
Table 7.1. Cartesian coordinates of BLG(2+2) before optimization.....	79
Table 7.2. Fractional coordinates of BLG(2+2) before optimization.....	79
Table 7.3. Cartesian coordinates of BLG(2+2) after geometry optimization.	79
Table 7.4. Fractional coordinates of BLG(2+2) after geometry optimization.	79
Table 7.5. Z-matrix of BLG(2+2).	79
Table 7.6. Cartesian coordinates of BLG(4+4) before geometry optimization.....	80
Table 7.7. Fractional coordinates of BLG(4+4) before geometry optimization....	80
Table 7.8. Z-matrix of BLG(4+4).	80
Table 7.9. Cartesian coordinates of BLG(4+4) after geometry optimization.	81
Table 7.10. Fractional coordinates of BLG(4+4) after geometry optimization. ...	81
Table 7.11. Z-matrix of BLG(4+4).	81
Table 7.12. Cartesian coordinates of MBLG before geometry optimization.	82
Table 7.13. Fractional coordinates of MBLG before geometry optimization.....	82
Table 7.14. Cartesian coordinates of ReBLG after geometry optimization.	82
Table 7.15. Fractional coordinates of ReBLG after geometry optimization.....	83
Table 7.16. Z-matrix of ReBLG.	83
Table 7.17. Cartesian coordinates of WBLG after geometry optimization.....	83
Table 7.18. Fractional coordinates of WBLG after geometry optimization.....	84
Table 7.19. Z-matrix of WBLG.....	84
Table 7.20. Cartesian coordinates of MNBLG before geometry optimization.	84
Table 7.21. Fractional coordinates of MNBLG before geometry optimization....	85
Table 7.22. Cartesian coordinates of ReNBLG after geometry optimization.	85
Table 7.23. Fractional coordinates of ReNBLG after geometry optimization.	85
Table 7.24. Z-matrix of ReNBLG	86
Table 7.25. Cartesian coordinates of WNBLG after geometry optimization.....	86
Table 7.26. Cartesian coordinates of OsNBLG after geometry optimization.....	86
Table 7.27. Fractional coordinates of OsNBLG after geometry optimization.....	87
Table 7.28. Z-matrix of OsNBLG	87
Table 7.29. Cartesian coordinates of WOBLG before geometry optimization.....	87
Table 7.30. Fractional coordinates of WOBLG before geometry optimization....	89
Table 7.31. Cartesian coordinates of WOBLG after geometry optimization.....	90
Table 7.32. Fractional coordinates of WOBLG after geometry optimization.....	91
Table 7.33. Z-matrix of WOBLG.....	92
Table 7.34. Cartesian coordinates of ReOBLG before geometry optimization ...	93
Table 7.35. Fractional coordinates of ReOBLG before geometry optimization ...	94
Table 7.36. Cartesian coordinates of ReOBLG after geometry optimization.	95
Table 7.37. Fractional coordinates of ReOBLG after geometry optimization.....	96
Table 7.38. Z-matrix of ReOBLG	97
Table 7.39. Cartesian coordinates of OsOBLG after geometry optimization.	98

Table 7.40. Fractional coordinates of OsOBLG after geometry optimization.....	99
Table 7.41. Z-matrix of OsOBLG.....	100
Table 7.42. Bader charge volumes of MLG.....	113
Table 7.43. Bader charge volumes of BLG.....	113
Table 7.44. Bader charge volumes of ReBLG.....	115
Table 7.45. Bader charge volumes of WBLG.....	117
Table 7.46. Bader charge volumes of OsBLG.....	118
Table 7.47. Bader charge volumes of ReNBLG.....	119
Table 7.48. Bader charge volumes of WNBLG.....	120
Table 7.49. Bader charge volumes of OsNBLG.....	121
Table 7.50. The atomic charge volumes of ReOBLG structure.....	122
Table 7.51. The atomic charge volumes of WOBLG structure.....	123
Table 7.52. The atomic charge volumes of OsOBLG structure.....	124



LIST OF ABBREVIATIONS AND SYMBOLS

ATK	: Atomistic Tool Kit
BLG	: Bilayer Graphene
BPW91	: Becke exchange combined with Perdew-Wang-91 correlation functionals
C	: Carbon
CNT	: Carbon Nanotube
DFT	: Density Functional Theory
ext	: Electrostatic field expressions
GGA	: General Gradient Approximation
H	: Hartree expressions
HK	: Hohenberg-Kohn expressions
HOMO	: Highest Occupied Molecular Orbitals
KS	: Kohn-Sham expressions
LCAO	: Linear Combination of Atomic Orbitals
LUMO	: Lowest Unoccupied Molecular Orbitals
MLG	: Mono Layer Graphene
Os	: Osmium
OsBLG	: Osmium Intercalated Bilayer Graphene
OsNBLG	: N-doped Osmium Intercalated Bilayer Graphene
OsOBLG	: Osmium oxide Intercalated Bilayer Graphene
Re	: Rhenium
ReBLG	: Rhenium Intercalated Bilayer Graphene
ReNBLG	: N-doped Rhenium Intercalated Bilayer Graphene
ReOBLG	: Rhenium oxide Intercalated Bilayer Graphene
Th-Fe	: Thomas-Fermi expressions
VNL	: Virtual Nanolab
W	: Tungsten
WBLG	: Tungsten Intercalated Bilayer Graphene
WNBLG	: N-doped Tungsten Intercalated Bilayer Graphene
WOBLG	: Tungsten oxide Intercalated Bilayer Graphene
xc	: Exchange-correlation expressions

ACKNOWLEDGEMENTS

I wish to express my deepest gratitude to my supervisor Prof. Dr. İzzet MORKAN for his guidance, advice, criticism, encouragements, and insight throughout the research. I sincerely thank the rest of my thesis committee: Assoc. Prof. Dr. Bahadır ALTINTAŞ, and Assist. Prof. Dr. Erhan BUDAK, for their insightful comments, encouragement, and support. I would like to thank the other faculty members especially Prof. Dr. Ayşe UZTETİK MORKAN for her moral support and motivation. I would like to thank Dr. Seda KARABOĞA for friendship and support as my lab partner. I am grateful to all my friends Dr. Bedirhan GÜLTEPE, Dr. Cantürk AKBEN and Dr. Ahmet Yasin ŞENYURT, for their technical support and help to fix my crashed computer. I especially thank my mother Nilgün İLKİN, my father Ersan İLKİN for my life and all the sacrifices they made for me. I dedicate this thesis to my lovely son Attila Ozan for making my life meaningful. This last word of acknowledgment I have saved for my soul-mate, best friend and husband, Dr. Ercan Selçuk ÜNLÜ. I would not have finished this thesis without his great support, unconditional love, faith, and patience.

This study was supported by the BAİBU BAP., Grant Nr: 2016.03.03.1110

1. INTRODUCTION

As one of the most abundant element in universe, carbon has been known before the history itself (Greenwood N. N. 1997). In the era of nanotechnology, carbon has an outstanding importance in the scientific and technological areas with its unique allotropic forms. As an incredible element, carbon has the ability to bind itself and nearly all other elements in the periodic table. With an almost unlimited number of compounds, the carbon element has a very important role in a wide range of medicine, nutrition, energy and synthetic materials (Soukiassian and Rao, 2010; Hirsch, 2010).

Discovery of graphene has an important impact on nanotechnology research. Graphene structure was first proposed by the Canadian scientist Wallace in 1946 (Wallace 1947). He proposed that stacking one-atom thick graphene layers on top of each other could eventually form graphite. However, he also suggested that it was not experimentally possible to obtain one layer graphene sheet itself. Thus, two-dimensional graphene was considered to be an exclusively theoretical material until Novoselov and Geim isolated graphene using the Scotch tape method (Novoselov et al. 2004). They simply exfoliated graphite to obtain mono-layer graphene sheets (Figure 1.1 and Figure 1.2). This simple method had a revolutionary impact on starting forthcoming studies. Later, investigations elucidated important physical properties of graphene. Findings proved that it is a super-strong, very thin, transparent and extremely light material. In addition, it has extremely unusual electronic properties such as high electrical and heat conductivity. Today, there are thousands of publications in a wide range of scientific fields about graphene (Figure 1.3 and Figure 1.4). Data presented in Figure 1.3 and Figure 1.4 were received from Web of Science (2018).

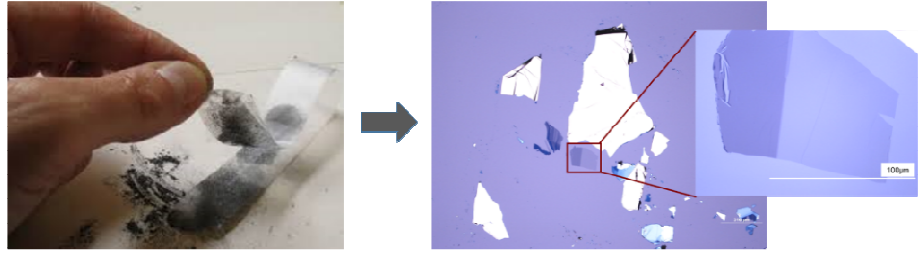


Figure 1.1. Optical image of monolayer graphene (Terse-Thakoor, Badhulika & Mulchandani 2017).

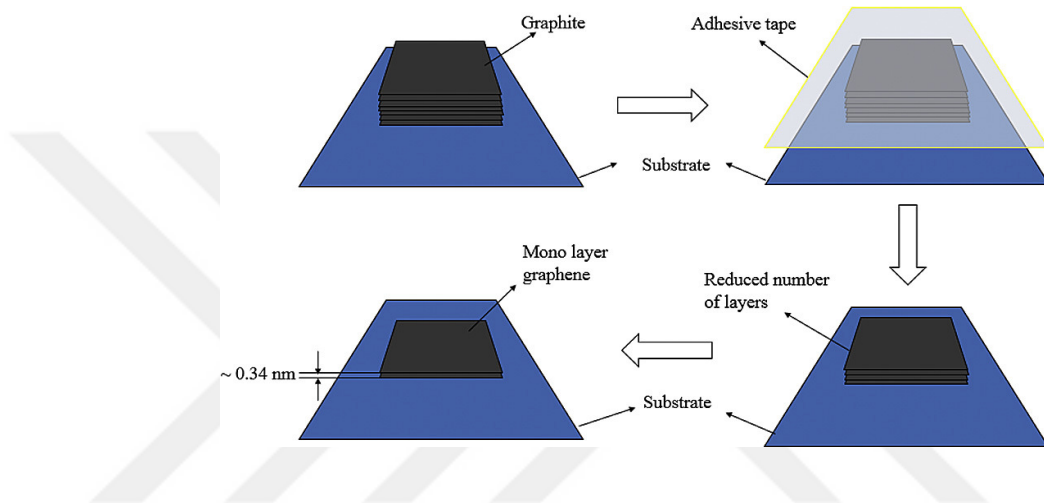


Figure 1.2. Steps in Mechanical exfoliation method on a substrate (Dasari et al. 2017).

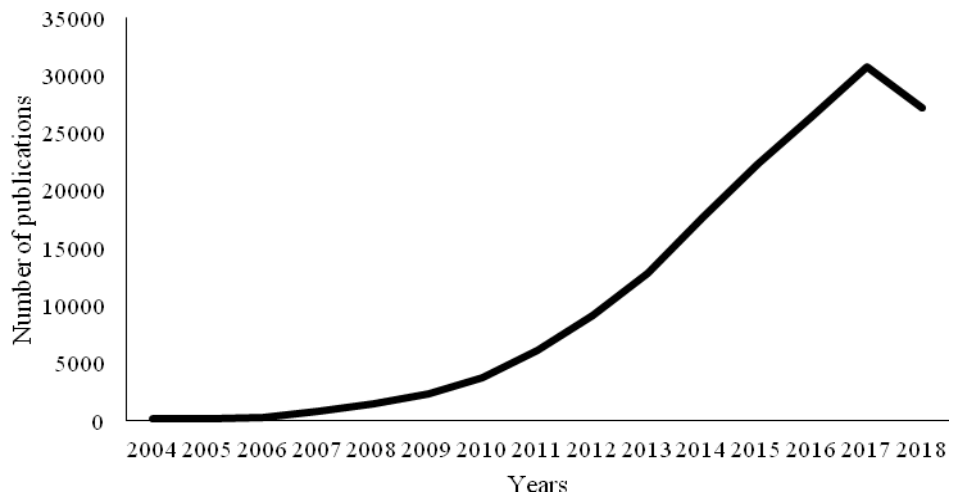


Figure 1.3. Papers and patents in graphene research between 2004 and 2018.

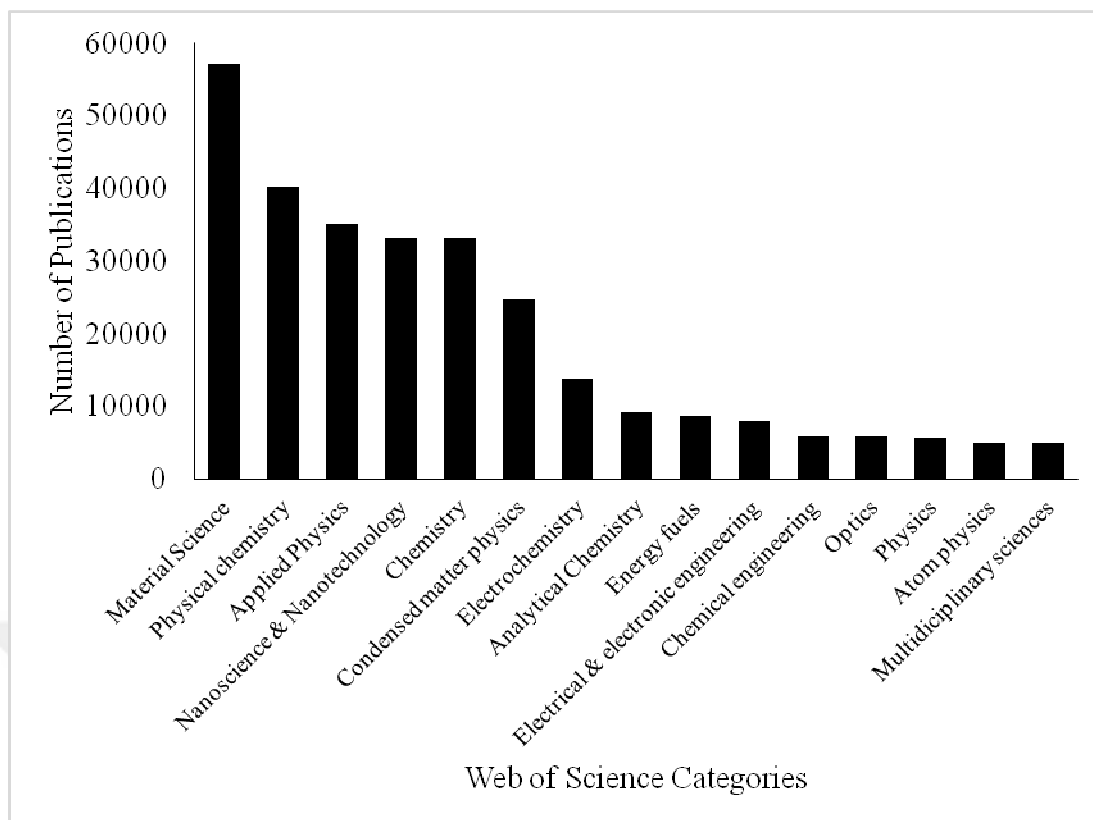


Figure 1.4. Top research areas of graphene used studies.

1.1 Carbon Nanomaterials

Carbon atom can show three types of hybridization (sp , sp^2 , and sp^3) depending on the number of mixing atomic orbitals in bonds (Figure 1.5). In sp hybridization, $2s$ and $2p$ orbitals are mixing to form two sp orbitals and leaving two p orbitals in unchanged state. The sp orbital consists of 50% of each s and p characters. Each sp orbital has one lobe larger than the other. When two sp orbitals (four lobes) set together, the larger lobes face together in linear 180° orientation. In sp^2 hybridization, one $2s$ and two $2p$ orbitals are hybridized to form three sp^2 orbitals consisting of 33% s and 67% p characters. To minimize the electronic repulsion, three sp^2 orbitals oriented with 120° angle where unchanged p_z orbitals perpendicular to the plane. In sp^3 hybridization, one $2s$ and three $2p$ orbitals are mixed to form four sp^3 orbitals that each orbital has 75% p and 25% s characters. The sp^3 hybrids are oriented at 109° angle to each other in tetrahedral geometry.

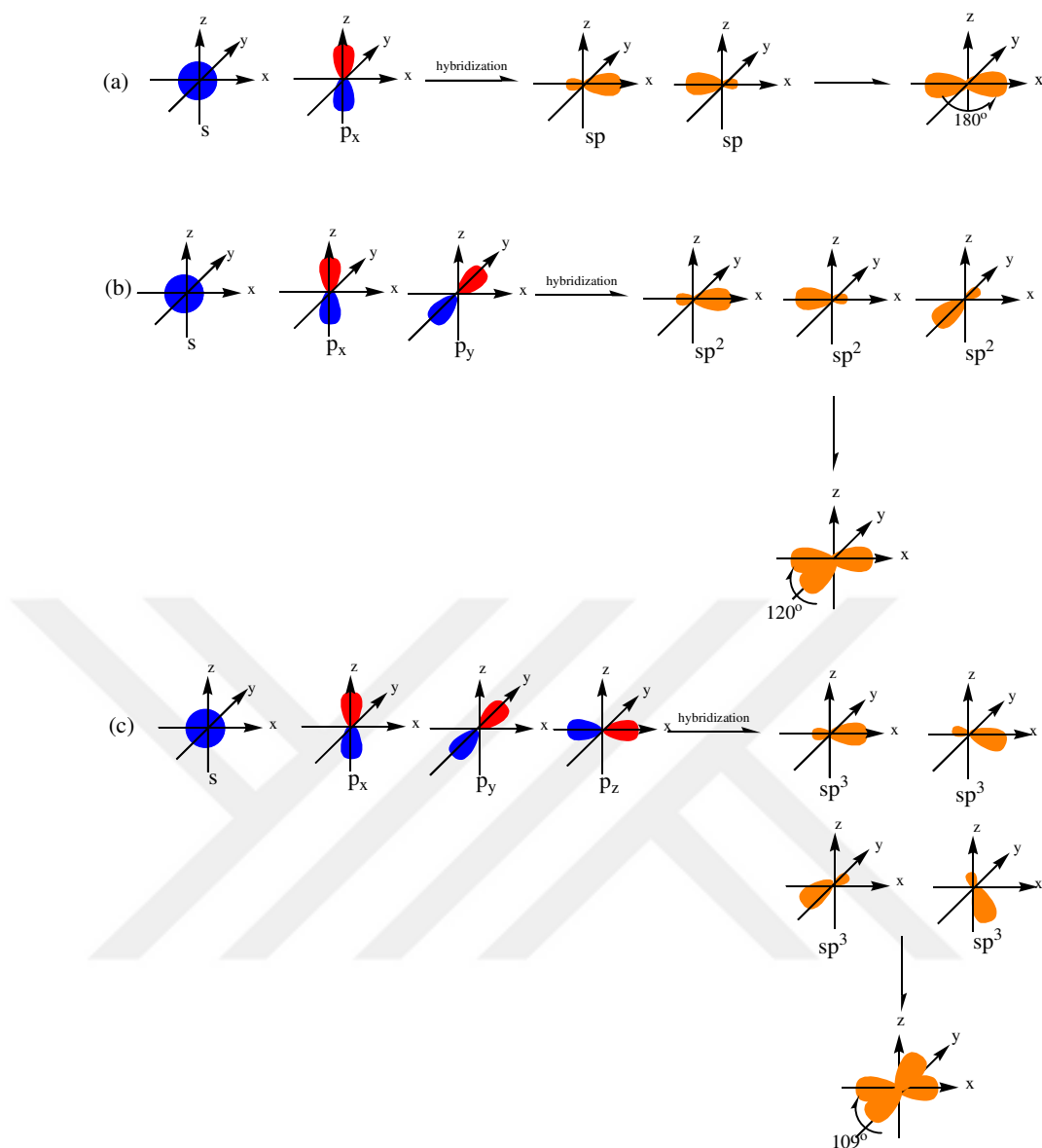


Figure 1.5. Possible hybridizations of carbon. (a) sp hybridization, (b) sp^2 hybridization, (c) sp^3 hybridization; note that there are unhybridized p orbitals in sp and sp^2 that are not shown here (Brinkley 1933).

When the orbitals overlap between two atoms, a chemical bond is formed between C atoms. For instance, in the case of sp^2 hybridization, there are three sp^2 hybrid orbitals can form bonds with other three C atoms. This overlapping hybrid orbitals create stronger covalent bonds (σ -bonds) in plane, while unhybridized p_z orbital forms weaker out-of-plane π -bond (Brinkley, 1933; Greenwood NN, 1997).

Aforomentioned hybridization types enable carbon atoms to form four different allotropes (Figure 1.6). Carbon allotropes are categorized by their

dimensions: i- Zero-dimensional (0D) fullerenes and buckyballs; ii- One-dimensional (1D) carbon nanotubes (CNTs); iii- Two-dimensional (2D) graphene; iv- three-dimensional (3D) diamond and graphite (Katsnelson, 2007; Li et al., 2015).

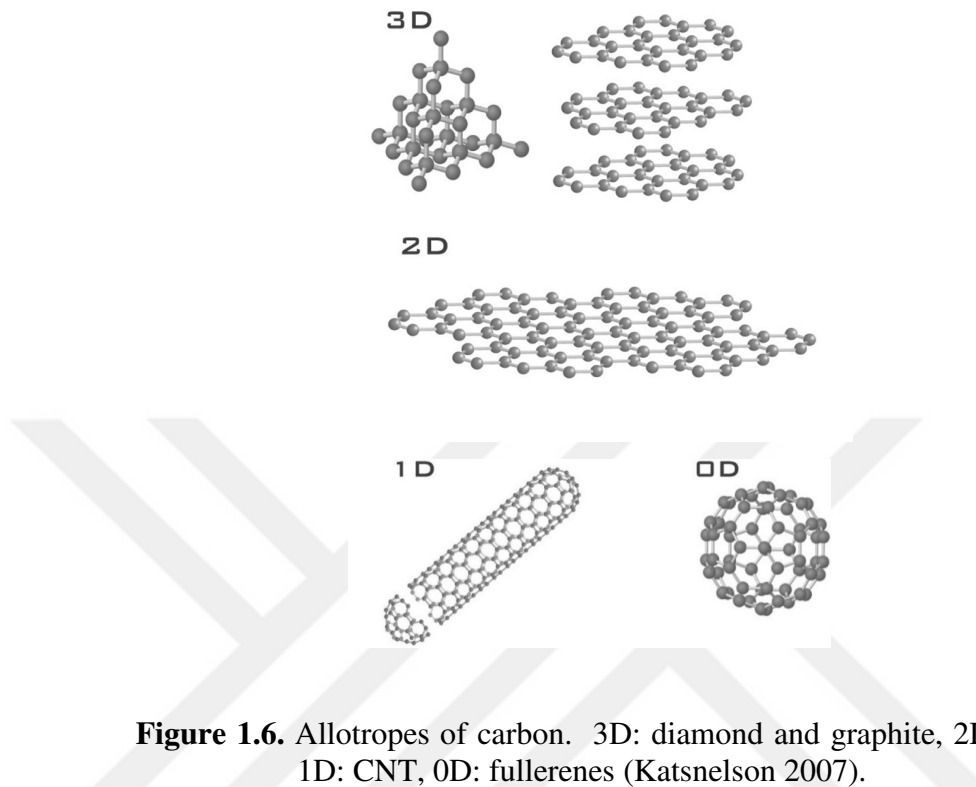


Figure 1.6. Allotropes of carbon. 3D: diamond and graphite, 2D: graphene, 1D: CNT, 0D: fullerenes (Katsnelson 2007).

3D carbon allotropes are bulk materials while others are classified under nanomaterials. Nanomaterial studies for carbon allotropes started with the discovery of C_{60} fullerene (i.e. Buckminsterfullerene) (Kroto et al. 1985). Fullerene is a zero-dimensional series of hollow carbon molecules that form a closed cage (viz. buckyballs). In 1991, Sumio discovered carbon nanotubes (CNTs) with a cylindrical nanostructure (Iijima and Ichihashi, 1993). Two decades after the discovery of these carbon allotropes, Novosolov and Geim discovered graphene in 2004 (Novoselov et al., 2004).

1.2 Atomic structure of Graphene

Graphene is a hexagonal honeycomb structure consisting of one-atom thick sp^2 hybridized carbon atoms in two-dimension (Allen, Tung and Kaner, 2010; Soldano, Mahmood and Dujardin, 2010). Novoselov described graphene as the

“mother” of all graphitic carbon allotropes in other dimensions (Geim & Novoselov 2007). For example, stacking several layers of graphene sheets forms a three dimensional graphite while rolling graphene sheets with different boundaries leads to formation of one dimensional carbon nanotubes. Buckyballs can be produced by wrapping a graphene segment into a sphere structure. The formation scheme of these structures is illustrated in Figure 1.7 (Geim and Novoselov, 2007).

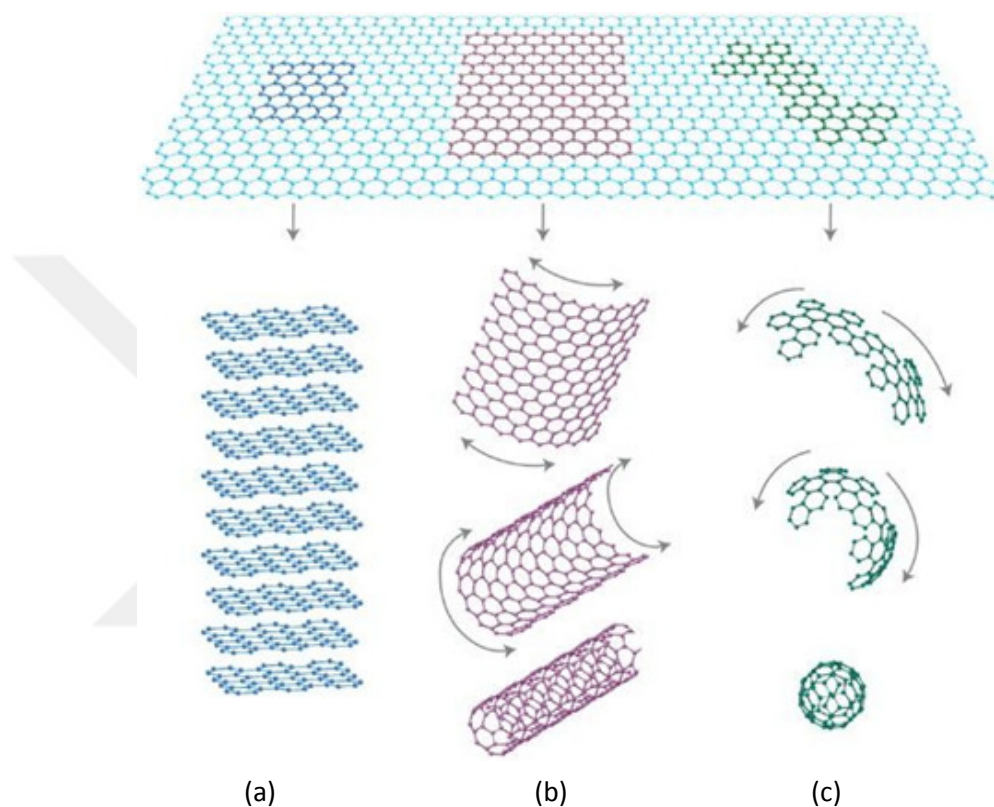


Figure 1.7. Graphene, basic building block for graphitic materials. a) 3D graphite, b) 1D carbon nanotube, and c) 0D graphite (Geim and Novoselov, 2007).

As previously mentioned, the $2s$ orbital overlap with $2p_x$ and $2p_y$ orbitals forming three sp^2 hybrid orbitals in graphene which results with stronger σ bonds. The strength of these bonds are more than sp^3 interactions in diamonds. They are responsible for defined mechanical properties of graphene. On the other hand, the unhybridized p_z electrons are weakly bounded to the nuclei. They are responsible for relative delocalization of electrons and in turn π bond formation (Figure 1.8). Hybridization of π - and π^* -bands between π -bands is responsible for graphene’s electronic properties. One-atom thick layer of graphene shows hexagonal structure which requires alignment of three σ -bonds on each lattice. In this structure model,

binding of sp^2 hybridized carbon atoms with surrounding hybridized carbon atoms causes the formation of a benzene ring. Within this molecule, each atom donates an unpaired electron where bond length of carbon-carbon interaction is 0.142 nm (Figure 1.9). (Soldano, Mahmood and Dujardin, 2010).

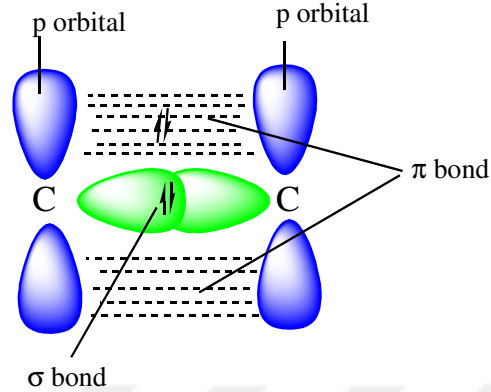


Figure 1.8. The σ and π bonding in graphene.

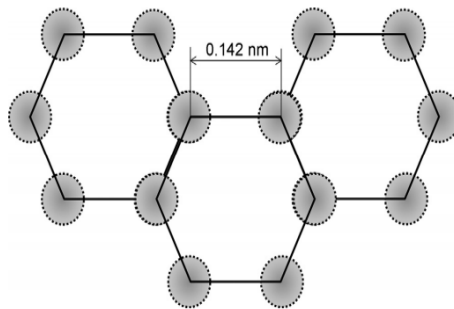


Figure 1.9. Lattice structure of graphene (Zhen and Zhu, 2018).

1.3 Electronic structure of Graphene

Graphene is considered as the thinnest material. The thickness of graphene layer is only 0.35 nm which is 1/200,000th the diameter of a human hair. Later studies of Novosolov and Geim showed that the electronic properties are highly depended on layer number of graphene (Geim and Novoselov, 2007). In order to understand graphene structures, some of the electronic structures of monolayer graphene, graphite and bilayer graphene are explained below.

1.3.1 Electronic properties of Monolayer Graphene

In general, crystal structure can be defined by two different components: lattice and basis. Lattice structure is a regular arrangement of points in space where a group of repeating atoms at every point in the lattice to form the crystal structure. The lattice can be generated by three primitive lattice translation vectors (*viz.* a_1 , a_2 and a_3). Any two lattice points can be connected by the translational vector (T) and can be formulated as:

$$T = n_1 a_1 + n_2 a_2 + n_3 a_3 \quad (1.1)$$

Defining the periodic structures of lattices depend on investigation of reciprocal lattice. Assuming m_i as an integer value and b_1 , b_2 and b_3 as the primitive translation factors of reciprocal lattice, general translation vector (G) between any two reciprocal lattice points can be calculated using following formula:

$$G = m_1 b_1 + m_2 b_2 + m_3 b_3 \quad (1.2)$$

As mentioned, one atom thick layer of graphene forms a hexagonal lattice with a honeycomb structure where each carbon atoms has four electrons in their valance shell. In order to fit the system into the usual Bloch state representation, it is essential to define the system as a triangular lattice with two basis carbon atoms per primitive cell. In this system, the equilateral parallelogram presents a unit cell with a_1 , a_2 lattice vectors and A1, B1 sublattices (Figure 1.10a). The hexagonal reciprocal lattice of graphene is defined in Brillouin zone with the high symmetry points labelled Γ , K, and M (Figure 1.10b). The High symmetry points of lattice can be formulated as:

$$\begin{aligned} \Gamma &= \{0, 0\} \\ n(r) &= \sum_{\alpha} f_{\alpha} |\varphi_{\alpha}(r)|^2 \\ n(r) &= \sum_{ij} D_{ij} \phi_i(r) \phi_j(r) \\ D_{ij} &= \sum_{\alpha} f_{\alpha} c_{\alpha i}^* c_{\alpha j} \\ \Delta(n) &= n(r) - \sum_{\mu} n^{atom}(r - R_{\mu}) \end{aligned} \quad (1.3)$$

$$K = \left\{ \frac{1}{3}, \frac{1}{3} \right\} \quad (1.4)$$

$$M = \left\{ 0, \frac{1}{2} \right\} \quad (1.5)$$

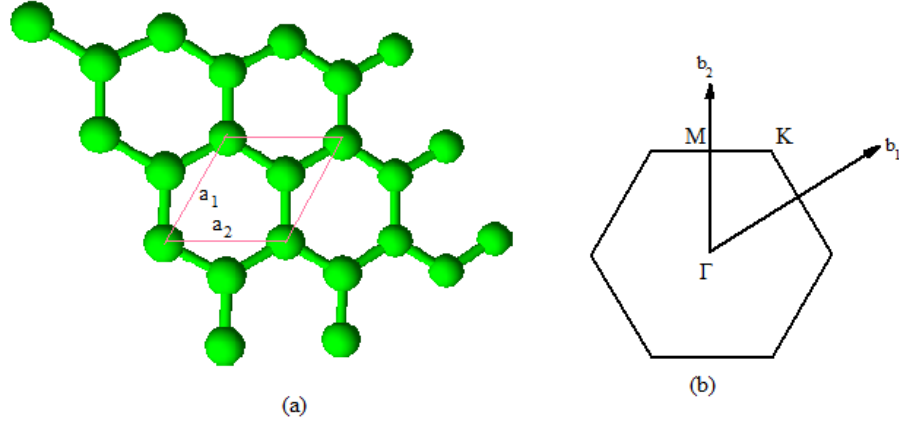


Figure 1.10. Graphene (a) The honeycomb structure, (b) The Brouillin zone

The real-space lattice vectors of graphene structure are given by the following equation where lattice constant $a = \sim 1.4 \text{ \AA}$:

$$a_1 = \frac{a}{2}(3, \sqrt{3}) \quad (1.6)$$

$$a_2 = \frac{a}{2}(3, -\sqrt{3}) \quad (1.7)$$

In a simple model, the nearest neighbor to tight-binding Hamiltonian consist of only π orbital in each atom. The nearest neighbor distance is $\frac{a}{\sqrt{3}}$. The vectors connecting to these nearest neighbor atoms are given below.

$$\delta_1 = \frac{a}{2}(1, \sqrt{3}) \quad (1.8)$$

$$\delta_2 = \frac{a}{2}(1, -\sqrt{3}) \quad (1.9)$$

$$\delta_3 = a(-1, 0) \quad (1.10)$$

The tight-binding model is required to define electron motion. Thus, it is suitable to introduce the operator (c) to system with $c_{\alpha j, R_i}^\dagger$. R_i refers to the position where the operator produces an electron on the lattice site while α denotes the atom sublattice and j denotes the plane. Therefore, the tight-bonding Hamiltonian can be written as given in Equation 1.11 where t (approximately 3 eV for graphene) represents the energy associated with the bouncing of electrons between neighboring π -orbitals.

$$H_{t.b.} = -t \sum_{R_i} \sum_{j=1,2,3} \left(c_{A1, R_i}^\dagger c_{B1, R_i + \delta_j} + h.c. \right) \quad (1.11)$$

Next, it is possible to define Fourier-transformed operators where N represents the number of unit cells in the system.

$$c_{\alpha j, R_i} = \frac{1}{\sqrt{N}} \sum_k e^{ik \cdot R_i} c_{\alpha j, k} \quad (1.12)$$

According to this basis, the tight-binding Hamiltonian:

$$H_{t.b.} = \sum_k \left[\zeta(k) c_{A1, k}^\dagger c_{B1, k} + \zeta^*(k) c_{B1, k}^\dagger c_{A1, k} \right] \quad (1.13)$$

where

$$\zeta(k) = -t \sum_k e^{ik \delta_i} = -t e^{(ik_x a/2)} \left[2 \cos \left(\frac{k_y a \sqrt{3}}{2} \right) + e^{i3k_x a/2} \right] \quad (1.14)$$

Since the sublattice structure can be described for the systems by a spinor, $\psi_k^\dagger (c_{A1, k}^\dagger, c_{B1, k}^\dagger)$, the tight-binding Hamiltonian can be expressed as:

$$H_{t.b.} = \sum_k \psi_k^\dagger \begin{pmatrix} 0 & \zeta(k) \\ \zeta^*(k) & 0 \end{pmatrix} \psi_k \quad (1.15)$$

The primitive lattice vectors of b_1 and b_2 reciprocal lattices can be estimated by using the equations 1.2 and 1.3. The following equations can be used to calculate b_1 and b_2 vectors.

$$b_1 = \frac{2\pi}{3a}(1, \sqrt{3}) \quad (1.16)$$

$$b_2 = \frac{2\pi}{a}(1, -\sqrt{3}) \quad (1.17)$$

The encircled K and K' corners of the Brillouin zone of graphene have the coordinates defined with:

$$K = \frac{2\pi}{3\sqrt{3}a}(\sqrt{3}, 1) \quad (1.18)$$

$$K' = \frac{2\pi}{3\sqrt{3}a}(\sqrt{3}, -1) \quad (1.19)$$

If these corners of Brillouin zone expand correlated to $\mathbf{k} = \mathbf{K} + \mathbf{q}$ and, following equations can be written.

$$\zeta(q) \approx \frac{3at}{2} e^{\frac{i\pi}{6} + \frac{iq_x a}{2}} (q_x + iq_y) = v_F q e^{i\left(\phi - \frac{\pi}{6}\right)} \quad (1.20)$$

$$\zeta(q') \approx \frac{3at}{2} e^{\frac{i\pi}{6} + \frac{iq_x a}{2}} (q'_x + iq'_y) = v_F q e^{i\left(\phi' - \frac{\pi}{6}\right)} \quad (1.21)$$

In the tight-binding model, the Fermi-Dirac velocity is given by $v_F = 3ta$. However, the extra phase of $\pi/6$ in the equation above can be absorbed into the phases of B1 wavefunctions. In addition, during the construction of wavefunctions in both inequivalent corners of Brillouin zone, $\pi/6$ is not necessary since it is the same for both K and K' points.

Alternatively, it is possible to use other pairs of corners of Brillouin zone since two Bloch states are equivalent. If the system defines b using the the other pair of corners in Brillouin zone instead of K and K' points, then these points can be described as $\mathbf{K} = \frac{4\pi}{3\sqrt{3}a}(0, -1)$ and $\mathbf{K}' = -\mathbf{K}$. So, the equation is transformed to:

$$\zeta(q) \approx \frac{3at}{2} (-q_y + iq_x) = iv_F q e^{i\phi} \quad (1.22)$$

$$\zeta(q') \approx \frac{3at}{2} (q'_y + iq'_x) = iv_F q e^{-i\phi'} \quad (1.23)$$

This alternate has an advantage of easier implementation of time reversal symmetry. When the time reversal is k to $-k$, it results with the anti-unitary operator of complex

conjugate operation. As a consequence, time reversal exchange of the K and K' points in this alternative convention is presented in Figure 1.11.

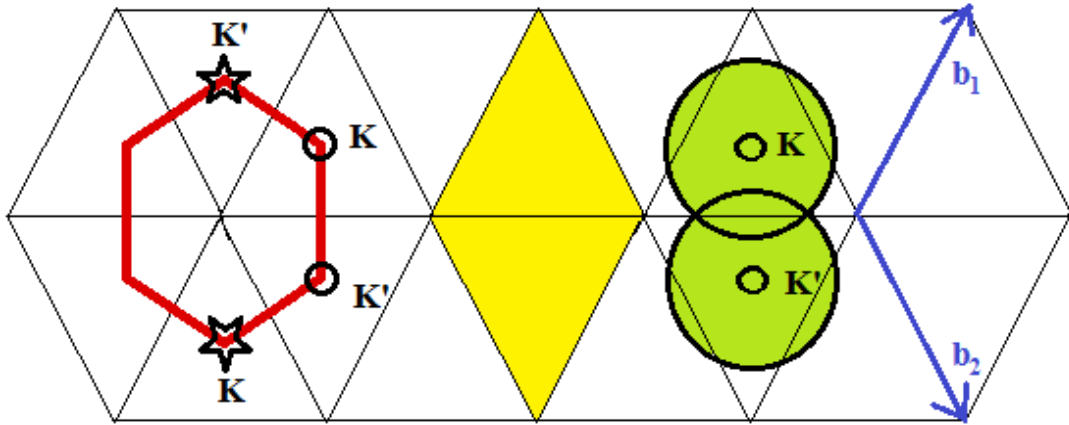


Figure 1.11. The reciprocal lattice of graphene. It is a triangular lattice resulting in a hexagonal Brillouin zone. The two choices of the K and K' points are shown as the circles and the stars in the corners of the BZ.

For either convention, when the appropriate rotation of the coordinate system is established, the Hamiltonian forms close to the K point resulting with a two dimensional Dirac Hamiltonian of mass-free Fermions as shown in the following equation.

$$H_{Dirac} = v_F \sum_q \psi_q^\dagger \begin{pmatrix} 0 & q_x + iq_y \\ q_x - iq_y & 0 \end{pmatrix} \psi_q \quad (1.24)$$

The final spectrum measured from the K-point is linear in the momentum, $E_{\pm}(q) = \pm v_F q$. This linear dispersion relation is unusual in condensed matter systems.

“Dirac point” can be defined as the contact points between the two bands. Dirac point of the bands in graphene is given at zero energy (Figure 1.12). Interestingly, there are two symmetrical Dirac points for graphene due to two existing sublattices in its structure. Thus, the energy at Dirac points is zero, and graphene is a gapless semiconductor.

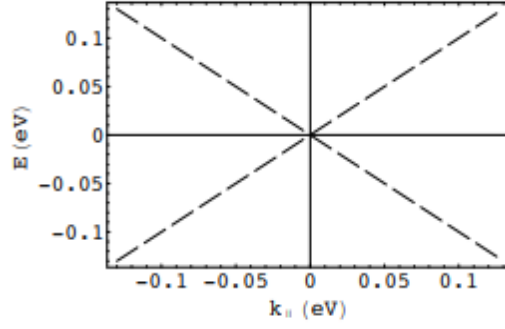


Figure 1.12. The “Dirac cone” dispersion of the quasiparticles in graphene.

The Dirac Hamiltonian equation is not acceptable for all points in the Brillouin zone. For instance, when the momentum is far from the corners of Brillouin zone, the lattice structure will appear in the dispersion, and it cannot be cylindrically symmetric. Still, linear spectrum gives acceptable approximation to study the low energy properties close to the Dirac point. However, it is required to introduce a cutoff value (Λ) to arrange the formula at high energies because of the finite band width. Then, the linear spectrum is assumed to be valid for momenta, $v_F q \ll \Lambda$. Λ term can be obtained by demanding the number of states conserved within the linear approximation in the Brillouin zone. As shown in Figure 1.11, two circles of radii Λ covers the Brillouin zone and estimated by $2\pi\Lambda^2 = (2\pi)^2/A_u$ where A_u is the area of the real space unit cell with $A_u = \sqrt{27}a^2/2$. In the natural unit, the Fermi-Dirac velocity

is equal to 1 which implies that $\Lambda \approx t\sqrt{\pi\sqrt{3}} \approx 7eV$. The term “natural unit” implies energies and frequencies that have the same units as momenta and wave-numbers. Thus, the units of momenta is oftenly given in eV. For an electron pocket with a radius given by Q in eV, the resulting electron density is $-v_4\sigma^*$

$$n = \frac{Q^2}{\pi} = \left(\frac{Q}{t}\right)^2 \frac{4}{9\pi a^2} \approx Q^2 7.8 \times 10^{13} \text{ cm}^{-2} \quad \text{including both K-points and spin projections.}$$

1.3.2 Electronic properties of Graphite

As mentioned, formation of graphite requires stacking of graphene layers by Van der Waals interactions with approximately 3.44 Å interplane distance.

Depending on the orientation of graphene layers, graphite can exist in two stacking forms (viz. ABAB and ABCABC sequences) (Figure 1.13). The ABAB sequence, known as Bernal stacking, is found in hexagonal crystal form while the ABCABC sequence is found in rhombohedral form. For both sequence forms, there are four carbon atoms in a unit cell of graphite (Figure 1.13c). The primitive lattice vectors are given in the following equation where $a = 2.461 \text{ \AA}$ is the lattice constant:

$$a_1 = a(1,1,0) \quad (1.25)$$

$$a_2 = a \left(-\frac{1}{2}, \frac{\sqrt{3}}{2}, 0 \right) \quad (1.26)$$

$$a_3 = a \left(0, 0, \frac{c}{a} \right) \quad (1.27)$$

The nearest neighbor distance in-plane is 1.421 \AA . The a_3 vector is perpendicular to the layers in c-axis where distance value (c) is 6.708 \AA , and the interplanar distance is calculated by $c/2$. The bonding strength between planes is weaker than that found in-plane bonds. The distance between nearest neighbor atoms on a plane is a factor of 2.36, which is larger than the distance between successive planes.

Reciprocal lattice vectors can be given in terms of primitive translation vectors as:

$$b_1 = \frac{2\pi}{\Omega} (a_2 \times a_3) \quad (1.28)$$

$$b_2 = \frac{2\pi}{\Omega} (a_3 \times a_1) \quad (1.29)$$

$$b_3 = \frac{2\pi}{\Omega} (a_1 \times a_2) \quad (1.30)$$

where Ω is the volume of the unit cell and given as $\Omega = |a_1 \cdot (a_2 \times a_3)|$. By using equation 1.2 and equation 1.4, the primitive translation vectors of the reciprocal lattice of graphite can be found as follows:

$$b_1 = \frac{2\pi}{a} \left(1, \frac{1}{\sqrt{3}}, 0 \right) \quad (1.31)$$

$$b_2 = \frac{2\pi}{a} \left(0, \frac{2}{\sqrt{3}}, 0 \right) \quad (1.32)$$

$$b_3 = \frac{2\pi}{a}(0,0,1) \quad (1.33)$$

Thus, the reciprocal lattice of graphite is hexagonal in the first Brillouin zone with the high symmetry points labelled as Γ , K, and H (Figure 1.13d). The High symmetry points of lattice;

$$\Gamma = \{0,0,0\} \quad (1.34)$$

$$K = \left\{ \frac{1}{3}, \frac{1}{3}, 0 \right\} \quad (1.35)$$

$$M = \left\{ 0, \frac{1}{2}, 0 \right\} \quad (1.36)$$

$$H = \left\{ \frac{1}{3}, \frac{1}{3}, \frac{1}{2} \right\} \quad (1.37)$$

$$A = \left\{ 0, 0, \frac{1}{2} \right\} \quad (1.38)$$

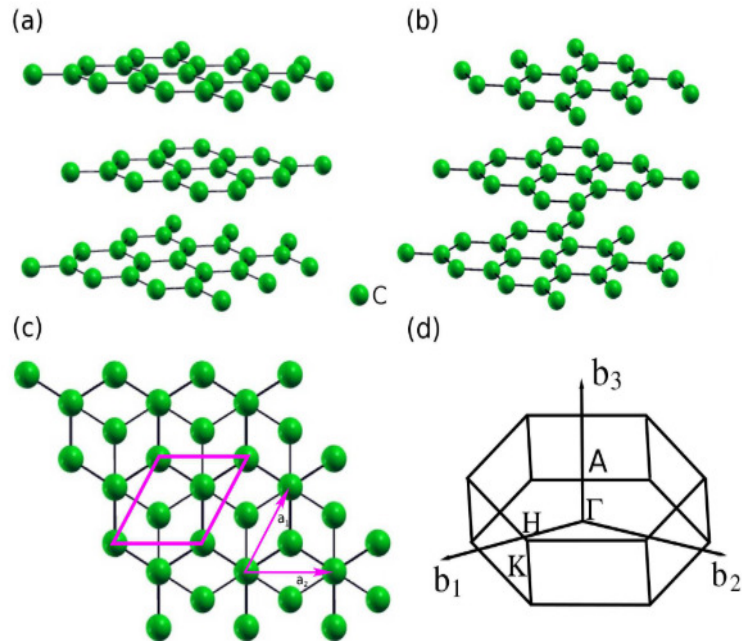


Figure 1.13. Graphite (a) AB- (b) ABC-. (c) Unit cell. It is the equilateral parallelogram (solid lines) with a_1 and a_2 lattice vectors. (d) The Brillouin zone.

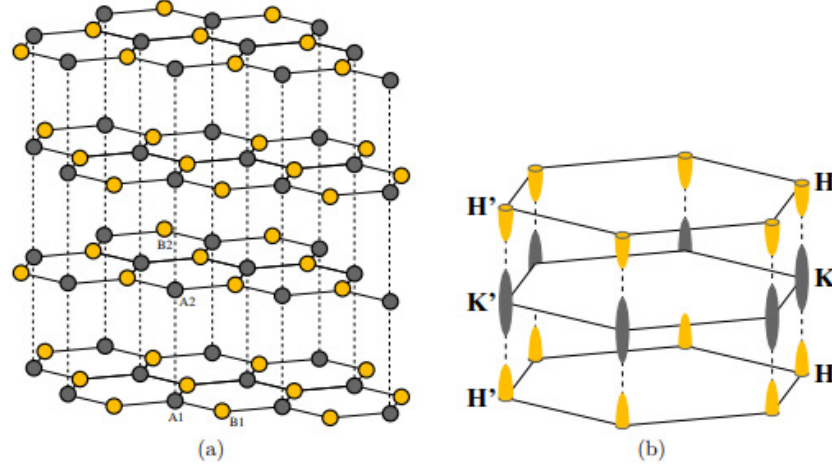


Figure 1.14. Graphite (a) The lattice structure (b) The hexagonal Brillouin zone. A, B letters represents atoms while 1, 2 represents corresponding layers.

The Bernal phase is the most favorable form of graphite. Figure 1.14 represents lattice structure of ABAB sequence shaped by two planes and four atoms in the unit cell where the A and B atoms are inequivalent. Represented four-component (A1-B1 and A2-B2) spinor can be estimated by:

$$\psi_k^\dagger = [c_{A1,k}^\dagger, c_{B1,k}^\dagger, c_{A2,k}^\dagger, c_{B2,k}^\dagger] \quad (1.39)$$

The Hamiltonian for the system can be generally described as:

$$H_{kin} = \sum_q \psi_q^\dagger H_0(q) \psi_q \quad (1.40)$$

4x4 matrix $H_0(p)$ close to the K point can be calculated by:

$$H_0(p) = \begin{pmatrix} \Delta + \frac{\gamma_5 \Gamma^2}{2} & v_F p e^{i\phi} & \gamma_1 \Gamma & -v_4 v_F p \Gamma e^{-i\phi} \\ v_F p e^{-i\phi} & \frac{\gamma_2 \Gamma^2}{2} & -v_4 v_F p \Gamma e^{-i\phi} & v_3 v_F p \Gamma e^{i\phi} \\ \gamma_1 \Gamma & -v_4 v_F p \Gamma e^{-i\phi} & \Delta + \frac{\gamma_3 \Gamma^2}{2} & v_F p e^{-i\phi} \\ -v_4 v_F p \Gamma e^{-i\phi} & v_3 v_F p \Gamma e^{i\phi} & v_F p e^{i\phi} & \frac{\gamma_2 \Gamma^2}{2} \end{pmatrix} \quad (1.41)$$

In the matrix, $v_3 = \frac{\gamma_3}{\gamma_0}$ and $v_4 = \frac{\gamma_4}{\gamma_0}$, and $v_F p e^{i\phi}$ expressions come from the in-plane graphene dispersion. Hopping terms regard to nearest neighboring planes are different depending on the pair of atoms: $\gamma_1 (A \leftrightarrow A)$, $\gamma_2 (B \leftrightarrow B)$, and γ_3 and γ_4 . They denotes a hopping between next nearest plane for B,(A) atoms. Thus, Δ

denotes the difference in on-site energies of atoms since they have different environments.

$$M_1(p) = \begin{pmatrix} 1 & 0 & 0 & 0 \\ 0 & e^{-i\phi} & 0 & 0 \\ 0 & 0 & 1 & 0 \\ 0 & 0 & 0 & e^{i\phi} \end{pmatrix} \quad (1.42)$$

The previous matrix used to perform the gauge transformation $H_1 = M_1^\dagger(\phi)H_0M_1(\phi)$ which moves all of $e^{\pm i\phi}$ phase factors to the V_a term:

$$H_1(p) = \begin{pmatrix} \Delta + \frac{\gamma_5\Gamma^2}{2} & v_F p & \gamma_1\Gamma & -v_4 v_F p \Gamma \\ v_F p & \frac{\gamma_2\Gamma^2}{2} & -v_4 v_F p \Gamma & v_3 v_F p \Gamma \\ \gamma_1\Gamma & -v_4 v_F p \Gamma & \Delta + \frac{\gamma_5\Gamma^2}{2} & v_F p \\ -v_4 v_F p \Gamma & v_3 v_F p \Gamma & v_F p & \frac{\gamma_2\Gamma^2}{2} \end{pmatrix} \quad (1.43)$$

This form clearly shows that the V_a term is responsible for trigonal distortion of the bands and breaking cylindrical symmetry structure. The symmetric/asymmetric combinations of A atoms that generates bonding/antibonding bands can be produced by the matrix:

$$M_2 = \begin{pmatrix} 1/\sqrt{2} & 0 & -1/\sqrt{2} & 0 \\ 0 & 1 & 0 & 0 \\ 1/\sqrt{2} & 0 & 1/\sqrt{2} & 0 \\ 0 & 0 & 0 & 1 \end{pmatrix} \quad (1.44)$$

Then these bands are permuted with the matrix:

$$M_3 = \begin{pmatrix} 1 & 0 & 0 & 0 \\ 0 & 0 & -1 & 0 \\ 0 & 1 & 0 & 0 \\ 0 & 0 & 0 & -1 \end{pmatrix} \quad (1.45)$$

Next, the transformed Hamiltonian $H_2 = M_3^\dagger M_2^\dagger H_1 M_2 M_3$ becomes:

$$H_2 = \begin{pmatrix} \Delta + \frac{\gamma_5 \Gamma^2}{2} + \gamma_1 \Gamma & 0 & (v_4 \Gamma - 1)v_F p / \sqrt{2} & (v_4 \Gamma - 1)v_F p / \sqrt{2} \\ 0 & \Delta + \frac{\gamma_5 \Gamma^2}{2} + \gamma_1 \Gamma & (1 + v_4 \Gamma)v_F p / \sqrt{2} & -(1 + v_4 \Gamma)v_F p / \sqrt{2} \\ (v_4 \Gamma - 1)v_F p / \sqrt{2} & (1 + v_4 \Gamma)v_F p / \sqrt{2} & \frac{\gamma_2 \Gamma^2}{2} & v_3 v_F p \Gamma e^{-3i\phi} \\ (v_4 \Gamma - 1)v_F p / \sqrt{2} & -(1 + v_4 \Gamma)v_F p / \sqrt{2} & v_3 v_F p \Gamma e^{-3i\phi} & \frac{\gamma_2 \Gamma^2}{2} \end{pmatrix} \quad (1.46)$$

This matrix is the overall gauge transformation of a Slonczewski-Weiss-McClure model for graphite which is generally written as:

$$H_{SWMC} = \begin{pmatrix} E_1 & 0 & H_{13} & H_{13}^* \\ 0 & E_2 & -H_{23} & -H_{23}^* \\ H_{13}^* & H_{23}^* & E_3 & H_{33} \\ H_{13} & -H_{23} & H_{33}^* & E_3 \end{pmatrix} \quad (1.47)$$

where

$$E_1 = \Delta + \gamma_1 \Gamma + \frac{\gamma_5 \Gamma^2}{2} \quad (1.48)$$

$$E_2 = \Delta - \gamma_1 \Gamma + \frac{\gamma_5 \Gamma^2}{2} \quad (1.49)$$

$$E_3 = \frac{\gamma_3 \Gamma^2}{2} \quad (1.50)$$

$$H_{13} = \frac{1}{\sqrt{2}} (-\gamma_0 + \gamma_4 \Gamma) e^{i\alpha} \zeta \quad (1.51)$$

$$H_{23} = \frac{1}{\sqrt{2}} (\gamma_0 + \gamma_4 \Gamma) e^{i\alpha} \zeta \quad (1.52)$$

$$H_{33} = \gamma_3 \Gamma e^{i\alpha} \zeta \quad (1.53)$$

Table 1.1 represents most widely used values for Slonczewski-Weiss-McClure parameters (Brandt, 1988; Chung and Lu, 2002).

Table 1.1. Typical values of Slonczewski-Weiss-McClure parameters.

γ_0	γ_1	γ_2	γ_3	γ_4	γ_5	$\gamma_6 = \Delta$	ϵ_F
3.16	0.39	-0.02	0.315	0.044	0.038	0.008	-0.024
3.12	0.377	-0.020	0.29	0.120	0.0125	0.004	-0.0206

These common parameters show that in the Brillouin zone electrons and holes are near to K and H points, respectively. These electron and holes pockets are mainly generated by coupling of γ_2 in the tight binding model resulting with a hopping among B atoms of next close planes. This process involves a hopping of a distance to maximum 7 Å.

Comparison of deriving Slonczewski-Weiss-McClure parameters for 2D graphene and bulk graphite is a major focus in graphene related studies. Studies suggested an important difference between the graphite and bilayer graphene based on the analysis of Ramanscattering and a number of *ab initio* calculations (Zhang et al., 2008). Yet, these theoretical studies does not include a clear discussion of the Slonczewski-Weiss-McClure parameters.

1.3.3 Electronic properties of Bilayer Graphene

As a nanomaterial, bilayer graphene consists of two graphene sheets. It is a system intermediate between monolayer graphene and graphite. Bilayer graphene can be obtained in three forms: AA stacking, AB (or Bernal phase) stacking, and twisted bilayer. AA stacking form is the simplest structure where each carbon atom of the second layer is placed exactly above the aligned atom of the first carbon sheet (Liu et al., 2009). AB stacking form is the most stable structure where half of the carbon atoms of the top layer are above the aligned carbon atoms of the lower layer while other atoms lie above the centers of the lower-layer hexagons (Rozhkov et al., 2016). Twisted bilayer graphene is also a stable structure where the top carbon layer is rotated with respect to the lower layer by θ angle (Lopes dos Santos, Peres and Castro Neto, 2007).

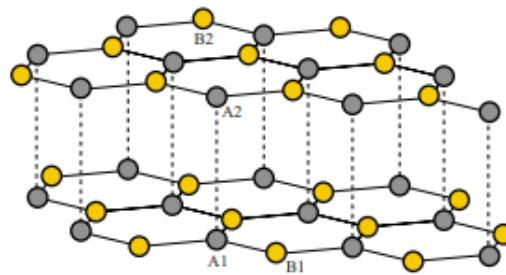


Figure 1.15. Lattice structure of the graphene bilayer.

Bernal (AB) stacking graphene (Figure 1.15) consists of two coupled graphene layers of carbon atoms — each of them are in the honeycomb lattice structure. These two planes have inequivalent sites namely A1-B1 and A2-B2 on the graphane layers. Since A, B atoms are equivalent in their physical properties with inequivalent layers, it gives the advantage to evaluate two layers together. The

aforementioned A1-B1 and A2-B2 notations are also valid for tight bonding electronic model of bilayer graphene. So, using the four-component spinor (equation 1.30) and Hamiltonian matrix (equation 1.32) defined for the graphite with $\Gamma = \mathbf{1}$ and $\gamma_2 = \gamma_3 = \mathbf{0}$ parameters lead to:

$$H_0(p) = \begin{pmatrix} \Delta & v_F p e^{i\phi} & t_{\perp} & -v_4 v_F p e^{i\phi} \\ v_F p e^{-i\phi} & 0 & -v_4 v_F p e^{-i\phi} & v_3 v_F p e^{i\phi} \\ t_{\perp} & -v_4 v_F p e^{i\phi} & \Delta & v_F p e^{-i\phi} \\ -v_4 v_F p e^{i\phi} & -v_4 v_F p e^{-i\phi} & v_F p e^{i\phi} & 0 \end{pmatrix} \quad (1.54)$$

Two-dimensional bilayer graphene system is only relative to the atomic positions; therefore, hopping term between A1(B1) and A2(B2) atoms are local in real space. Thus, the t_{\perp} constant in momentum space is defined for Hamiltonian matrix. The hopping term, $B1 \rightarrow A1$ [$A1 \rightarrow B1$], in graphene improves to the factor $\zeta(k)$ [$\zeta^*(k)$], where $\zeta(k)$ defined as:

$$\zeta(k) = -t \sum_k e^{ik \cdot \delta_i} = -t e^{ik_x a/2} \left[2 \cos\left(\frac{k_y a \sqrt{3}}{2}\right) + e^{i3k_x a/2} \right] \quad (1.55)$$

The geometrical role of A and B atoms alternate between planes 1 and 2, so $A2 \rightarrow B2$ [$B2 \rightarrow A2$] hopping gives rise to the factor $\zeta(k)$ [$\zeta^*(k)$] in Fourier space. The opposite direction in the $B1 \rightarrow B2$ hopping associates with $v_3 \zeta^*(k)$ factor where $v_3 = v_2/\mathbf{0}$. Here, the hopping energy is v_2 and $v_1 = \mathbf{0}$. Likewise, $B1 \rightarrow A2$ hopping direction similar to $B1 \rightarrow A1$ hopping leads to $v_4 \zeta(k)$ term along with $B1 \rightarrow A2$ hopping. Therefore the full tight-binding Hamiltonian matrix becomes:

$$H_{t,b}(k) = \begin{pmatrix} \Delta & \zeta(k) & t_{\perp} & -v_4 \zeta^*(k) \\ \zeta^*(k) & 0 & -v_4 \zeta^*(k) & v_3 \zeta(k) \\ t_{\perp} & -v_4 \zeta(k) & \Delta & \zeta^*(k) \\ -v_4 \zeta(k) & v_3 \zeta^*(k) & \zeta(k) & 0 \end{pmatrix} \quad (1.56)$$

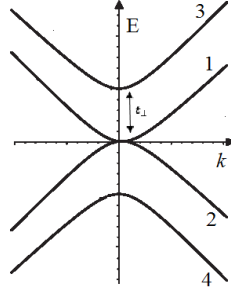


Figure 1.16. Dispersions in the bilayer graphene. Four bands near K-point labeled by the numbers 1 to 4 in the bilayer graphene system.

If the expressions in the Equation.1.55 expands close to the K point, the characteristic behaviour of the bands obtained from this equation force band 3 and band 4 to move away from the Dirac point by the energy of t_{\perp} (Figure 1.16). In addition, the potential energy parameter V can be included in the planes of bilayer graphene. That term generally generated by an electric field perpendicular to layers. Voltage applied systems has a gap in the spectrum unlike natural gapless bilayer graphene system. When V parameter is included to hoppings from the tight-binding picture by expanding matrix in Equation 1.46 close to the K-point, then the matrix becomes:

$$H_0(p) = \begin{pmatrix} \frac{V}{2} + \Delta & \sigma & t_{\perp} & -v_4 \sigma^* \\ \sigma^* & \frac{V}{2} & -v_4 \sigma^* & v_3 \sigma \\ t_{\perp} & -v_4 \sigma & -\frac{V}{2} + \Delta & \sigma^* \\ -v_4 \sigma & v_3 \sigma^* & \sigma & -\frac{V}{2} \end{pmatrix} \quad (1.57)$$

Two of the bands are moved away from the Dirac point by inter plane hopping term energy with $V \ll t_{\perp}$. Thus, the application of tranverse voltage opens a gap in the spectrum. The existence of this gap was also experimentally confirmed (Rozhkov et al., 2016). In bilayer graphene studies, tailoring this gap attracts attention from both theoretical and experimental studies. The possibility of obtaining semiconductor graphene with controlled gap is a promising area with a wide range of applications.

1.4 Optical Properties of Graphene Structures

The optical properties of graphene-based structures have been attracted by researchers due to the discovery of outstanding optical properties of graphene. Considering the optical properties of graphene, they are the most promising material for future technologies as optoelectronic devices. It is obvious that most of graphene related studies have been focused on electronic behaviours of graphene like structures and less information is available for optical properties of these materials. However, demonstration of the universal conductivity at different energy levels, increased the value of experimental and theoretical studies regarding to optical behaviours of graphene systems. So, in order to understand these extraordinary optical properties of graphene based systems, optical conduction and transitions should be discussed in details.

1.4.1 Optical conductance of graphene structures

The optical conductance of single layer graphene can be defined as:

$$\sigma = \sigma_{\pi-\pi^*} + \sigma_{\sigma-\sigma^*} \quad (1.58)$$

where $\sigma_{\pi-\pi^*}$ and $\sigma_{\sigma-\sigma^*}$ terms indicate conductance contributions from interband transitions of $\pi-\pi^*$ and $\sigma-\sigma^*$. The transitions between σ and π bands are forbidden due to the wavefunction symmetry. Optical conductance can be shown as a complex number for the transitions:

$$\sigma_{\pi-\pi^*} = \sigma_{r1} + i\sigma_{i1} \quad (1.59)$$

The real and imaginary conductivity of monolayer graphene is represented as:

$$\sigma_{r1} = \sigma_0 \left[\frac{1}{2} + \frac{(\hbar\omega)^2}{72\xi^2} \right] x \left(\tanh \frac{\hbar\omega + 2\mu}{4k_B T} + \tanh \frac{\hbar\omega - 2\mu}{4k_B T} \right) \quad (1.60)$$

$$\sigma_{i1} = \sigma_0 \left[\frac{\mu}{\hbar\omega} \frac{4}{\pi} \left(1 - \frac{2}{9} \frac{\mu^2}{\xi^2} \right) - \log \frac{|\hbar\omega + 2\mu|}{\hbar\omega - 2\mu} \left(\frac{1}{\pi} + \frac{1}{36\pi} \left(\frac{\hbar\omega}{\xi} \right)^2 \right) \right] \quad (1.61)$$

In tight bonding model ξ , the closest neighbor hopping parameter value for unhybridized p_z electrons is approximately 3 eV that μ is the chemical potential according to the Dirac point, r_0 is the universal optical conductance in the 1, m, t of massless Dirac band structure, and $\hbar\omega$ is the incident photon energy:

$$\sigma_0 = \frac{\pi e^2}{2 h} = \frac{e^2}{4\hbar} \sim 6.08 \times 10^{-5} \Omega^{-1} \quad (1.62)$$

In the case of low doping ($\mu=0$ and $T=300$ K and $\hbar\omega=550$ nm), $\sigma_{\pi} = 1.016\sigma_0$ and σ_{π} is calculated approximately zero. When $\sigma_{\pi-\pi^*}$ is nearly equal to σ_0 , the optical conductance of graphene at $\pi - \pi^*$ transitions is almost identical to the universal optical conductance.

The $\sigma - \sigma^*$ transitions in the optical conductance results with a phase shift of optical waves, since the energy gap is larger than visible photon energies. For multilayer graphene structures, $\sigma - \sigma^*$ transitions have more critical role.

The $\sigma - \sigma^*$ bands can be modelled via the dielectric constant as:

$$n = \sqrt{\frac{\partial}{\partial_0}} = \sqrt{1+x} \quad (1.63)$$

In Equation 1. 63, the susceptibility term $x = \frac{e^2 N}{mc_0 \omega_0^2} \frac{\omega_0^2}{\omega_0^2 - \omega^2 + j\omega\Delta\omega}$ defined for a two-level system where N is the number of charges, and ω_0 is resonant angular frequency. It is more convenient to use Lorentzian function for better estimation of far below bands since the $\sigma - \sigma^*$ transitions have energy bands for visible photons. So, for a large detuning, the susceptibility term equation can be simplified as:

$$x = \frac{e^2}{m\partial_0} \frac{\hbar^2}{\partial_0^2 - \partial^2} N \quad (1.64)$$

If σ defines as a function of x ,

$$\sigma_{\sigma-\sigma^*} = i\omega\partial_0 x \delta = i \frac{e^2}{m} \frac{\partial \hbar}{\partial_0^2 - \partial^2} N \delta \quad (1.65)$$

where δ represents thickness of graphene, and m represents the bare electron mass. The charge density of $\sigma - \sigma^*$ bands must be taken into account for determination of $N\delta$. From the calculations of primitive unit cell area, $N\delta$ term can be calculated as

$$N\delta = \frac{2}{|a_1 \times a_2|} = \frac{2}{\frac{\sqrt{3}}{2} a^2} = 3.82 \times 10^{19} m^{-2} \quad (1.66)$$

Therefore, the contributions of $\sigma - \sigma^*$ transitions to the conduction band is $\sigma_{\sigma-\sigma^*} = 0.85r_0i$. So, the total conductance of graphene is:

$$\begin{aligned} \sigma &= \sigma_{\pi-\pi^*} + \sigma_{\sigma-\sigma^*} \\ \sigma &= (\sigma_0 + 0i) + (0 + 0.85r_0i) \\ \sigma &= \sigma_0 [1 + 0.85i] \end{aligned} \quad (1.67)$$

1.4.2 Refractive Index

As an optical phenomena, the refractive index is the measure of light-bending ability of a specific medium. The optical properties of graphene-based structures can be described by the refractive index measurements. So, the bulk graphite can be used in order to model the optical response of graphene by the means of refractive index.

The refractive index of graphene can be defined from the optical conductivity, displacement \vec{D} , magnetic field \vec{H} , and surface current \vec{J} in the Maxwell equations:

$$\vec{D} = \epsilon_0 \vec{E} + \vec{P} = \epsilon_0 \epsilon_r \vec{E} \quad (1.68)$$

$$\vec{J} = \frac{\sigma}{d} \vec{E} \quad (1.69)$$

$$\nabla \times \vec{H} = \frac{\delta \vec{D}}{\delta t} = \vec{J} + \epsilon_0 \frac{\delta \vec{E}}{\delta t} \quad (1.70)$$

\vec{P} indicates the dielectric polarization, ϵ_0 represents free space permittivity, and ϵ_r shows relative material permittivity. By the substitution of Equation 1.50, it can be simplified as following when $\epsilon_r = 1 + \sigma/j\omega\epsilon_0$:

$$\frac{\sigma}{\delta} \vec{E} + i\omega\epsilon_0 \vec{E} = i\omega\epsilon_0 \epsilon_r \vec{E} \quad (1.71)$$

Then, the definition of refractive index of the medium is $n = \sqrt{\epsilon_r \mu_r}$ which reveals the transmission efficiency of the medium. When linear susceptibility (μ_r) equals to zero then the refractive index (n) is $\sqrt{\epsilon_r}$. Therefore, the refractive index of graphene

becomes $n = \sqrt{\epsilon_r} = \sqrt{1 + \sigma/j\omega\epsilon_0}$.

The optical character of graphene is directly related to its honeycomb hexagonal lattice structure of carbon atoms. The relation of linear energy dispersion on graphene layer enables the distribution of surface plasmons. They are charge density waves moving at the graphene interface and electric materials. This allows gating the materials easily by varying their plasmonic states, broadly. In other words, graphene is a feasible material for plasmonic applications from terahertz to mid point infrared frequencies due to flexible plasma states. Structural gating consists of two varieties (*viz.* back-gating and top-gating). Both of them can accommodate the carrier charge concentrations of graphene with proper modifications. The tuned carrier concentration (N) with an applied voltage of V can be defined as:

$$N = \frac{\epsilon_{DC} |V_G - V_{CNP}|}{ed} \quad (1.72)$$

where ϵ_{DC} represents the dielectric constant, V_G represents the voltage applied between graphene and back-gate, and V_{CNP} is the voltage of the charge neutrality point. The strength of the tuning of graphene depends on its surrounding dielectric environment. So, it is important to examine the range of dielectric properties for graphene.

1.4.3 Optical properties of bilayer graphene

Bilayer graphene shows similar properties with monolayer graphene such as high electrical mobility, high mechanical strength, flexibility and chemical stability. On the other hand, the structure difference between bilayer and monolayer graphene leads to a plethora of different electronic and optical properties. The most notable differences are the ability to open a band gap and the infrared activity of the Γ -point optical phonon (Mak et al., 2009; Mccann and Koshino 2013; Xia et al., 2010; Zhang et al., 2009).

The gamma-point optical phonon in pristine bilayer graphene has a small electrical dipole moment. That, it can be detected in infrared absorption spectrum (Cappelluti, Benfatto and Kuzmenko, 2010). However, the corresponding phonon has zero electrical dipole for monolayer graphene, since A- and B- sublattices are equivalent. In addition, the bilayer graphene systems consist of only one type of atoms, and it has a dipole moment for the lattice vibration, surprisingly. The dipole moment in the E_u vibrational mode comes from the inequivalent A1(A2) and B1(B2) atoms. The vibrations between the atoms replacing in one direction on dimer site and the atoms replacing in the other direction on non-dimer site creates a macroscopic dipole moment with coupling of light. The E_g vibrational mode of pristine bilayer graphene has zero dipole moment. In addition, asymmetric doping in upper and lower layers of graphene cause E_g mode to have a dipole moment and to become IR-active, as well (Cappelluti et al., 2012; Cappelluti, Benfatto and Kuzmenko, 2010). The vibrational phonon modes of bilayer graphene structures are given in the Figure 1.17a.

The IR-activity of the optical phonon in bilayer graphene structure can be detected on IR-spectroscopy. The phonon IR-spectra of bilayer graphene depends mostly on the Fermi energy and electric field across two layers of graphene. Figure 1.17b shows the contribution of the phonon at different gates to the optical conductivity of bilayer graphene (Cappelluti et al., 2012; Cappelluti, Benfatto and Kuzmenko, 2010; Kuzmenko et al., 2009; Tang et al., 2010). Both shape and intensity of the peak depend on the gate voltage (V_g). Phonon peak is nearly invisible at $V_g = -30$ V. However, the phonon gains intensity with the increase in doping of

both electron and hole sites, and it creates Fano asymmetric line-shape (Fano, 1961). In addition, the magnitude of E_u vibrational mode dipole moment is smaller than those of typical spectra. This can be explained by charged phonon theory where dipole moment and IR-activity is strengthened by charge carriers. The Fano line-shape in the spectra can be explained by the optical transition through phonon excitation which causes a wide optical absorption spectra from electronic transitions and reveals a Fano resonance system (Fano, 1961).

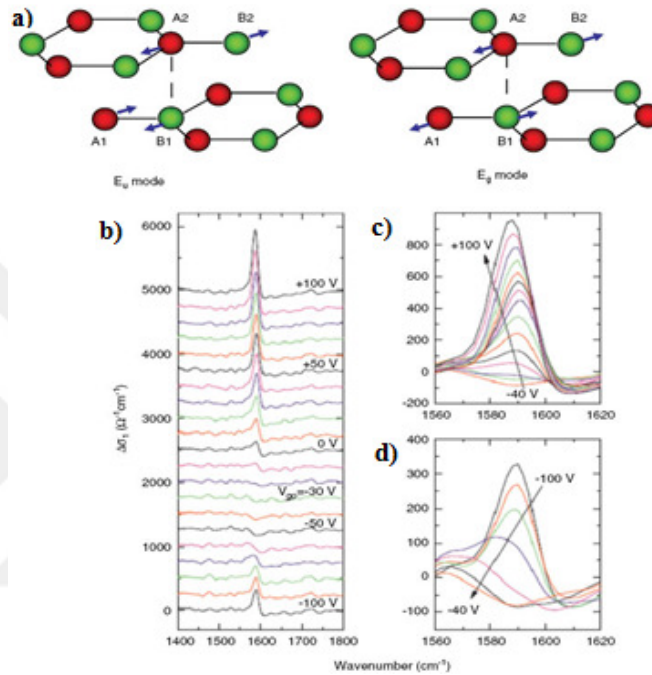


Figure 1.17. Tunable Fano resonance in back-gated bilayer graphene. a) Sketch of the E_u phonon and E_g phonon modes. b) Extracted optical conductivity in the phonon region for different gate voltages. c, d) The expanded view of the phonon spectra in the electron and hole doping regime.

1.5 Tailoring the graphene-based structures

Graphene possess zero band gap that weakens its potential in the field of semiconductors. It increases the number of studies on functionalization of graphene structures and its derivatives with organic and inorganic molecules. To modify electronic structure of graphene based systems, doping, intercalation and striping would be useful.

1.5.1 Nitrogen Doping

One of the most widely used method for tuning and controlling the electronic properties of graphene-based systems is doping with heteroatoms. For substitutional doping of graphene, boron and nitrogen are the best candidates. They both have atomic sizes, hole acceptor capabilities and electron donor capabilities similar to carbon atoms in graphene. Doping with boron causes graphene to behave like a p-type material whereas doping with nitrogen causes graphene to behave like an n-type material. In addition, nitrogen doping results a direct substitution of carbon atoms in the lattice structure due to the one extra electron in nitrogen atom.

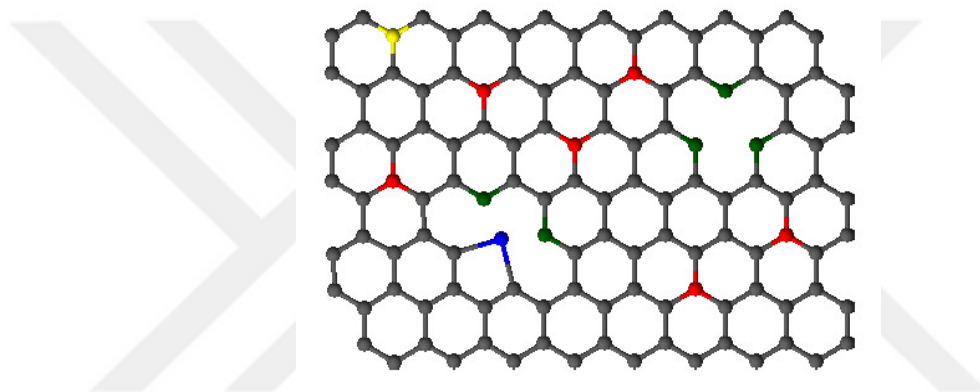


Figure 1.18. Schematic representation of different types of N atoms in graphene; graphitic [red atoms (bulk), yellow (edge)], pyridinic (green atoms) and pyrrolic N (blue).

Nitrogen doping of graphene provides three different bonding configurations (Figure 1.18); pyridinic nitrogen, pyrrolic nitrogen and the graphitic nitrogen. In pyridinic N doping, each nitrogen atom is bonded to two carbon atoms by donating one π -electron to the π system. In the pyrrolic N doping, nitrogen atoms are incorporated into the heterocyclic rings where nitrogen atom is bonded to two carbon atoms contributing two π -electrons to the π system. Finally, in graphitic N doping, the nitrogen atoms replaced with carbon atoms in the graphene plane. Graphitic N-doped configuration can change the local density state around the Fermi level which may play an important role in tailoring the electronic properties of graphene-based systems.

Nitrogen doped graphene was first synthesized by Wei in 2009. Later, extraordinary properties of nitrogen functionalized graphene have been explored. There are several potential applications proposed for using nitrogen functionalized graphene systems such as development of lithium batteries, hydrogen storage technologies, biosensors and catalysts in oxygen reduction reactions. In addition to the experimental studies, many theoretical studies have also been dedicated to the nitrogen-doping graphene with a focus of turning it to semiconductor materials. The spin-polarized band structures from the studies for different nitrogen doping models is given in Figure 1.19. It can be seen that, pristine graphene shows zero band gap with 6V vacancies where the Dirac point close to K point is stable. However, in the graphitic N-doping band structure, there is ~ 0.04 eV change at Fermi level which causes an opening in band gap.

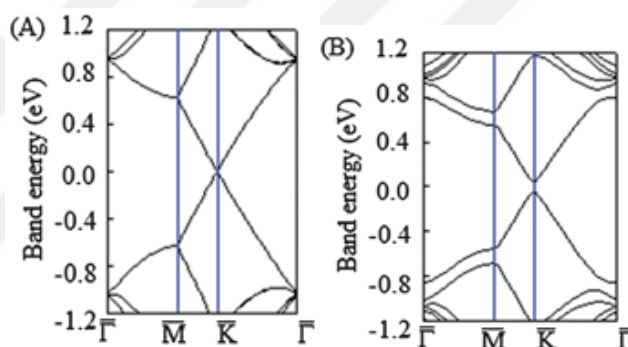


Figure 1.19. Calculated band structures. (a) ideal graphene (b) graphitic N-doped graphene.

Thus, nitrogen doping of graphene-based systems provide the possibility of tuning the band gap of graphene. Converting the electronic properties from semimetal to semiconductor by increasing the number of dopants allows applications in wide range of electronic devices.

1.5.2 Metal Intercalation

Intercalation takes place by inserting different species between two dimensional graphene layers. It is an effective way to tailor electronic properties of these systems. Metal interactions with monolayer graphene and bilayer graphene have been investigated by both experimental and theoretical aspects. Novoselov et al.

continued their studies with exploring surface interactions between one-atom thick graphene and Au, Fe, and Cr metals by using scanning transmission electron microscopy (Zan et al., 2011). According to Takashi and co-workers intercalation takes place when metal atoms are inserted between two graphene layers. They experimentally synthesized Li-intercalated bilayer graphene on SiC(0001) substrate and characterized the substance by low-energy electron diffraction (LEED) and angle-resolved photoemission spectroscopy (ARPES) (Sugawara et al., 2011). Their studies led the development of nano-scale lithium ion batteries. In 2014 Wang and co-workers investigated the energetics of Li, Na, K alkali metal intercalations between graphite layers by Van der Waals density functionals. Their study showed that the intercalation of alkali metals induces a small increase in bond lengths between two carbon atoms neighboring to alkali metals without any breakage of hexagonal symmetry (Wang, Selbach and Grande, 2014). Two years ago, superconductivity in calcium intercalated bilayer graphene was suggested by using *in situ* electrical transport measurements by Hasegawa and co-workers (Ichinokura et al., 2016). The development of computational tools for density functional theory calculations have been showed significant efforts in nanomaterial science field. However, the interactions of transition metal in bilayer graphene systems has not been investigated in details using computer based systems. Nakada and Ishii investigated the decorations of alkali, alkali earth and transition metals on graphene structure by using DFT calculations. In most cases, the studies showed that metal atom tends to locate on the hexagonal adsorption site (H) while some of the metal atoms may prefer bridge (B) or top (T) adsorption site of hexagonal structure (Figure 1.20) (Nakada, Torobu and Ishii, 2012).

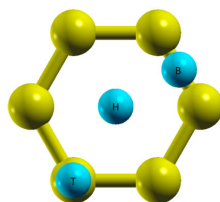


Figure 1.20. Three adsorption sites on the graphene surfaces. H: hexagonal, B: bridge and T: top.

For example, the intercalation of transition metal chromium was reported as most stable form when it interacts on the hexagonal (H) adsorption site of graphene

sheets (Bui et al., 2013). The sandwich like graphene-Cr-graphene structure is presented in Figure 1.21. Giovanetti reported the interactions between graphene and different transition metal atoms (Al, Ag, Cu, Au, and Pt). Their results showed that weakening the graphene-metal bond causes approximately 0.5 eV shift in the Fermi level in DFT calculations. The interactions of nickel and copper on graphene was investigated theoretically by Xu and Buehler (Xu and Buehler, 2010). They demonstrated that the adhesive energy of nickel-graphene was much stronger than energy of copper-graphene. Decorating transition metal atoms on graphene layers reveals magnetic behaviour which is the main topic of spintronics. The spintronic applications of graphene-ferromagnet interfaces of Co(111) and Ni(111) were explained by Maassen and co-workers by using DFT calculations. They reported that spin efficiencies of Co(111) and Ni(111) as 80% and 60%, respectively. In addition, Liao reported the stable structure configurations of scandium- and titanium-intercalated bilayer graphene structures using first-principle calculations (Liao et al., 2016). In general, the effect of transition metal intercalation on graphene-based systems alters the electronic and magnetic behaviour of the defective system (Figure 1.22) (Zhang et al., 2017). Recently, the structures and electronic properties of VB transition metals intercalated with bilayer graphene have been studied. Adding some VB metals (vanadium, niobium and tantalum) between two graphene layers can lead to control the band structure of bilayer graphene. In summary, this study showed that tuning of the electronic band gap between valence and conduction bands results with appearance of a Dirac cone only in vanadium-intercalated bilayer graphene (Pakhira, Lucht and Mendoza-Cortes, 2018).

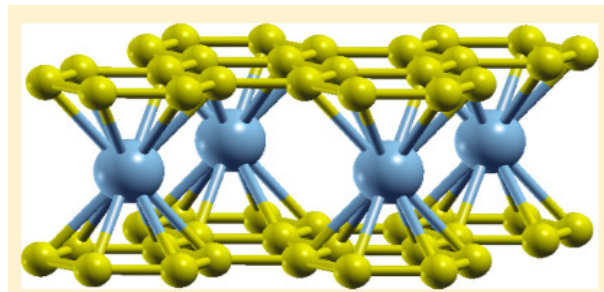


Figure 1.21. The sandwich like graphene-Cr-graphene structure (Zhang et al., 2017).

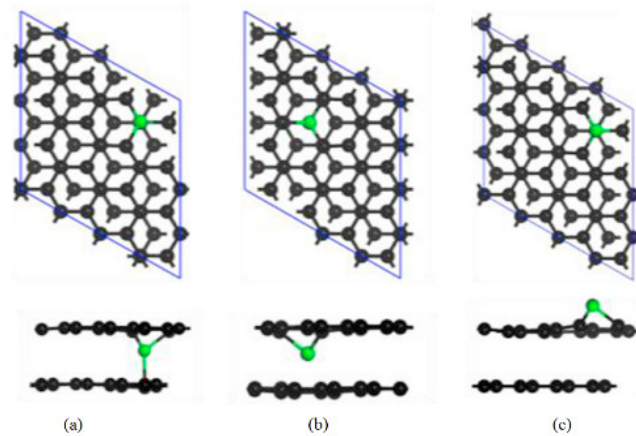


Figure 1.22. The effect of transition metal atoms on defective BLG (TM@dBGLs, TM = Ti-Fe) (Zhang et al., 2017).

In conclusion, bilayer graphene shows high potential for nanomaterial related research and applications. In this study, we aimed to explore electrical and optical properties of bilayer graphene systems by tailoring the band gap structure. This study is motivated to fulfill the gap in the literature by presenting valuable data on transition metal-intercalated graphene systems. We calculated structural properties of N-doped bilayer graphene intercalated with rhenium, tungsten, osmium and their oxides. The main motivation of this study to increase the understanding of bilayer graphene nanoparticles to guide further experimental approaches on nanocatalyst synthesis.

2. AIM AND SCOPE OF THE STUDY

Graphene is one of the most studied topic due its remarkable properties. Over the past decade, graphene research has promised potential applications especially for high efficient batteries, solar cells, corrosion prevention systems, electrical devices and medicinal technologies.

There are several studies focusing on bilayer graphene which shows similar properties to graphene. The results suggest that bilayer graphene shows superior characteristics when compared to mono layer graphene. The richer electronic structure in bilayer graphene give rise to many outstanding phenomena with the potential applications for modifying electronic states through interlayer-coupling.

Tailoring the band gap of bilayer graphene structure is crucial for investigation of electronic and optical properties of such systems. There are several methods such as applying an electric field, heteroatom doping and metal intercalation to modify electronic band gap. The main object of this thesis study is to tune electronic properties of bilayer graphene systems by intercalation of transition metal atoms between graphene layers by using *ab initio* first principle density functional theory calculations. There are limited number of studies on this subject since the investigations on metal-intercalated graphene systems have started just a decade ago. The data produced in this study will contribute understanding the effects of inserting transition metals between bilayer graphene sheets.

In this study, first principles *ab initio* density functional computational methods were used for exploring the electronic structure of bilayer graphene systems. To modify electrical and optical properties of bilayer graphene systems, nitrogen doping and intercalation of some rare transition metal atoms (rhenium, tungsten and osmium) between layers of graphene were applied to computational calculations. The objectives of this study are the following:

1. Building of bilayer graphene structures and geometry optimizations
2. Calculations of bond lengths and total energies
3. Analysing the molecular dynamic simulations

4. Analysing the band structures and effective masses of bilayer graphene systems
5. Analysing the electronic properties of bilayer graphene systems by the means of electron density, electron difference density and electron localization density.
6. Analysing the optical properties of bilayer graphene systems by the means of adsorption, refractive index, dielectric constant and phonon energy.



3. MATERIALS AND METHODS

There are two common approaches to derive the electronic spectra of graphene systems, as well as many other materials: the “*ab-initio*” Density Functional Theory (DFT) calculations and the tight-binding approximation (Rozhkov et al., 2016) . In many cases, hopping amplitudes in tight-binding approximations are calculated by DFT method.

In this study, the Atomistic-ToolKit (ATK) (version 2017.2) (Atomistix Toolkit version 2017.2 2017) software package (Synopsys QuantumWise A/S) was utilized to carry out the *ab initio* DFT calculations for geometry optimizations and investigations of electronic and optical properties for transition metal (Re, W, Os) incalated BLG systems. First-principles DFT calculations were performed by using generalized gradient approximation (GGA) for the exchange–correlation interactions. The BPW91 basis set was used for DFT calculations with linear combination of atomic orbitals (LCAO) calculator while setting electron temperature 300 K, k points (3, 3, 1), mesh cutoff 75 Hartree.

In the following subsections, the Density Functional theory (DFT) and Quantumwise ATK-VNL Nanolab and its related functional theory will be evaluated to understand the methodology about the computational studies in this work.

3.1 Density Functional Theory

As an advanced theoretical formalism, Density Function Theory is mainly based on the theories stated by Hohenberg and Kohn in 1964 (Hohenberg and Kohn, 1964). Among the importance of these theorems, DFT has become more popular in practise with the Kohn and Sham approach (Kohn and Sham, 1965).

3.1.1 The Hohenberg-Kohn theorems

Density Functional Theory is mainly based on the Hohenberg-Kohn (HK) theorems. The statement of the first HK theorem is the replacement of wavefunction by the ground state electron density with no loss of information. The second theorem is the equivalent of the variational principle in standard quantum mechanics. Before the giving detailed explanation for two theorems, it is convenient to give the Hamiltonian. First two terms are universal and the third term defines the Hamiltonian as:

$$H = T + V_{ee} + V_{ext} \quad (1.73)$$

The first Hohenberg-Kohn theorem states that the external potential of any system $\tilde{V}_{ext}(\mathbf{r})$, is incomparably determined by the particle density of the ground state, $\rho_0(\mathbf{r})$. Since the Hamiltonian is mainly specified by the external potential, it can be said that it is determined by ground state electron density. In other words, Hohenberg and Kohn proved that the electron density is the main variable where the external potential energy defines uniquely the charge density and vice versa. Also ground state density is a basic variable to obtain the information about the electron densities.

The Second HK theorem is the ‘‘Variational Principle’’ which can be expressed only in terms of the charge density:

$$E_v[\rho(\vec{r})] = F[\rho(\vec{r})] + \int V_{ext}(\vec{r})\rho(\vec{r})d\vec{r} \geq E_0 \quad (1.74)$$

$$F[n(r)] = T_s[n(r)] + E_H[n(r)] + E_{xc}[n(r)] \quad (1.75)$$

$$E_H[n(r)] = \frac{1}{2} \iint \frac{n(r_1)n(r_2)}{|r_1 - r_2|} dr_1 dr_2 \quad (1.76)$$

As presented in the equations, the second HK theorem states that if and only if the input density is ρ_0 , $E_v[\rho(\vec{r})]$ delivers the lowest energy.

3.1.2 Kohn-Sham Equation

Kohn and Sham described a non-interacting reference system in which the electrons have no interaction and live in an external potential. Thus, their ground state electron density is equal to the electron density of interacting system. This system is called as Kohn-Sham system where the electrons refer as the Kohn-Sham electrons and the external potential refers as Kohn-Sham potential.

For a such system with zero interacting electrons, Slater determinant is the right wave-function and the kinetic energy can be defined as:

$$T_s = -\frac{1}{2} \sum_i^N \phi_i | \nabla^2 | \phi_i \quad (1.77)$$

For non-interacting reference system where the electrons moves only in an effective potential $V_s(\vec{r}_i)$, the Hamiltonian can be written as:

$$H_s = -\frac{1}{2} \sum_i^N \nabla_i^2 + \sum_i^N V_s(\vec{r}_i) \quad (1.78)$$

The Hamiltonian operator H_s includes no interaction between electrons for that reason it defines a non-interacting system. For each specific orbital we have:

$$f^{KS} = -\frac{1}{2} \nabla^2 + V_s(\vec{r}) \quad (1.79)$$

The f^{KS} operator which is a one-electron Kohn-Sham operator can be defined as:

$$f^{KS} = -\frac{1}{2} \nabla^2 + V_s(\vec{r}) \quad (1.80)$$

So for any specific orbital in a real system we can have:

$$\left[-\frac{1}{2} \nabla^2 + V_H(\vec{r}) + V_{xc}(\vec{r}) + V_{ext}(\vec{r}) \right] \phi_i(\vec{r}) = H_{KS} \phi(\vec{r}) = \epsilon_i \phi_i(\vec{r}) \quad (1.81)$$

$$V_{KS}(r) = \int \frac{n(r')}{|r-r'|} dr' + V_{xc}(r) + V_{ext}(r) \quad (1.82)$$

$$V_H(r) = \int \frac{n(r')}{|r-r'|} dr', \quad V_{xc}(r) = \frac{\delta E_{xc}}{\delta n(r)}, \quad n(r) = \sum_{i=1}^N |\phi_i(r)|^2 \quad (1.83)$$

In these equations the exact kinetic energy of the Kohn-Sham reference system is used as that of the real, interacting one. The true kinetic energy of the interacting system is not equal to the kinetic energy in the non-interacting system. Also the residual part has been added to the exchange-correlation energy E_{xc} which contains a number of unknowns. The V_{xc} as the exchange-correlation potential can be defined as the derivative of E_{xc} with respect to $n(r)$.

As a result, the Kohn-Sham approach is an exact theory in principle. The exchange-correlation energy E_{xc} has a good approximation, and the calculation is easier than the Hartree-Fock approach.

3.2 Quantumwise ATK-VNL Nanolab and its related functional theory

Atomistix ToolKit (ATK) and Virtual Nanolab (VNL) are included in a commercial software package by Quantumwise Snopsis Inc. that offers unique capabilities for simulating electrical transport properties of nanodevices on the atomic scale. The program scripted in Python and based on an open architecture that integrates a with a graphical user interface. Quantum ATK-VNL uses both accurate first-principles density functional theory and fast semi-empirical methods and classical potentials. Since 2006, the software used by many research laboratories, governments and companies with more than a thousand scientific publication. That numbers reveals that Quantumwise ATK-VNL is a useful tool for investigation of electronic and optical properties of nano-scale structures.

In this study, we mainly used the classical DFT to calculate the properties of bilayer graphene nanoclusters. To understand the algorithms in the Quantumwise ATK-VNL, many-body problem should be given by the means of different approximations and methods. These can be listed as Schrödinger Equation,

Variational Principle, Born-Oppenheimer Approximation, Mean Field Approach, Hatree-Fock Approximation, and Thomas-Fermi Approach

In the time dependent Schrödinger Equation,

$$-\frac{\hbar^2}{2m}\nabla^2\Psi(\vec{r},t)+V(\vec{r},t)\Psi(\vec{r},t)=i\hbar\frac{\partial\Psi(\vec{r},t)}{\partial t} \quad (1.84)$$

If potential assumed to be time independent, then the equation becomes as,

$$-\frac{\hbar^2}{2m}\nabla^2\Psi(\vec{r},t)+V(\vec{r},*)\Psi(\vec{r},t)=i\hbar\frac{\partial\Psi(\vec{r},t)}{\partial t} \quad (1.85)$$

When this equation is solved by separation of variables method, $\Psi(\vec{r},t)=\varphi(\vec{r})f(t)$ is inserted to the equation 3.13, and separate sides of equation with different variables become equals to constant E . This yields:

$$i\hbar\frac{d}{dt}f(t)=Ef(t)\Rightarrow f(t)=\exp\left(-i\frac{E}{\hbar}t\right) \quad (1.86)$$

$$\left[-\frac{\hbar^2}{2m}\nabla^2+V(\vec{r})\right]\varphi(\vec{r})=E\varphi(\vec{r}) \quad (1.87)$$

Using equations 3.14 and 3.15, we get the time independent Schrödinger Equation which describes the stationary states. The final form of this equation is shown in

Equation 3.16 where Hamiltonian $H=-\frac{\hbar^2}{2m}\nabla^2+V(\vec{x})$.

$$H\varphi(x)=E\varphi(\vec{r}) \quad (1.88)$$

If the state represented by following wavefunction form then, it is called stationary.

$$\Psi(x,t)=\varphi(x)f(t)=\varphi(x)\exp\left(-i\frac{E}{\hbar}t\right) \quad (1.89)$$

The probability of finding an electron in x and t can be described as $\|\Psi(x,t)\|^2$ for a stationary state which is time independent.

$$\|\Psi(x,t)\|^2 = \left\| \varphi(x) \exp\left(-i\frac{E}{\hbar}t\right) \right\|^2 = \|\varphi(x)\|^2 \quad (1.90)$$

The first step of solving the Schrödinger Equation is to set up the specific Hamiltonian operator for an atom or a molecule system. Then, the eigenfunctions ψ_i and corresponding eigenvalues E_i of Hamiltonian operator should be found. Once the eigenfunction is defined, all the properties can be determined by applying the proper operators to the wavefunction. This simple approach is not suitable for the exact solution of Schrödinger Equation for atomic and molecular systems. In this case, the variational principal method offers a solution by systematical approach to the ground state wavefunction ψ_0 . In the principal state for a trial wavefunction ϕ , the expectation value of \hat{H} should be even or higher than the true energy of ψ_0 :

$$E[\phi] = \frac{\langle \phi | \hat{H} | \phi \rangle}{\langle \phi | \phi \rangle} \quad (1.91)$$

$$E[\phi] \geq E_0 \quad (1.92)$$

For the many-body system, Hamiltonian can be written as a collection of atoms:

$$H = T_e + T_N + V_{e-e} + V_{N-N} + V_{e-N} \quad (1.93)$$

$$\begin{aligned} T_e &= -\frac{1}{2} \sum_i \nabla_i^2 \\ V_{e-N} &= \sum_i \left[\sum_l V(\bar{R}_l - \vec{r}_i) \right] \\ V_{e-e} &= \sum_i \sum_{j \neq i} \frac{1}{|\vec{r}_i - \vec{r}_j|} \end{aligned} \quad (1.94)$$

$$H\Psi(r_1, \dots, r_n, R_1, \dots, R_N) = E_{tot} \Psi(r_1, \dots, r_n, R_1, \dots, R_N) \quad (1.95)$$

This is called as the Born-Oppenheimer approximation where the electrons are treated as quantum particles in the field. It has the advantage of mass difference

between electron and nuclei. Nuclei has a greater mass than electron. Thus, the Born-Oppenheimer approximation allows electrons to move in a field of fixed nuclei. Since the nuclei has no motion, the kinetic energy is zero, and the repulsion between nuclei-nuclei is almost a constant. In this case, Hamiltonian can be reduced and called as electronic Hamiltonian:

$$H = T_e + V_{e-e} + V_{e-N} \quad (1.96)$$

Thus, according to the Born-Oppenheimer approximation the Schrödinger Equation can be simplified as:

$$H_{elec} \Psi_{elec} = E_{elec} \Psi_{elec} \quad (1.93)$$

The many-body problem is very complicated to get a single wave function. Thus, the mean field approximation is used for complicated calculations. According to the Hartree, in the independent particle model each electron moves in an effective potential which represents the average effect of the repulsive interactions and the attraction of the nuclei. So the mean field approximation described wavefunction for many-body system as follows:

$$\Psi(\vec{r}_1, \dots, \vec{r}_n) = \varphi_1(\vec{r}_1) \varphi_2(\vec{r}_2) \dots \varphi_n(\vec{r}_n) \quad (1.94)$$

$$\left[-\frac{1}{2} \nabla^2 + \sum_I V(\vec{R}_I - \vec{r}_i) + \sum_{j \neq i} \int |\varphi_j(\vec{r}_j)|^2 \frac{1}{|\vec{r}_j - \vec{r}_i|} d\vec{r}_j \right] \varphi_i(\vec{r}_i) = \epsilon \varphi_i(\vec{r}_i) \quad (1.95)$$

Here the effect of interactions of electrons with each other considered as a whole to make the calculation more simplified.

In the Hartree approximation, electrons are treated as distinguishable particles, but they are indistinguishable fermions. It is known that a set of identical fermions has an antisymmetric wavefunction according to the spin statistics. Therefore, when two electrons are exchanged, the sign of wave function must be changed from positive to negative in Hartree-Fock Approximation:

$$\Psi(\vec{r}_1, \vec{r}_2, \dots, \vec{r}_j, \dots, \vec{r}_k, \dots, \vec{r}_n) = -\Psi(\vec{r}_1, \vec{r}_2, \dots, \vec{r}_j, \dots, \vec{r}_k, \dots, \vec{r}_n) \quad (1.96)$$

Unlike the Hartree approximation, equation 3.28 contains an antisymmetric wavefunction, constructed via Slater determinant of individual orbitals:

$$\Psi(\vec{r}_1, \vec{r}_2, \dots, \vec{r}_n) = \frac{1}{\sqrt{n!}} \begin{vmatrix} \varphi_\alpha(\vec{r}_1) & \varphi_\beta(\vec{r}_1) & \cdots & \varphi_\nu(\vec{r}_1) \\ \varphi_\alpha(\vec{r}_2) & \varphi_\beta(\vec{r}_2) & \cdots & \varphi_\nu(\vec{r}_2) \\ \vdots & \vdots & \ddots & \vdots \\ \varphi_\alpha(\vec{r}_n) & \varphi_\beta(\vec{r}_n) & \cdots & \varphi_\nu(\vec{r}_n) \end{vmatrix} \quad (1.97)$$

To derive the Hartree equation, the self consistent field equation should be determined as:

$$\left[-\frac{1}{2} \nabla^2 + \sum_I V(\vec{R}_I - \vec{r}_i) \right] \varphi_\lambda(\vec{r}_i) + \left[\sum_\mu \int \varphi_\mu^*(\vec{r}_j) \frac{1}{|\vec{r}_j - \vec{r}_i|} \varphi_\mu(\vec{r}_j) d\vec{r}_j \right] \varphi_\lambda(\vec{r}_i) - \left[\sum_\mu \int \varphi_\mu^*(\vec{r}_j) \frac{1}{|\vec{r}_j - \vec{r}_i|} \varphi_\lambda(\vec{r}_i) d\vec{r}_j \right] \varphi_\mu(\vec{r}_i) = \varepsilon \varphi_\lambda(\vec{r}_i) \quad (1.98)$$

The Hartree equation depends on one-electron orbital which basically neglects other electrons in the system. Simultaneous integro-differential equations defines n number of orbitals. The solution of Hartree equation is repetitive, and it requires self consistency. Due to the Hartree-Fock approximation, the wave function is the main parameter that all information for the system can be retrieved from it. However, for each n electrons, there are a number of variables which leads to a serious problem because the actual systems contain too many atoms and a great number of electrons. This results with unmanageable wavefunction calculations. Thus, the Hartree-Fock approximation is convenient to use for atoms, only.

In 1927 Thomas and Fermi used the electron density instead of the wavefunction to get information about atoms and molecular systems. They used a local density approximation to obtain the kinetic energy term:

$$T(\vec{r}) = A\rho^{\frac{5}{3}}(\vec{r}) \quad (1.99)$$

With the combination of the classical expression for the potential of nuclei-electron, and that of electron-electron, the Thomas-Fermi expression for the energy of an atom can be described as

$$E_{Th-Fe}[\rho] = A \int \rho^{\frac{5}{3}}(\vec{r}) d\vec{r} + \int \rho(\vec{r}) V_{ex}(\vec{r}) d\vec{r} + \frac{1}{2} \iint \frac{\rho(\vec{r}_1)\rho(\vec{r}_2)}{|\vec{r}_1 - \vec{r}_2|} d\vec{r}_1 d\vec{r}_2 \quad (1.100)$$

This approach is not good for non-homogeneous systems because of poor approximation of true kinetic energy. However the Thomas-Fermi approach is very important since it is the ancestor of actual density functional theory.

In the self-consistent calculation of the Kohn–Sham equations the key parameter is the density matrix, which defines the electron density. The electron density then sets up an effective potential, which is given by the Hartree, exchange-correlation, and external potential. When the effective potential is known the Kohn–Sham Hamiltonian can be obtained. Quantumwise ATK-DFT can model the electronic and optical properties of many body systems by using the liner combination of atomic orbital (LCAO) calculator which provides a description of electronic structure using DFT and norm-conserving pseudopotentials. For a self consisting loop, Quantumwise ATK-DFT is used for calculating the effective potential, solving the Kohn-sham equations and evaluating the electron density and total every. The workflow chart of this study is given in the Figure 3.1.

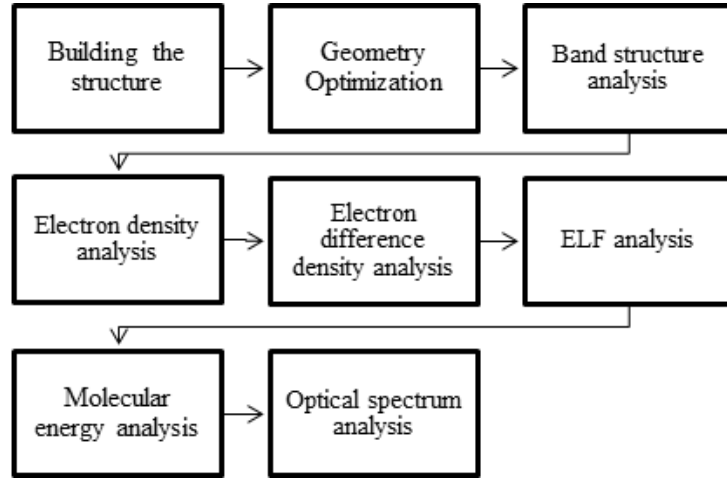


Figure 3.1. Workflow chart of the study.

Free total energies were calculated by equation 3.33 in ATK where n is the electron density, $T[n]$ is the kinetic energy of the Kohn-Sham orbitals, $E^{xc}[n]$ is the exchange-correlation energy, $E^H[n]$ includes all the electrostatic terms, $E^{ext}[n]$ is the interaction energy with an external field and $-\sigma S$ is the entropy contribution due to smearing of the occupation function.

$$F[n] = T[n] + E^{xc}[n] + E^H[n] + E^{ext}[n] - \sigma S \quad (1.101)$$

The effective potential, $V^{eff}[n]$, has three contributions, the first two terms are due to electron–electron interactions, which depend on the electron density.

$$V^{eff}[n] = V^H[n] + V^{xc}[n] + V^{ext} \quad (1.102)$$

The first term, $V^H[n]$, is the Hartree potential due to the mean-field electrostatic interaction between the electrons. The second term, $V^{xc}[n]$, is the exchange-correlation potential, which arises from the quantum mechanical nature of the electrons.

The potential V^{ext} represents any other electrostatic fields in the system. It can be separated into two contributions; the electrostatic potential of ions (given by norm-conserving pseudopotentials) and external electrostatic fields (given by one or more external sources).

The electron density of the many-electron system is given by the occupied eigenstates of the Kohn–Sham Hamiltonian. The key parameter in the self-consistent calculation of Kohn-Sham equations is the density matrix, which defines the electron density. For open systems, the density matrix is calculated using non-equilibrium Green’s functions while for closed or periodic systems it is calculated by diagonalization of the Kohn-Sham Hamiltonian. The electron density then sets up an effective potential that is given by the Hartree, exchange-correlation, and external potential allows us to obtain the Kohn-Sham Hamiltonian.

$$n(r) = \sum_{\alpha} f_{\alpha} |\varphi_{\alpha}(r)|^2 \quad (1.103)$$

where f_{α} is the occupation level denoted by α . For finite temperature calculation, the occupations are determined by the Fermi-Dirac distribution.

The electron density can be expressed in terms of the density matrix:

$$n(r) = \sum_{ij} D_{ij} \phi_i(r) \phi_j(r) \quad (1.104)$$

Where the density matrix is given by the basis set expansion coefficients $c_{\alpha i}$:

$$D_{ij} = \sum_{\alpha} f_{\alpha} c_{\alpha i}^* c_{\alpha j} \quad (1.105)$$

The electron difference density is simply defined as the electron valence density minus the neutral atom electron density. It is often convenient to compare the electron density of the many-body system to a superposition of individual atom-based electron densities. In order to understand the total electron charge density distributions it is efficient to examine difference in charge densities.

Electron difference density can be expressed as

$$\Delta(n) = n(r) - \sum_{\mu} n^{atom}(r - R_{\mu}) \quad (1.106)$$

where $\Delta(n)$ is the electron difference density and R_{μ} is the position of atom μ in the many-body system.

4. RESULTS AND DISCUSSIONS

4.1 Geometry Optimizations

Geometry optimization is the first step for further DFT calculations. The optimization of geometries involves minimizing the atomic forces for molecules and clusters, while for crystals, the shape and the size of the unit cell as well as any external pressure must also be taken into account. In this study, the geometry optimization calculations were performed for twelve different graphene structures; MLG, BLG(8+8), WBLG, ReBLG, OsBLG, BLG(32+32) WNBLG, ReNBLG, OsNBLG, WOBLG, ReBLG, OsOBLG. First-principles DFT calculations were performed by using generalized gradient approximation (GGA) for the exchange–correlation interactions. The BPW91 basis set was used for DFT calculations with linear combination of atomic orbitals (LCAO) calculator.

Bilayer graphene structure (AB stacking form) was built from graphite structure. The initial bilayer graphene structure contains 4 atoms; 2 atoms in each layer, (2+2). Repeating operations were applied on C-axis until the bilayer graphene pattern is suitable for transition metal intercalation. BLG (2+2), BLG (8+8) and BLG (32+32) structures were builded and calculated to optimize geometries. BLG(8+8) structure was chosen for transition metal intercalation where metal atoms were placed exactly in the center of graphene layers followed by optimization of geometries for each structure. Calculation parameters were set as 300 K electron temperature, k points (3,3,1) and 75 Hartree mesh cutoff. Geometrically optimized transition metal intercalated bilayer graphene structures (WBLG, ReBLG, OsBLG) were doped with nitrogen atoms by graphitic N-doped configuration. In graphitic N-doping, nitrogen atoms were replaced with carbon atoms to change local density state around the Fermi level. Geometry optimizations were carried out for designed N-doped structures (WNBLG, ReNBLG, OsNBLG). Finally, BLG (32+32) structure was chosen for transition metal oxide intercalation. Rhenium (VI) oxide, Tungsten (VI) oxide and Osmium (VI) oxide were placed exactly in the center of bilayer

graphene structure followed by geometry optimizations. The geometrically optimized MLG, BLG (2+2), BLG (8+8), BLG (32+32), WBLG, ReBLG, OsBLG, WNBLG, ReNBLG, OsNBLG, WOBLG, ReBLG, OsOBLG structures contain 2, 4, 16, 64, 17, 17, 17, 17, 17, 17, 17, 17, 17, 67, 75, 69 atoms, respectively (Figure 4.1).

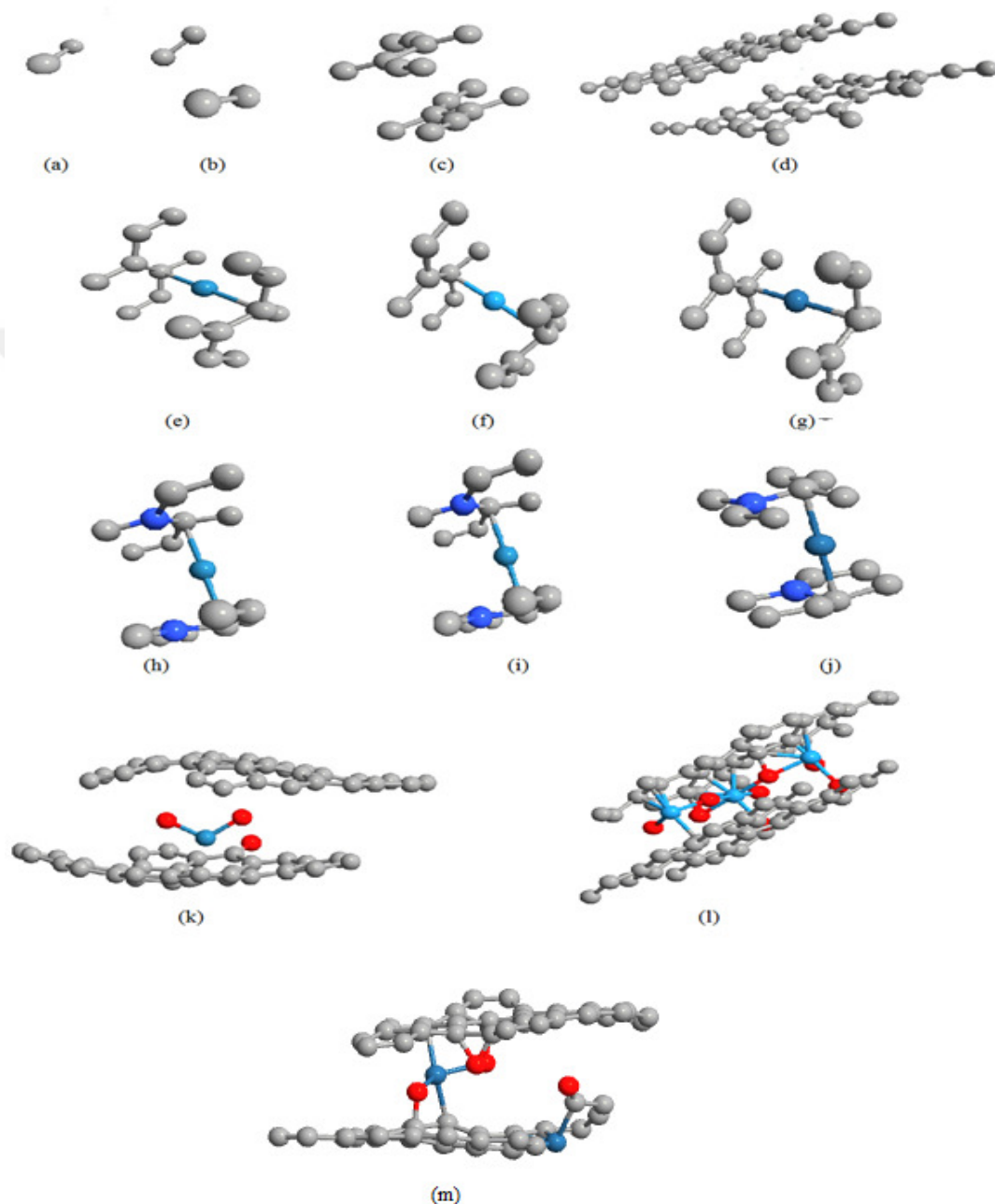


Figure 4.1. Optimized geometries of graphene structures (a) MGL, (b) BLG (2+2), (c) BLG (4+4), (d) BLG (32+32), (e) ReBLG, (f) WBLG, (g) OsBLG, (h) ReNBLG, (i) WNBLG, (j) OsNBLG, (k) ReOBLG, (l) WOBLG, (m) OSOBLG grey atoms represents carbons and blue one represents M: Re, W, Os, purple atoms represents nitrogen and red atoms represents oxygen atoms.

Bond lengths of metal bonded bilayer graphene structures were calculated before and after geometrical optimizations. Bond lengths between certain atoms in graphene structures were calculated and given in Table 4.1. It was shown that metal intercalation resulted with a distance widening between graphene layers. Although inserting a metal between graphene layer does not have an important effect on the C-C bond, nitrogen doping was shown to increase the layer distance. However, the insertion of metal oxides between graphene layers did not have common effect on bond lengths and layer distance, because rhenium (IV) oxides widening the layer distance, tungsten (VI) oxide narrows the layer distance.

Table 4.1 Bond lengths and distances between layers.

	C-C	M-C	C-N	C-O	Layer Distance
MLG	1.43				
BLG (2+2)	1.42				4.64
BLG (8+8)	1.44				4.36
ReBLG	1.43	2.37			4.25
WBLG	1.47	2.13			4.26
OsBLG	1.41	2.11			4.28
ReNBLG	1.43	2.15	1.44		4.37
WNBLG	1.44	2.17	1.44		4.32
OsNBLG	1.44	2.18	1.44		4.21
ReOBLG	1.42	2.36		1.24	5.73
WOBLG	1.42	1.87		1.39	3.65

Total energies of these graphene based structures were calculated, where k-point grid was 3x3x1 and the number of irreducible k-points was 5. Free total energies were calculated in ATK (Table 4.2).

Table 4.2. The total energies.

	Exchange-Correlation (eV)	Kinetic Energy (eV)	Electrostatic Energy (eV)	Entropy-Term (eV)	Total free energy (eV)
MLG	-900.9235	2064.5812	-3987.5916	-0.11946	-2824.0534
BLG	-769.26344	1709.9959	-3413.1910	-0.16284	-2472.6214
WBLG	-1105.5955	1950.7320	-3777.8264	-0.0393	-2932.8256
ReBLG	-1007.7792	2022.0774	-3925.3023	-0.0353	-2911.1295
OsBLG	-1041.57103	2103.07913	-4102.0871	-0.0156	-3040.6843
MNBLG	-1284.5901	1908.1415	-3951.5136	-0.0422	-3329.0044
WOBLG	-4701.8064	12573.7989	-30409.932	-0.9372	-22538.8766
ReOBLG	-3662.8427	8653.7755	-18445.402	-0.5159	-13454.9853
OsOBLG	-4066.2655	9841.7169	-22513.924	-0.4959	-16738.9685

The total free energies with external field, exchange-correlation, kinetic energy, electrostatic energy, entropy-term values are given in Table 4.2 for graphene

structures. Total energies of these structures showed that bilayer graphene has less free energy than mono layer graphene. In other words, the more layers added to the graphene structure, the more stable in hence it becomes. On the other hand, inserting metal between graphene layers caused an increase in all terms of energy; however inserting metal oxides to bilayer graphene lowered the free total energy, only.

4.2 Molecular Dynamic Analysis

Molecular dynamic (MD) analysis visualize the MD results for single atom configurations to large scale complex as radial/angular distribution function, local mass density profile, coordination number, neutron scattering factor and voidsize distrubituion.

The square of the angular distribution function shows the probability of finding the electron at dihedral angles. The square of radial distribution shows the probability of finding an electron at a given distance from the nucleus, whereas the square of radial distribution shows the probability of finding an electron at a given distance from the nucleus.

The Angular/radial distribution graphs of graphene structures were given in Figures 4.2 and 4.3. The angular and radial distributions of mono layer graphene shows only one peak at 120° however radial distribution of MLG shows three proportional peaks due to the even distributons of carbon atom in hexagonal honeycomb structure. On the other hand, the angular and radial distributions of bilayer graphene show numbers of uneven peaks because of Bernard stacking configuration. When metal atom inserted between layers of graphene, carbon-metal shows higher angular/radial distrubitions than carbon-carbon atoms, and the highest distrubition observed in MNBLG structures as expected. In addition, coordination number, mass density profile, and neutron scattering factor were also calculated and given in Figures 4.4, 4.5 and 4.6, respectively.

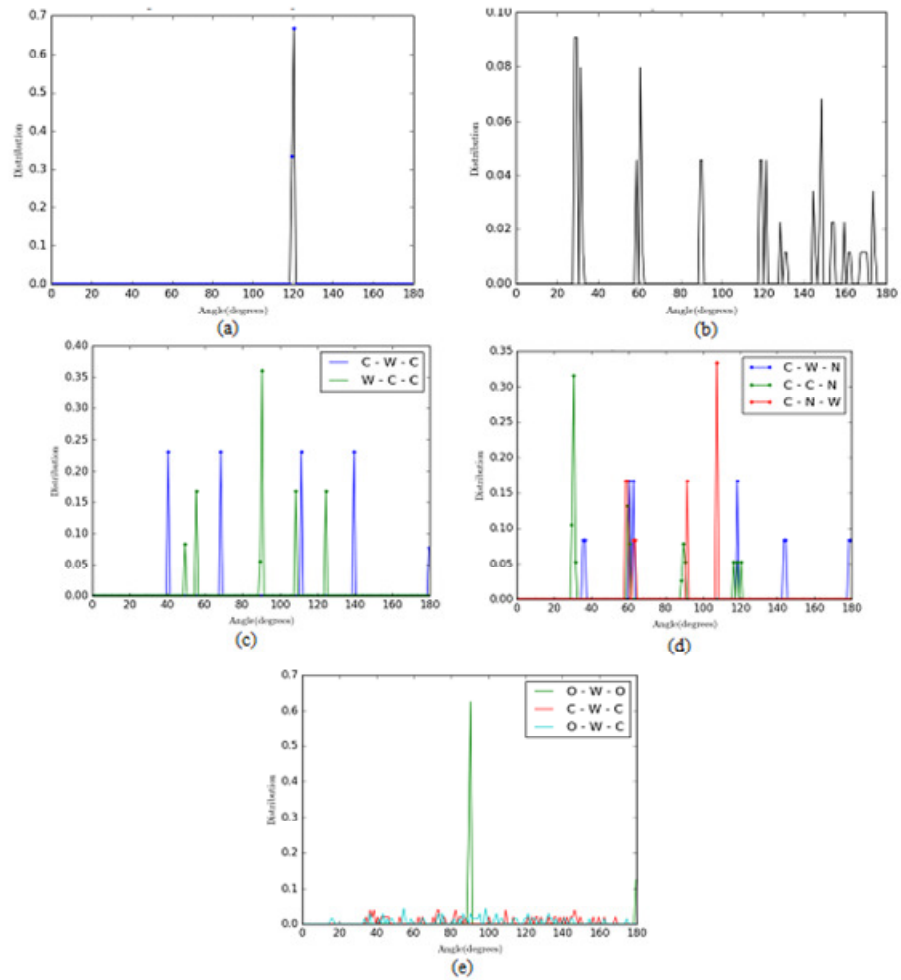


Figure 4.2. Angular distribution analysis. (a) MLG, (b) BLG, (c) WBLG, (d) WNBLG, (e) WOBLG.

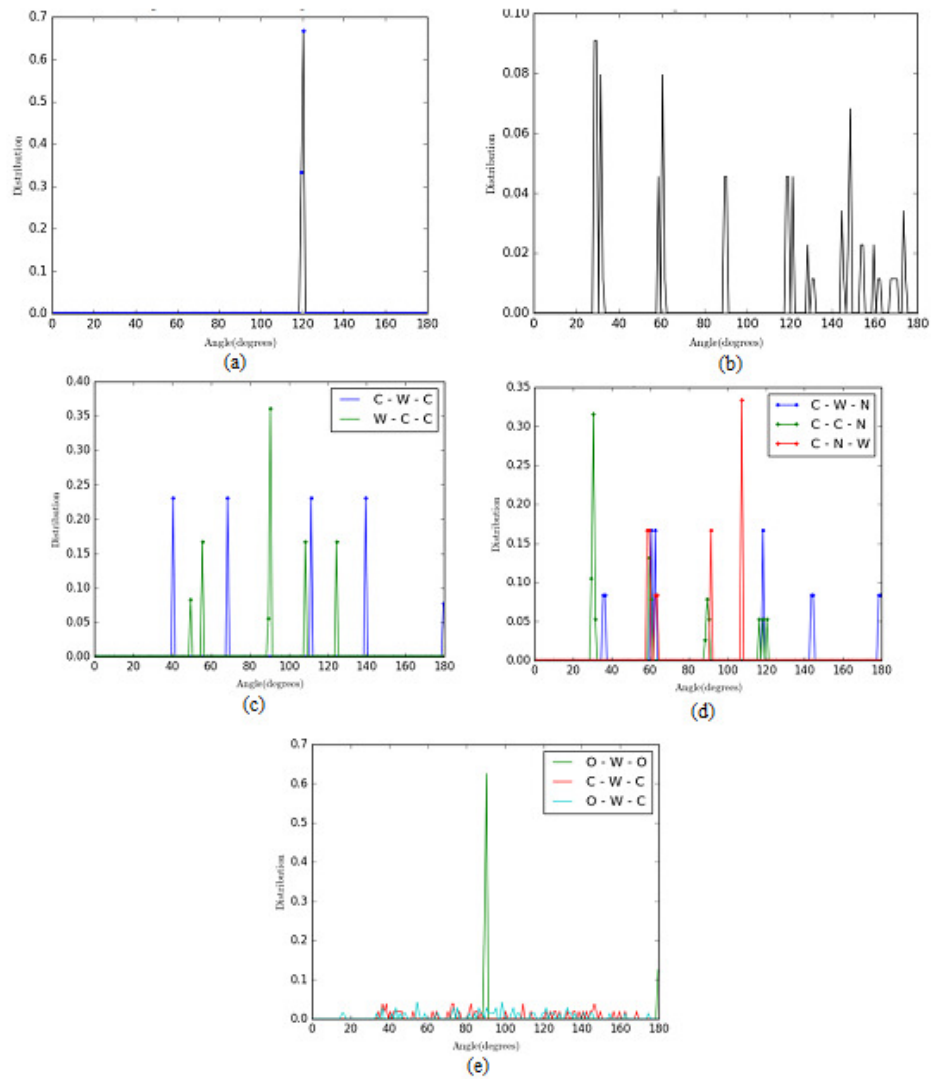


Figure 4.3. The radial distribution analysis. (a) MLG, (b) BLG, (c) WBLG, (d) WNBLG, (e) WOBLG.

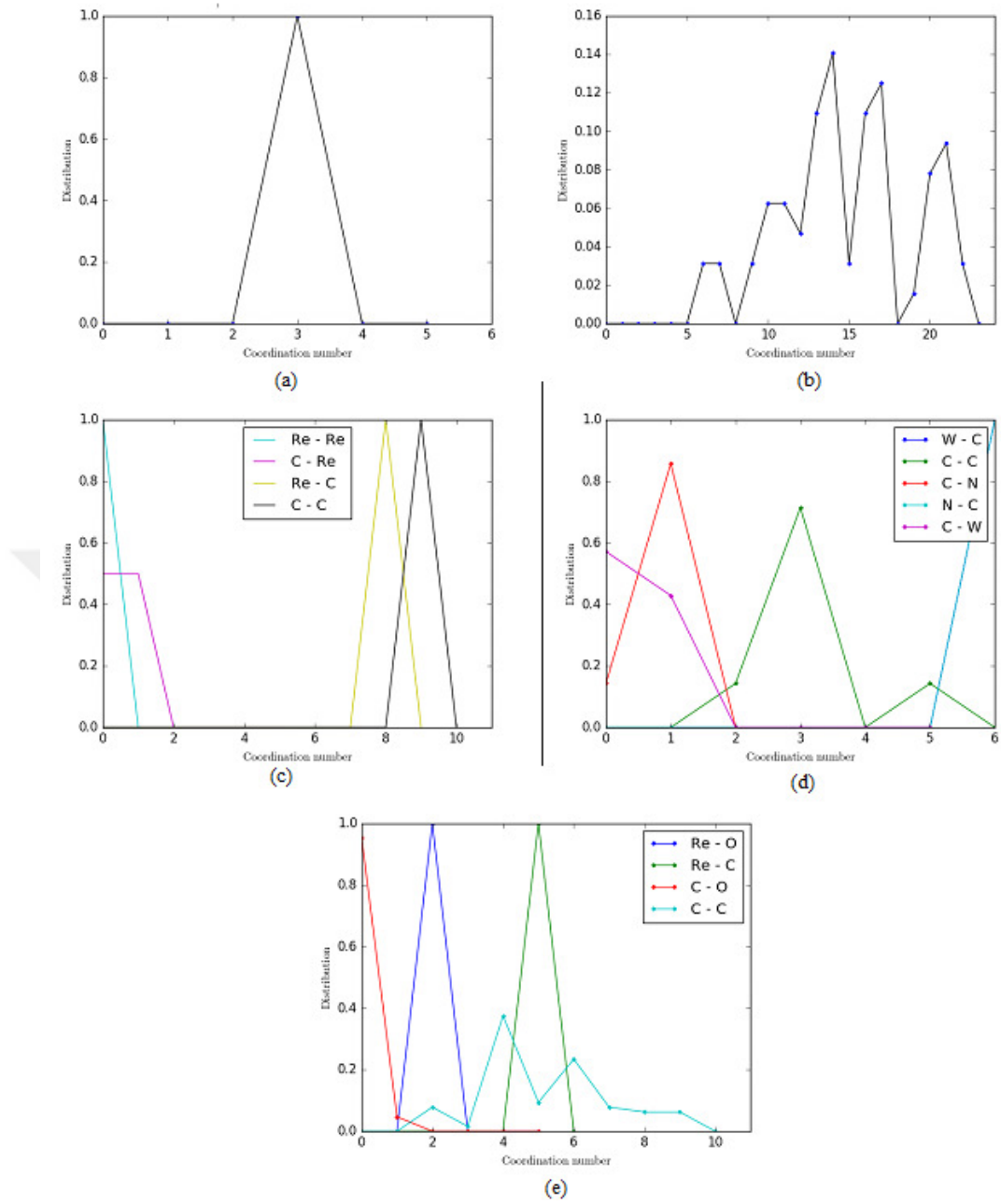


Figure 4.4. Coordination number distribution analysis. (a) MLG, (b) BLG, (c) ReBLG, (d) WNBLG, (e) ReOBLG.

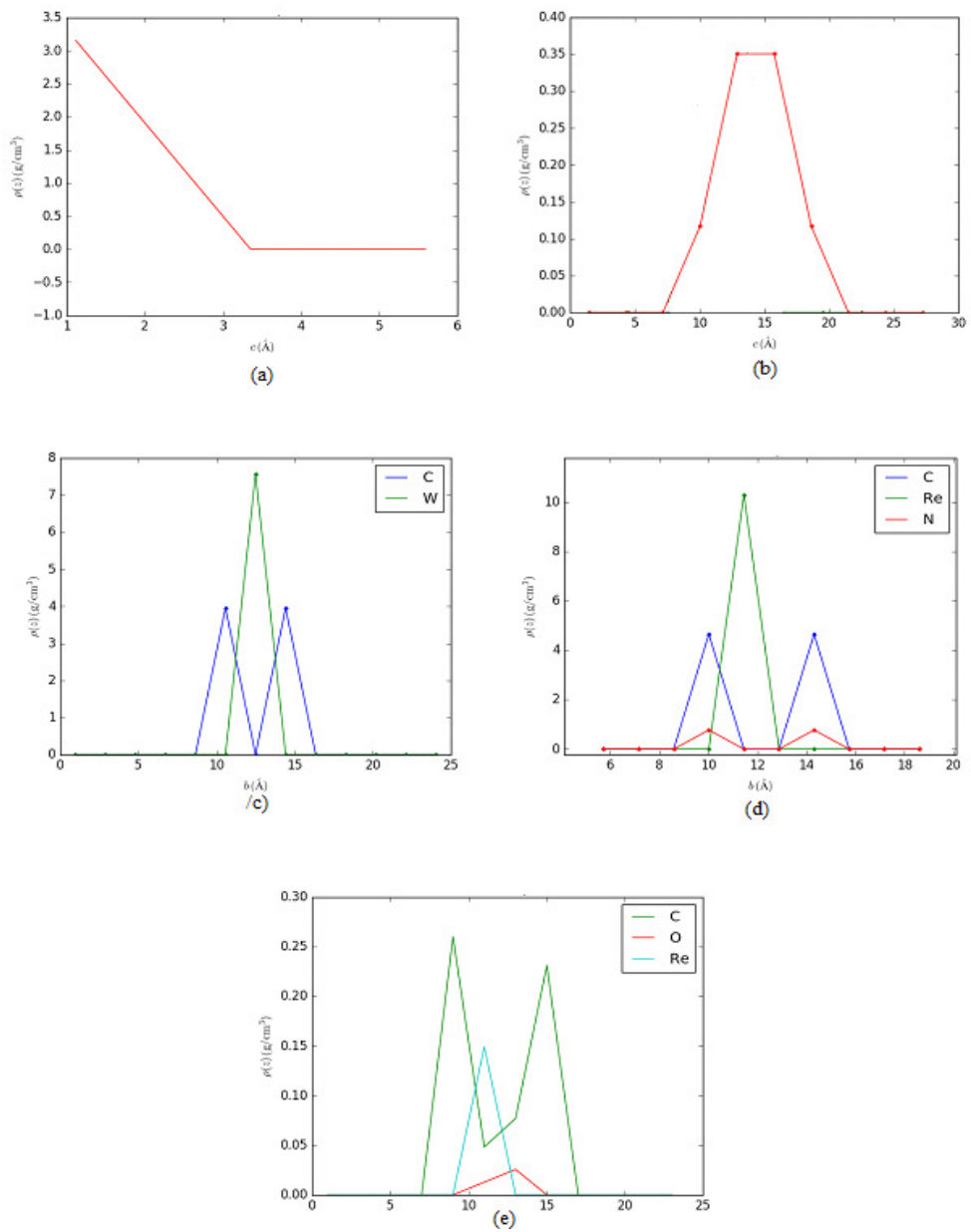


Figure 4.5. Mass density profiles analysis. (a) MLG, (b) BLG, (c) WBLG, (d) ReNBLG, (e) ReOBLG.

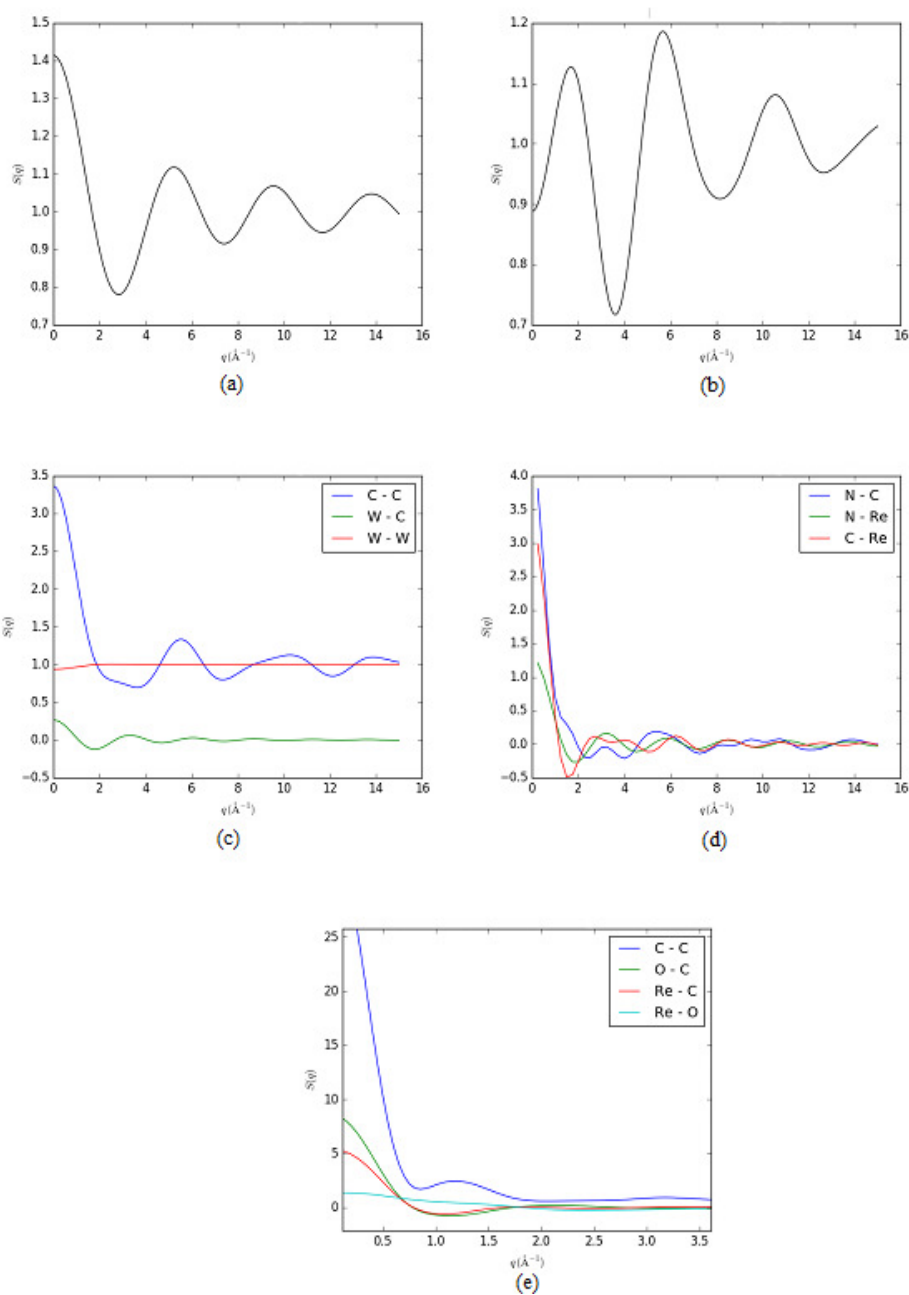


Figure 4.6. Neutron scattering factor analysis. (a) MLG, (b) BLG, (c) WBLG, (d) ReNBLG, (e) ReOBLG.

4.3 Band Structure Analysis

Band structure analysis is important for modification and tailoring the electronic properties for the compounds after structure relaxations. Band structure analysis was examined by using an *ab initio* pseudopotential approach using the exchange and correlation in the GGA Perdew Wang (BPW91) formalism. Band

structures of graphene, bilayer graphene and metal inserted bilayer graphene structure were given in Figure 4.7. Band structures of nitrogen doped metal bilayer graphene were given in Figure 4.8 and those of metal oxides inserted bilayer graphene structures were given in Figure 4.9.

Electronic band structure of graphene shows zero band gap at K point. For opening a band gap in bilayer graphene structure, an electric field could be applied by setting the voltage to 0 V for the first metallic region, and 10 V for the second. Bilayer graphene structures were enlarged by repeating operations in C-axis. Thus, BLG (8+8) was enlarged enough to cover entire hexagonal unit cell. The applied voltage results in 4 V/nm in the z direction, just above the field that has been found experimentally to open a band gap (Zhang et al., 2009). The theoretical lattice constant for bilayer graphene structure at 2.4612 Å band gap energy was found as 1.1682 eV at Fermi level. Intercalation of transition metals of tungsten, rhenium and osmium to a bilayer graphene resulted in narrowing band gap due to the decreasing of atomic radii of metals. Tungsten metal inserted bilayer graphene band gap was 0.04617 eV, structure with rhenium metal band gap was 0.086524 eV while osmium metal band gap was 0.11472 eV.

The band gap analyses showed nitrogen doping of metal inserted bilayer graphene structures results in a small broadening in band gap. For instance, WNBLG band gap was calculated as 0.076143 eV at Fermi level. This indicates that nitrogen doping and transition metal insertion lead to narrow the band gap and increasing the conductor character of structures.

The band structure analyses of metal oxides inserted bilayer graphene structures did not give efficient band structure data due to the high electron density in bulky systems. Therefore, ATK software cannot support the same route as metal inserted bilayer graphene structures.

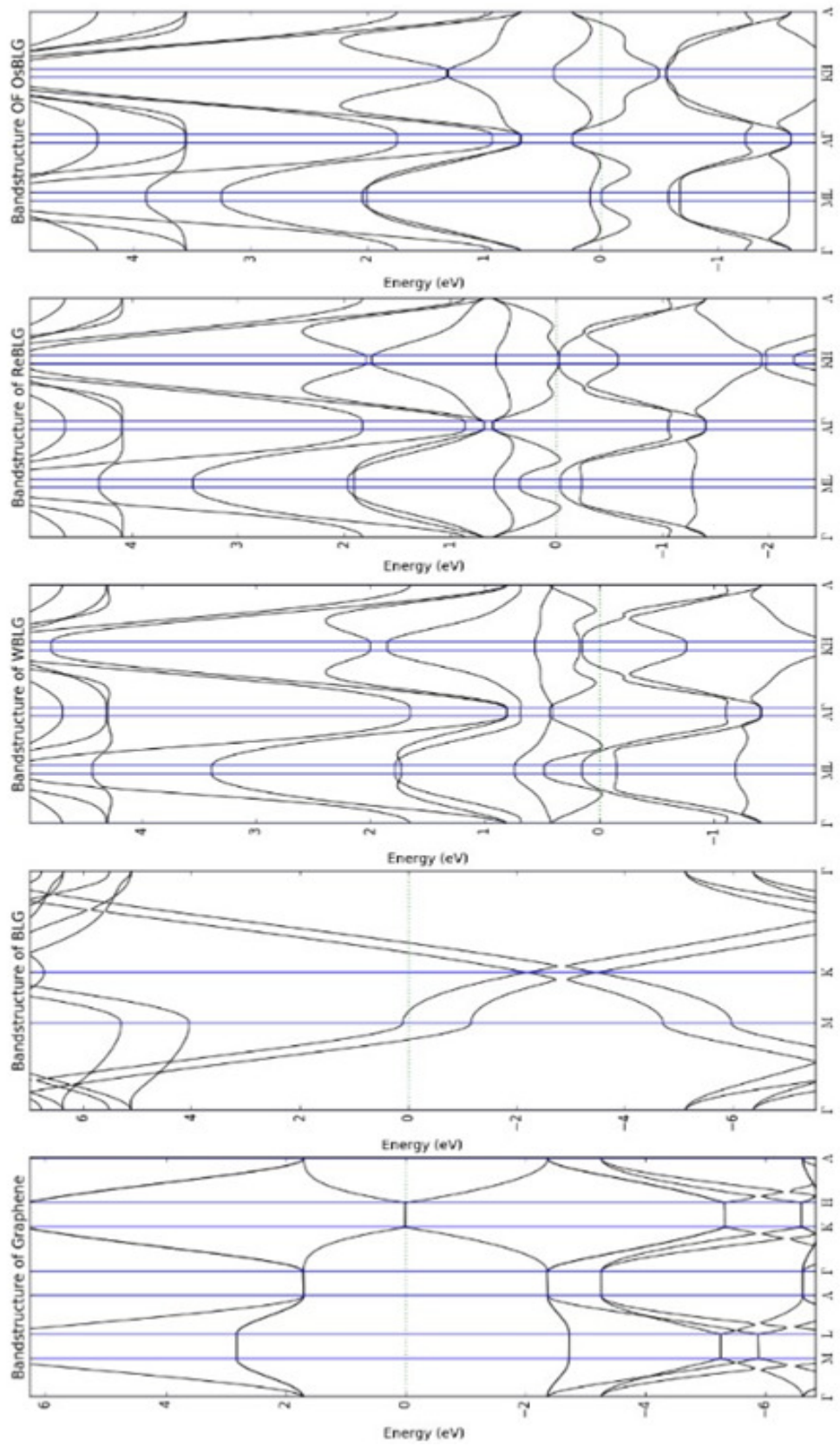


Figure 4.7. Band structures of graphene, BLG, WBLG, ReBLG and OsBLG.

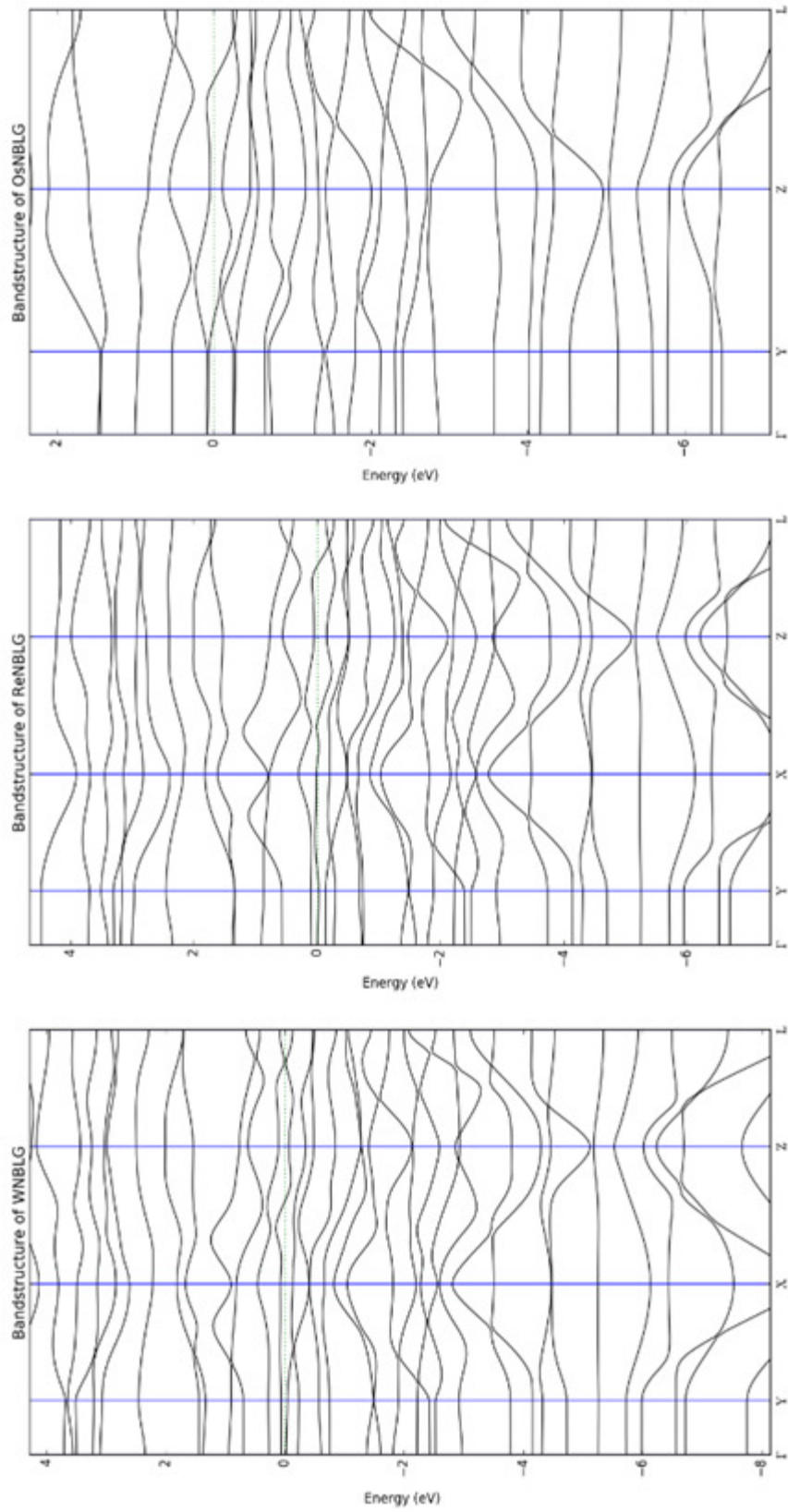


Figure 4.8. Band structures of nitrogen doped metal bilayer graphene. WNBLG, ReNBLG, OsNBLG.

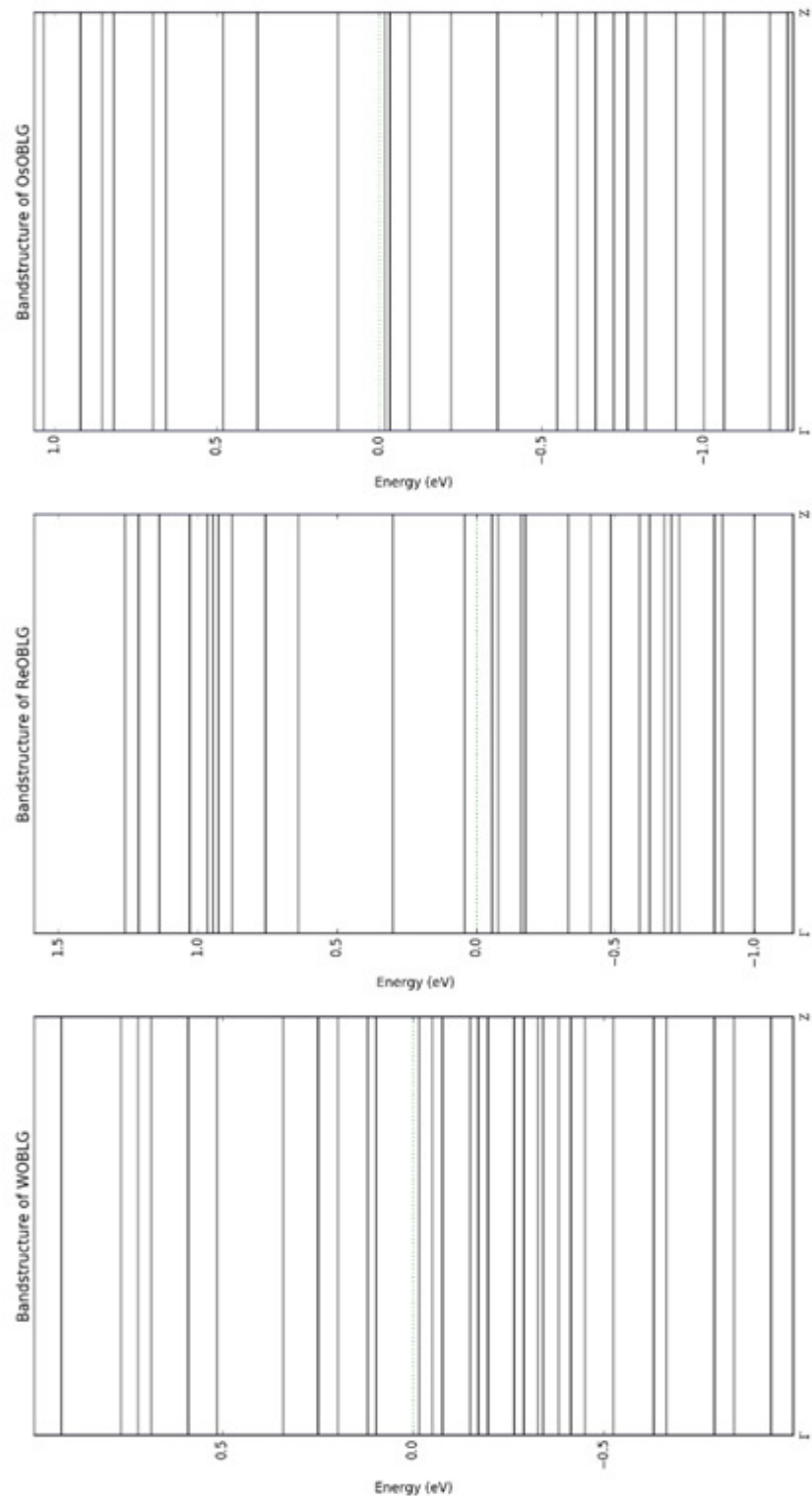


Figure 4.9. Band structures of metal oxides inserted bilayer graphene structures.

Brillouin zones of lattice structures are particular choices of the unit cells in reciprocal spaces. The planes are perpendicular to the connection line from the origin to each lattice point. *Brillouin zones* were represented in the Fig.4.10 for all the lattice structures.

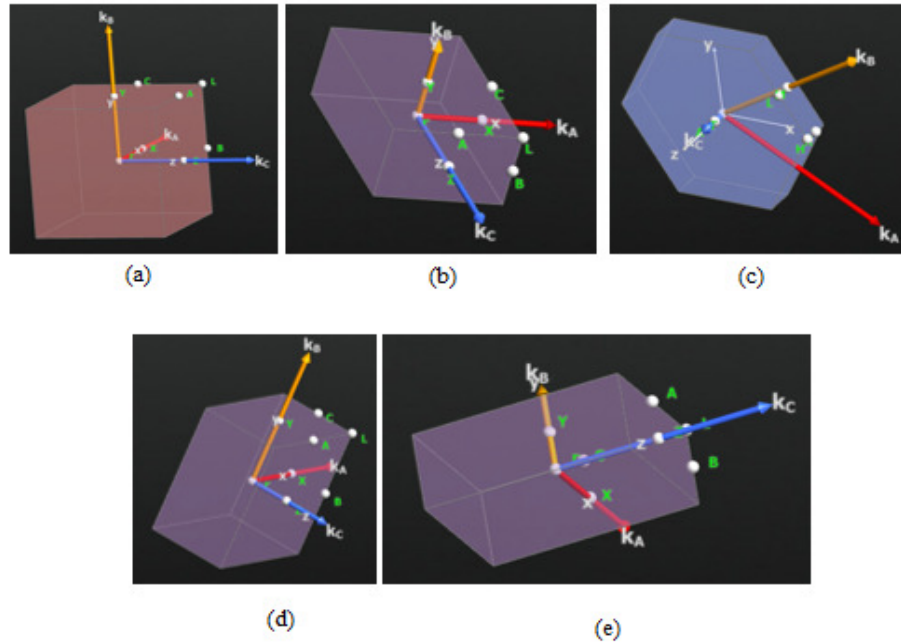


Figure 4.10. Brillouin zones. (a) MLG, (b) BLG, (c) WBLG, (d) WNBLG, (e) WOBLG.

Table 4.2 The effective mass analysis of all lattice structures.

	Band Index	Energy (eV)	m^* (m_e)
MLG	4	-13.403	0.233
	5	-13.403	0.088
BLG	4	-15.765	0.062
	5	-14.158	0.648
WGL	0	-19.663	1.440
	1	-19.514	1.448
ReGL	0	-20.324	1.442
	1	-20.138	1.448
WNBLG	0	-22.416	2.010
	1	-22.248	2.200
ReNBLG	4	-23.538	-0.426
	5	-20.619	11.369
OsNBLG	4	-23.274	-102.963
	5	-20.401	18.810
WOBLG	0	-76.316	3708918
	1	-75.677	-8854841.910
ReOBLG	0	-81.636	4970761.801
	1	-44.091	6442404.130
OsOBLG	0	87.120	2210512.452
	1	-86.147	-1308890.405

The effective mass of holes and electrons fitting a parabola to the minimum/maximum of the conduction/valence bands were computed for all lattice structures for various band index, and given in Table 4.2.

The chemical potentials were computed for each structure and modeled with GGA, BPW91 formalism by using numerical linear combination of atomic orbitals basis sets as given in Table 4.3.

Table 4.3. Chemical potential energies.

MLG	-4.264966 eV
BLG	-5.565939 eV
WBLG	-7.419938 eV
WNBLG	-6.655812 eV
WOBLG	-5.925405 eV

4.4 Electron Density

Electron densities of each structure were modeled with GGA BPW91 formalism by using numerical linear combination of atomic orbitals basis sets.

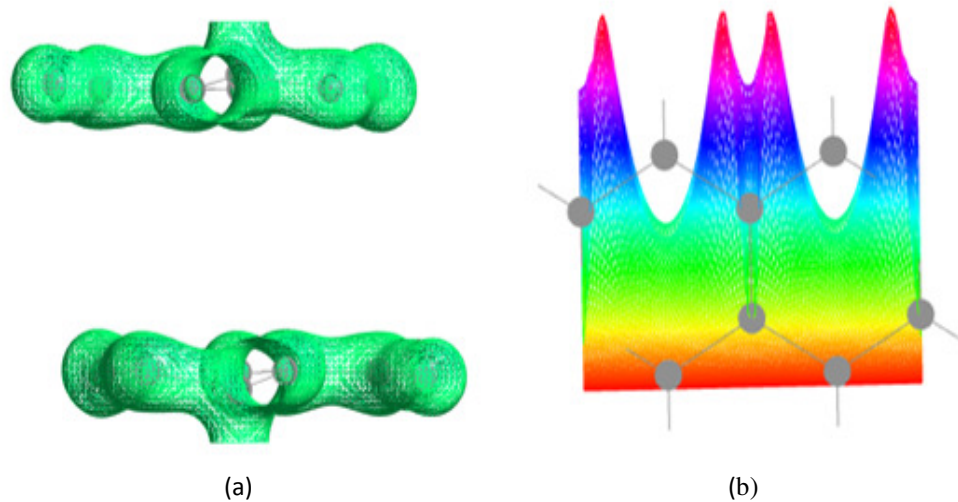


Figure 4.11. Electron density schemes of BLG. (a) isosurface, (b) cut-plane.

The electron density schemes of bilayer graphene structure in isosurface and 3D cut plane models for each structure were given in Figure 4.11. They show an equal distribution since there were only carbon atoms in Bernal stacking. Electron

density analysis of rhenium, tungsten and osmium metals intercalated to the center of bilayer graphene were carried out. The analyses showed that intercalation of rhenium metal to bilayer graphene leads to move the electron density through the central metal atom (Figure 4.12.a). Comparison of cut-plane illustrations of bilayer graphene (Figure 4.11.b) and transition metal intercalated bilayer graphene (Figure 4.12c) shows a significant change in charge density. Nitrogen doping and metal oxides intercalation also result in change of electron densities as shown in Figures 4.13 and 4.14, respectively. 1D projection plots were exported from the electron density analysis of ATK for sum of spin up and spin down projections of a, b and c axis with unit of $1/\text{Angs}^3$.

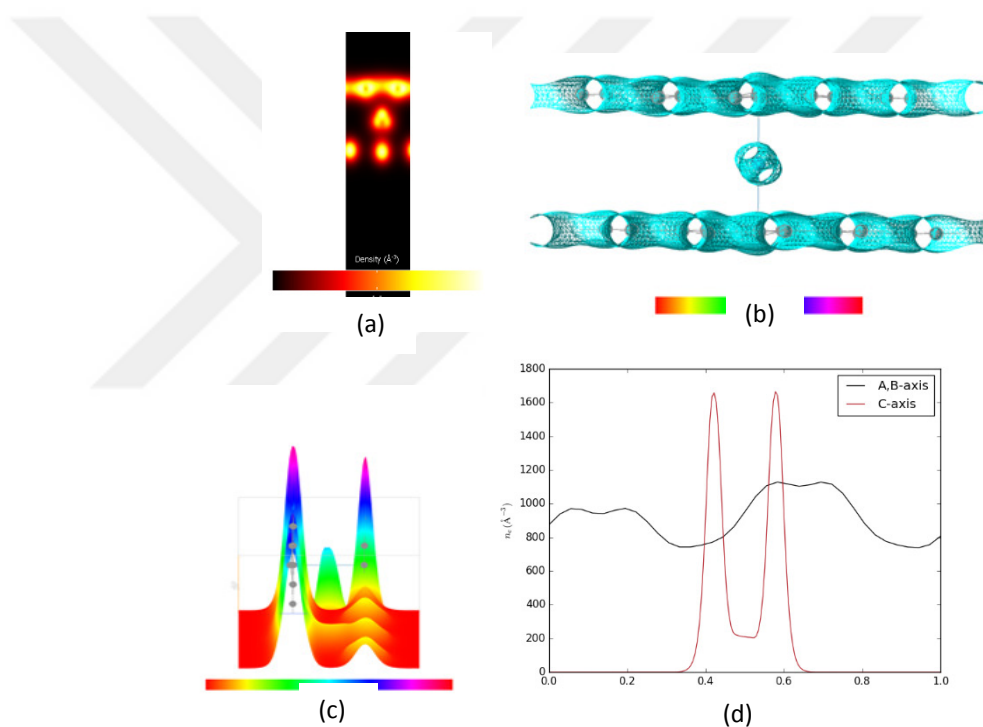


Figure 4.12. Electron density schemes of ReBLG. (a) isosurface-1, (b) isosurface-2 (c) 3D cut plane models and (d) 1D projection plot.

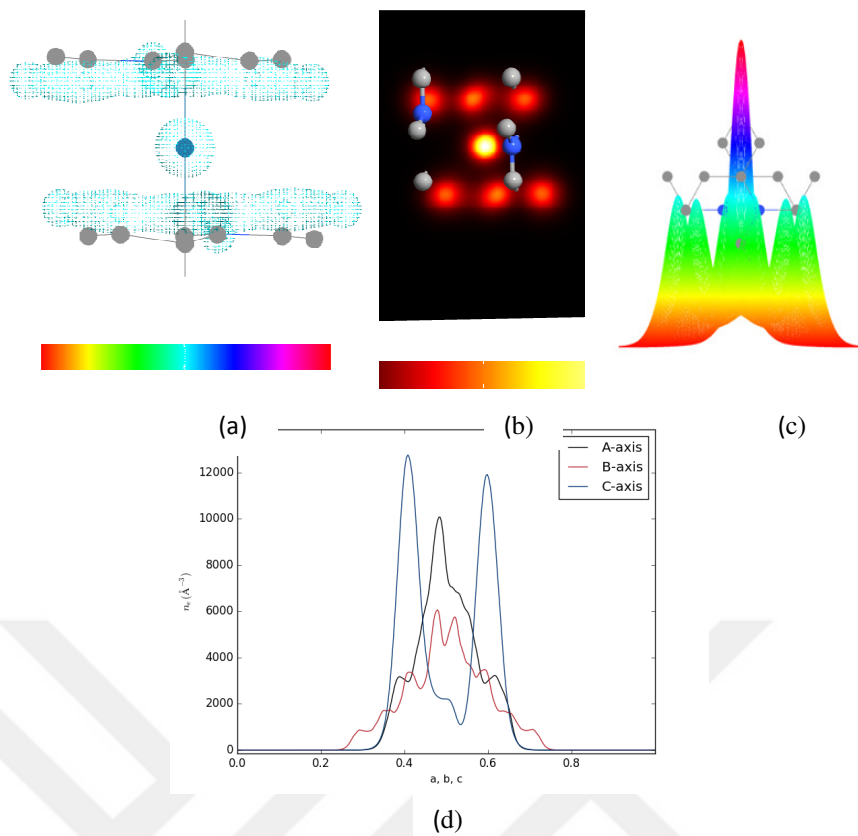


Figure 4.13. Electron density schemes of ReNBLG. (a) isosurface-1, (b) isosurface-2 (c) 3D cut plane models and (d) 1D projection plot

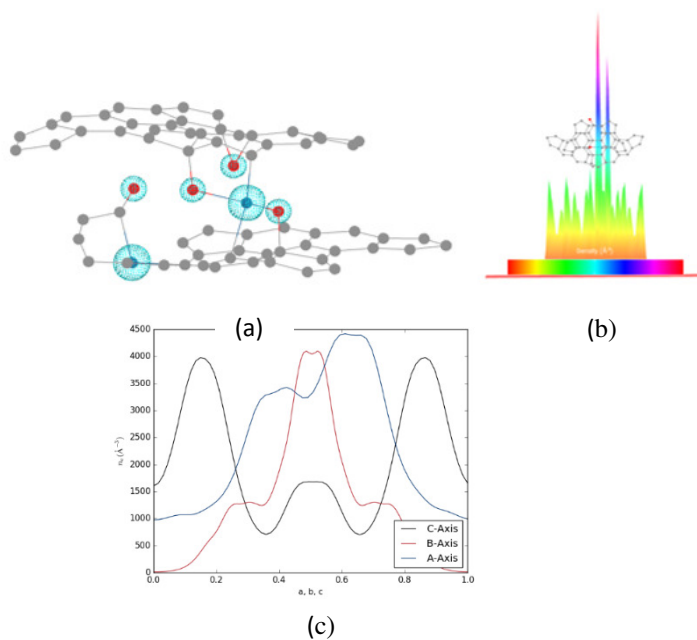


Figure 4.14. Electron density schemes of OsOBLG. (a) isosurface, (b) 3D cut plane models and (c) 1D projection plot

To understand the effect of changing atoms on the charge density, it is necessary to examine the partial charges in the structure. Richard Bader developed a method to divide molecules into atoms based on the electronic charge density. Bader analysis is a very useful method to examine the effects of dopants and metal intercalation on charge distribution. The overall Bader charge analysis is summarized in Figure 4.15 and Bader analysis of each structure are given in Appendix A.4.

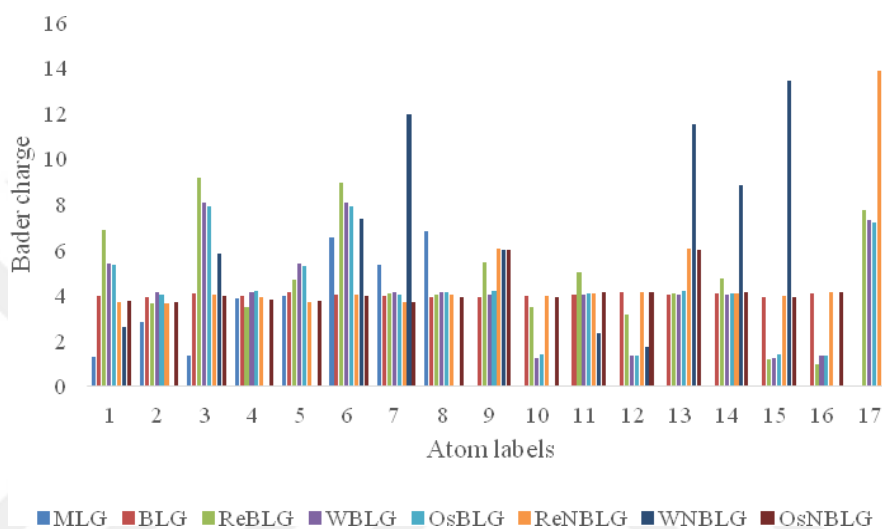


Figure 4.15. Summarization of Bader charges of the structures.

The Bader analysis revealed that charge distribution shows a significant change on carbon atoms which neighbouring metal and nitrogen atoms. Thus, total charge maxima is balanced by decreasing of charge density on the other carbon atoms in hexagonal carbon structure. Metal oxides inserted between the layers of bilayer graphene is shown in Figure 4.14. The topological scheme of charge density is legitimate when it is compared to the high total free energies and high electron density between the layers. This implies that transition metal oxide intercalation is not stable.

4.5 Electron Difference Density

Electron difference density models were computed by using LCAO basis sets of GGA exchange correlation B3PW91 formalism as shown in Figure 4.16.

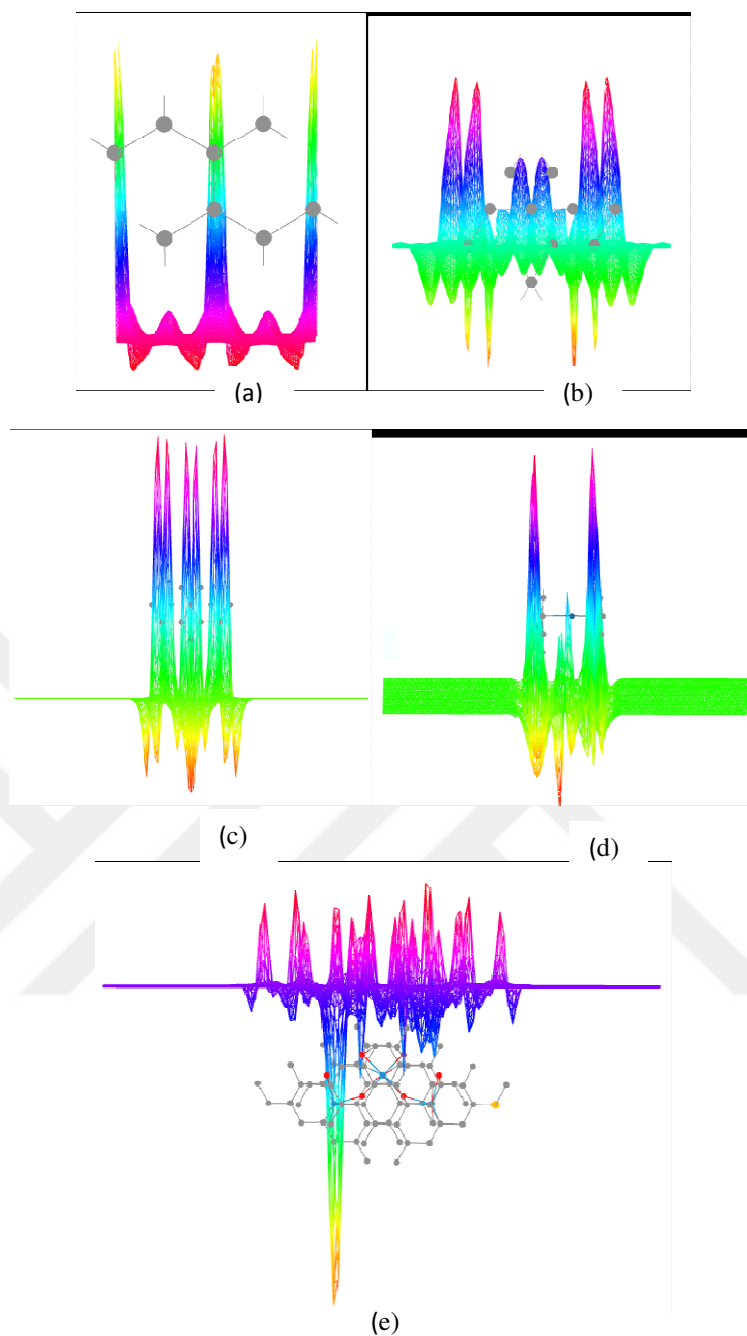


Figure 4.16. Electron difference density schemes. (a) MLG, (b) BLG, (c) MBLG, (d) MNBLG, (e) MOBLG.

Electron difference density analyses of graphene structures showed that oxygen in metal oxide structures consist of high charge difference with its electron-rich character. Nitrogen doped metal inserted bilayer graphene (MNBLG) showed unequal distribution of charge difference, whereas metal inserted bilayer graphene has equal distribution of electron difference density where metal and metal bonded carbon atoms have greater difference.

4.6 Electron Localizaiton Functions

The electron-localization function (ELF) was originally defined by Becke provides an alternative real-space function for the analysis of non-trivial bonding situations. ELF is a 3D function with the values between 0 to 1. ELF values closer to 1, basically represent the positions where the electrons are localized.

Electron localization function analysis of bilayer graphene structures were computed by first-principles DFT calculations using generalized gradient approximation (GGA) for the exchange–correlation interactions and BPW91 basis set for DFT with linear combination of atomic orbitals (LCAO) calculator as shown in Figure 4.17.

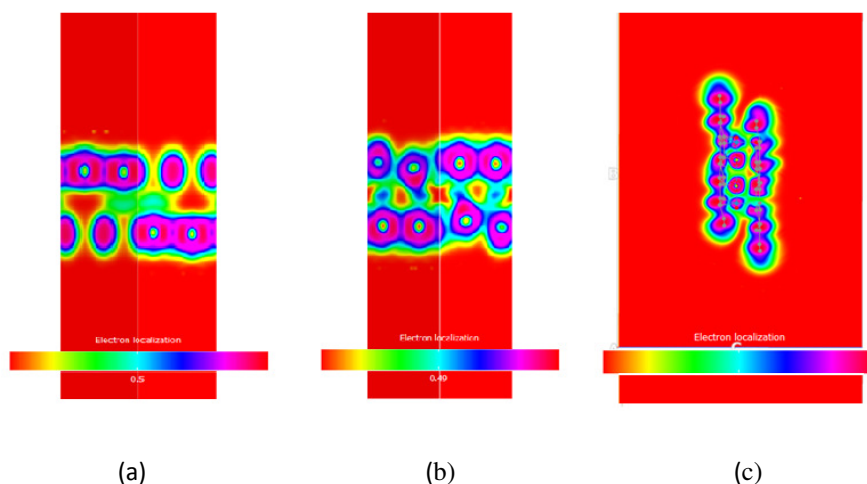


Figure 4.17. ELF models. (a) MBLG, (b) MNBLG (c) MOBLG.

Electron localization function schemes revealed that the molecular distribution of the pairs of electrons on each configuration can be visualized by means of the topological description of the ELF. The electrons were mostly localized in carbon atoms on graphene layers (pink areas).

4.7 Molecular Energy Analysis

Frontier molecular orbitals (*viz.* highest occupied molecular orbital (HOMO) and lowest unoccupied molecular orbital (LUMO)) give important parameters for

computational chemistry about π systems and transition mechanisms of electrons. To investigate chemical stability for both HOMO and LUMO energies, the energy difference between these molecular orbitals should be evaluated. For identification of HOMO and LUMO energies, molecular energy analysis were calculated by using the exchange–correlation interactions with BPW91 basis set for DFT. The molecular energy spectra of the structures were given in Figure 4.18. HOMO and LUMO energies of the structures calculated from molecular energy spectra are given in Table 4.4.

In summary, the energy difference between HOMO and LUMO shows a decreased when transition metal intercalation and N-doping applied to the pure bilayer graphene system. This change in HOMO-LUMO band gap can be explained by electronic transitions in MBLG, MNBLG, and MOBLG systems.

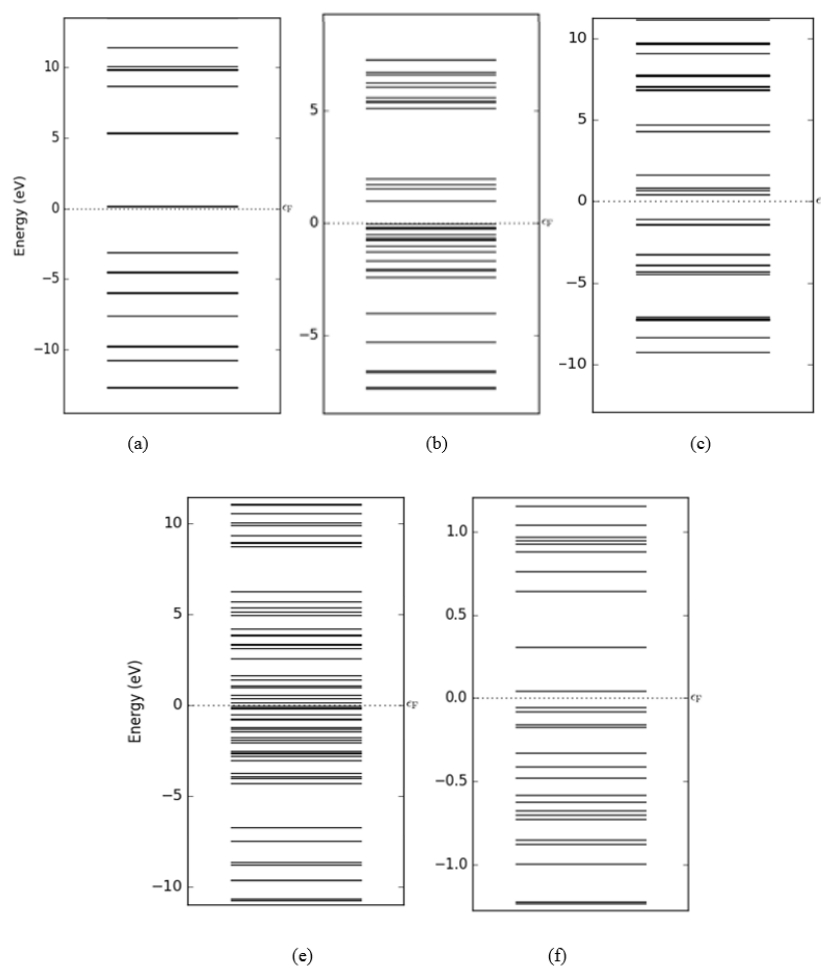


Figure 4.18. Molecular energy spectrum analysis. (a) MLG, (b) BLG, (c) ReBLG, (d) ReNBLG, (e) ReOBLG.

Table 4.4. Molecular energy spectra.

	HOMO (eV)	LUMO (eV)
MLG	-3.087631	5.75000
BLG	-0.0142857	1.0002
ReBLG	-1.0009	0.60021
ReNBLG	-0.17857	0.35714
ReOBLG	-0.06	0.041

4.8 Optical Properties

The optical spectroscopy analysis is a powerful tool to determine the overall band behavior of the structures. The optical spectrum analyses were performed by using the exchange–correlation interactions with basis set BPW91.

The energy absorption spectra are shown in Figures 4.19, 4.20 and 4.21 for graphene based structures. The optical absorption of pure bilayer graphene undergoes shift on metal intercalation and N-doping. The absorption of bilayer graphene reduces on intercalation and doping and increases again with transition metal oxide intercalation.

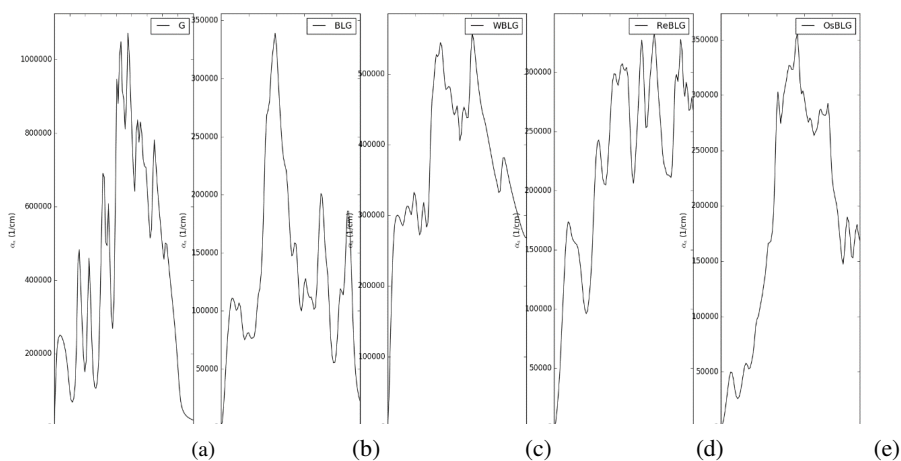


Figure 4.19. Energy-absorption spectra. (a) MLG, (b) BLG, (c) WBLG, (d) ReBLG, (e) OsBLG.

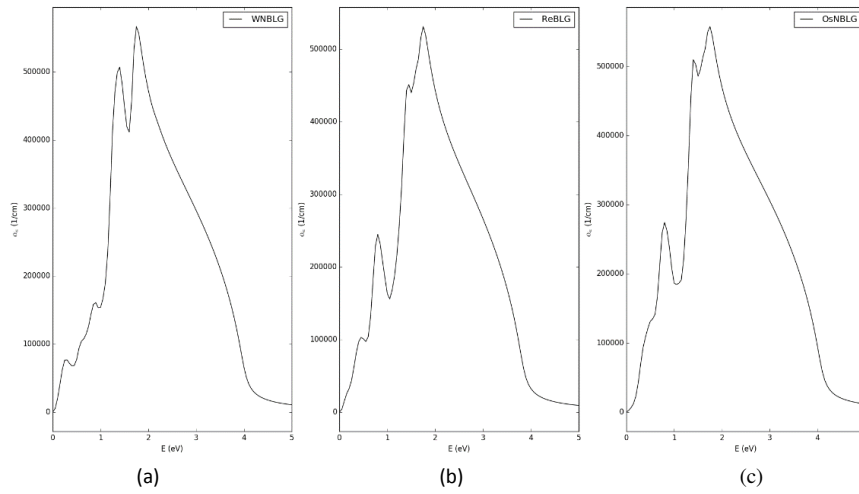


Figure 4.20. Energy-absorption spectra. (a) WNBLG, (b) ReNBLG, (c) OsNBLG.

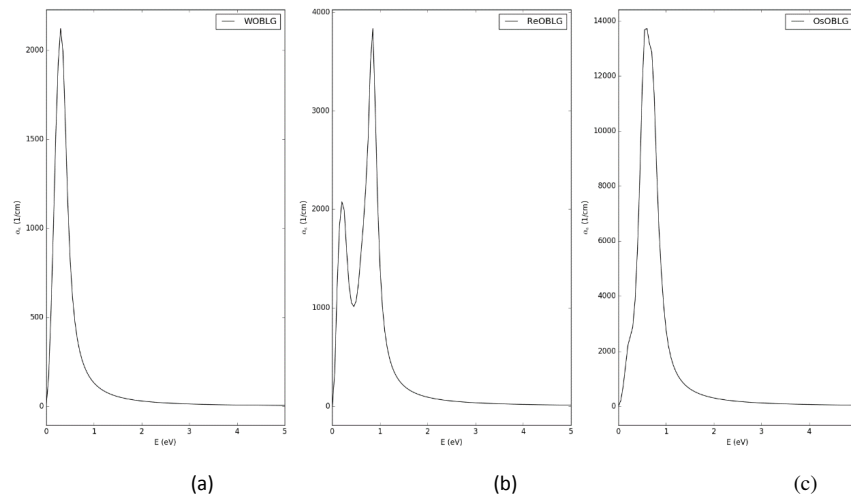


Figure 4.21. Energy-absorption spectra. (a) WOBLG, (b) ReOBLG, (c) OsOBLG.

Figures 4.22, 4.23 and 4.24 show the spectra of the real and imaginary parts of the complex dielectric function versus the photon energy. The lowest energy part of spectra (from 0 to 5.0 eV) is characterized by two sharp peaks of strongest intensity for metal inserted structures. This can be explained by electronic transitions from the valence band to the isolated low energy block in the conduction band.

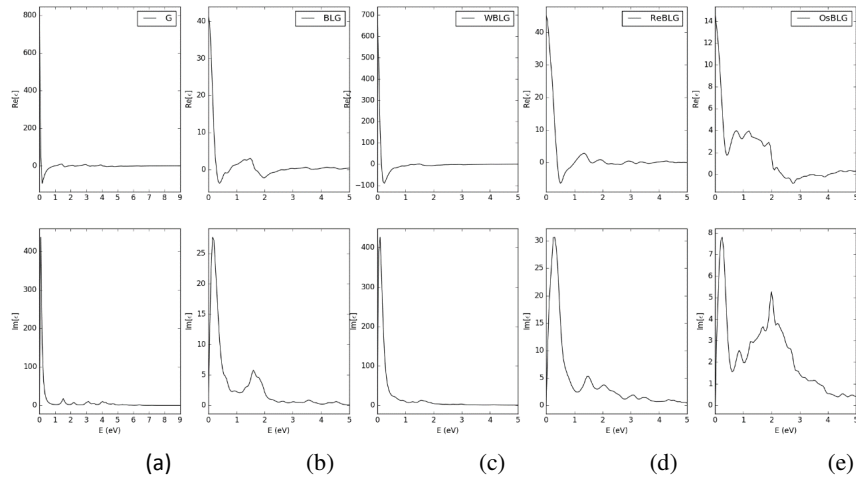


Figure 4.22. Energy-Dielectric constant spectra. (a) MLG, (b) BLG, (c) WBLG, (d) ReBLG, (e) OsBLG.

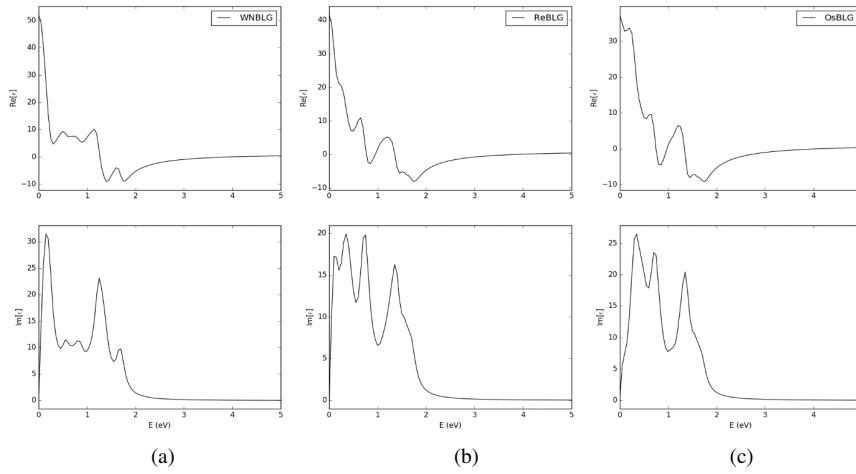


Figure 4.23. Energy-Dielectric constant spectra. (a) WNBLG, (b) ReNBLG, (c) OsNBLG.

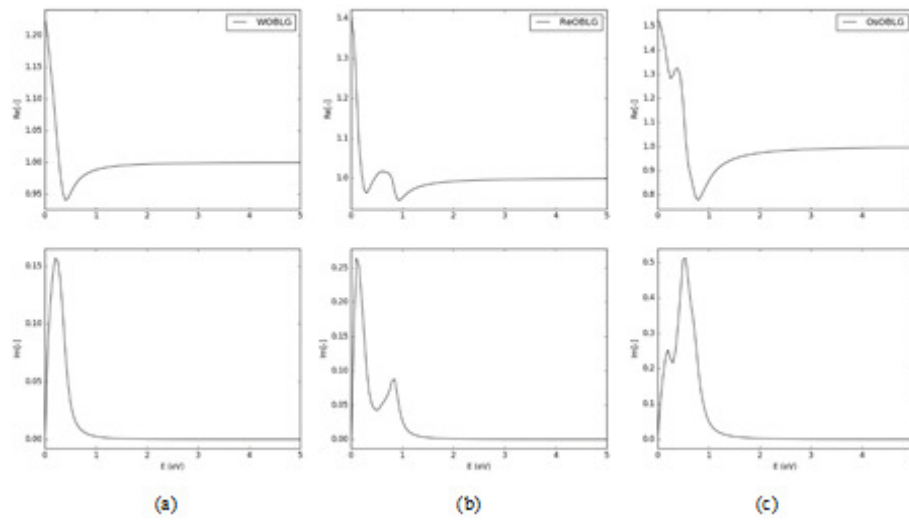


Figure 4.24. Energy-Dielectric constant spectra. (a) WOBLG, (b) ReOBLG, (c) OsOBLG.

Refractive index is related with the linear electro-optical coefficient that in turn determines the photorefractive sensitivity of the structure. Refractive index-energy spectra of the real and imaginary parts analysed as shown in Figures 4.25, 4.26 and 4.27. The refraction index reaches maximal values for the energies near the absorption threshold of bilayer graphene systems.

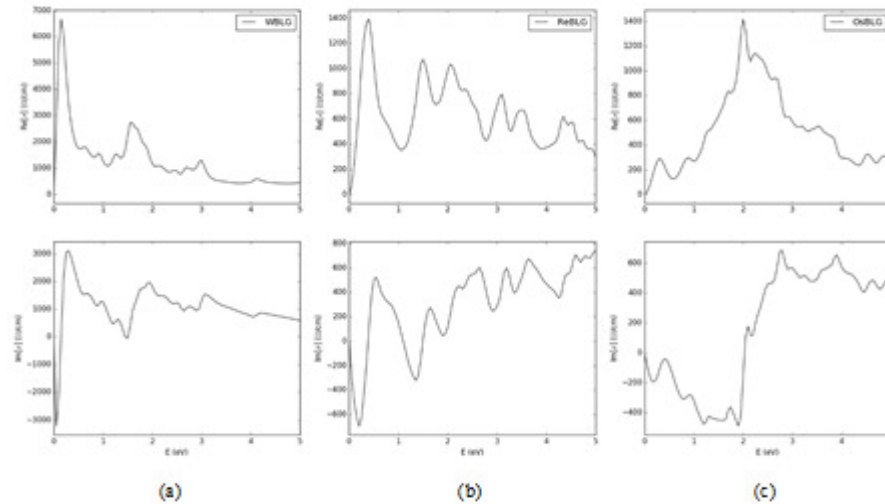


Figure 4.25. Energy-optical conductivity spectra. (a) WBLG, (b) ReBLG, (c) OsBLG.

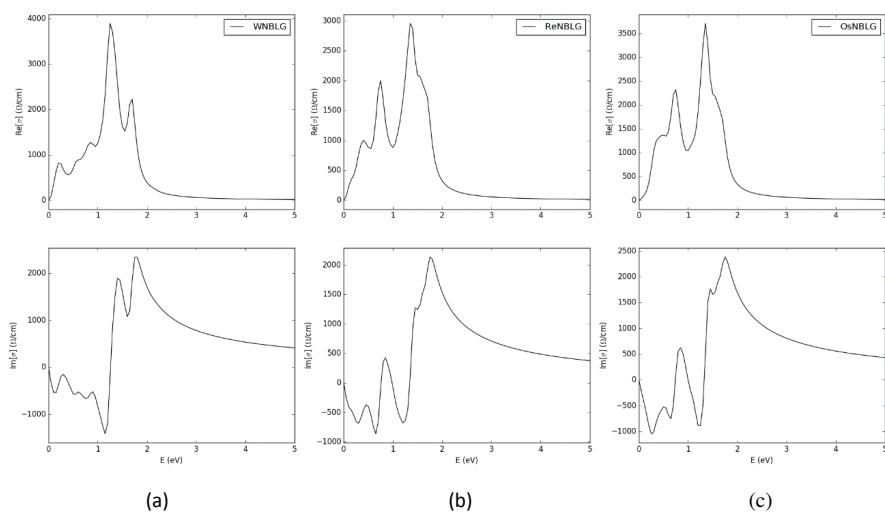


Figure 4.26. Energy-optical conductivity spectra. (a) WNBLG, (b) ReNBLG, (c) OsNBLG.

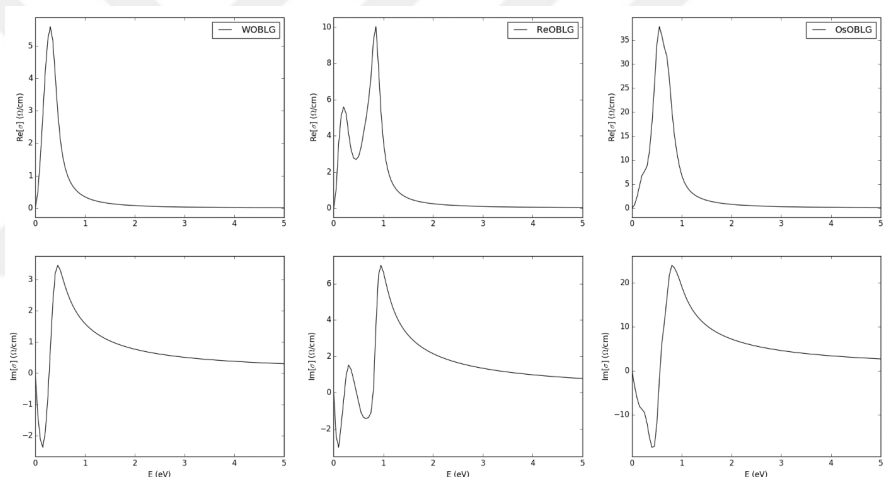


Figure 4.27. Energy-optical conductivity spectra of WOBLG, ReOBLG and OsOBLG.

Finally, absorption-wavelength spectra were analyzed by using the exchange–correlation interactions with BPW91 basis set and shown in Figures 4.28, 4.29 and 4.30.

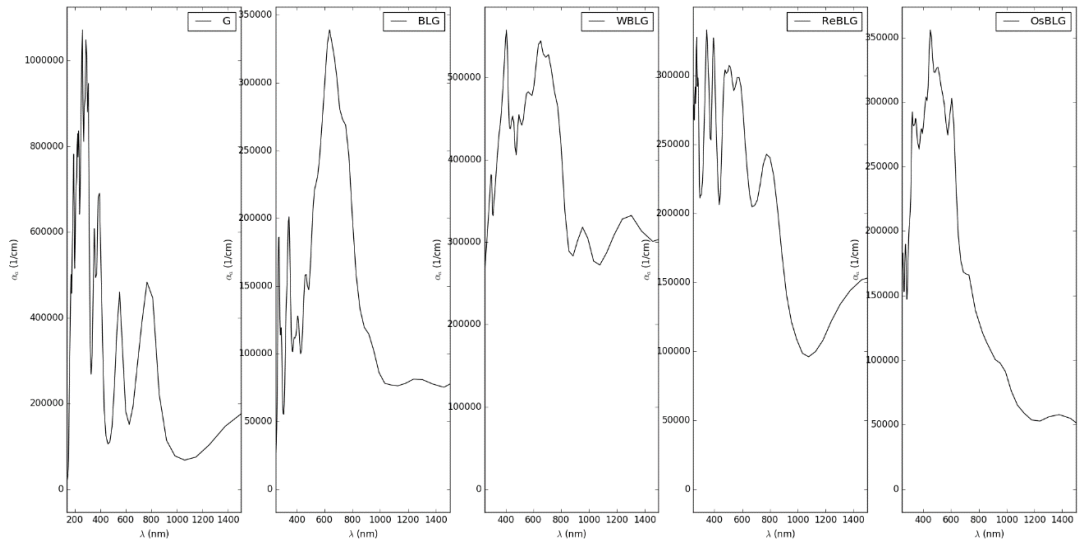


Figure 4.28. Absorption-wavelength spectra of MLG, BLG, WBLG, ReBLG and OsBLG.

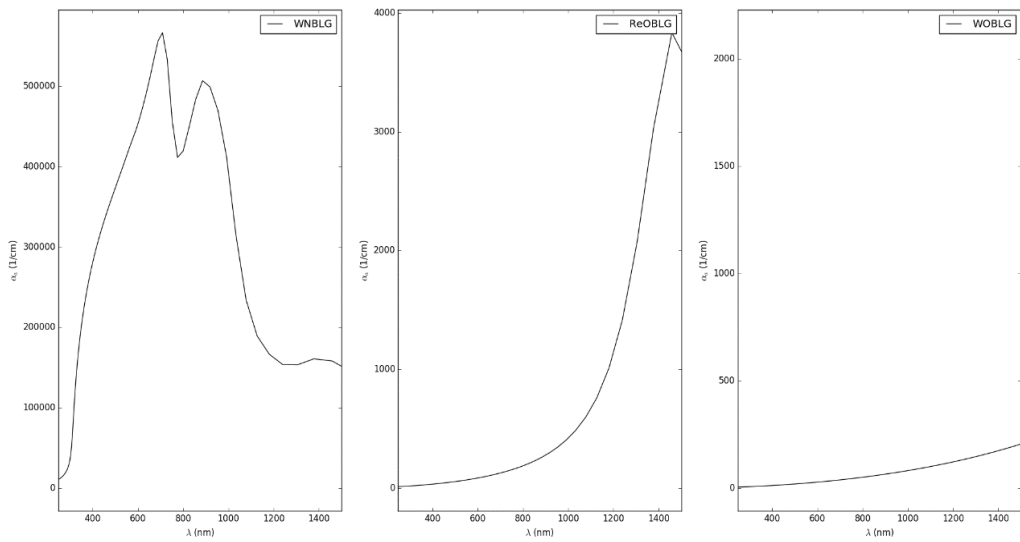


Figure 4.29. Absorption-wavelength spectra of WNBLG, ReNBLG and WNBGL.

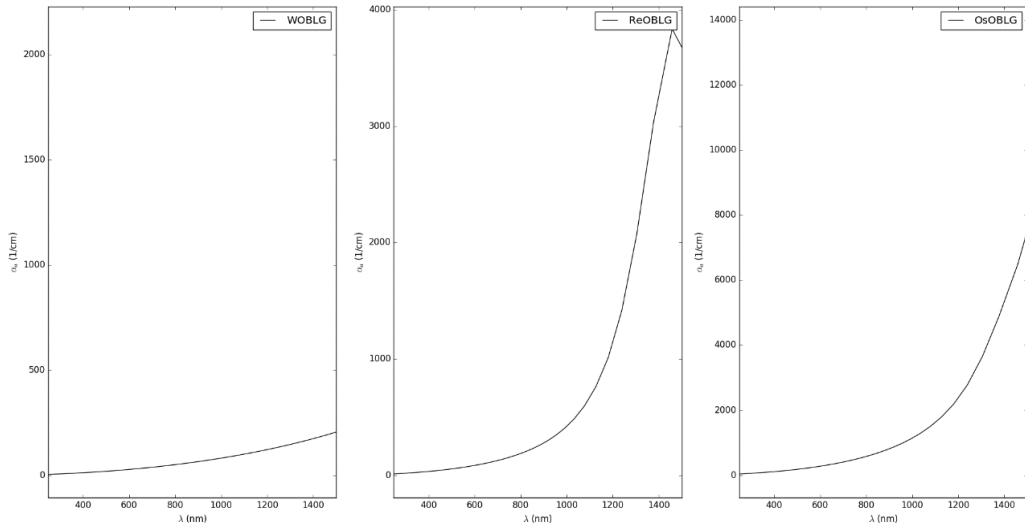


Figure 4.30. Absorption-wavelength spectra of WOBLG, ReOBLG and OsOBLG.

The optical absorption-wavelength spectra of designed structures show legitimate results with energy-absorption spectra. Absorption of pure bilayer graphene is 400 nm. The absorption-wavelength spectra rises with metal intercalation (~600 nm) and N-doping (~500 nm). The relation of wavelength shift on absorption spectra is consistent with total free energy calculations of the bilayer graphene systems.

5. CONCLUSIONS AND RECOMMENDATIONS

In this study, we have shown the first principles *ab initio* density functional computational methods for exploring the electronic structure of BLG systems with nitrogen doping of BLG and intercalation of some rare transition metal atoms (M: W, Re, Os) between layers of graphene. Structural comparison with MLG structure was carried out. All twelve different graphene based nanostructures modeled from the lattice constant of graphite structure and geometry optimization calculations were carried out for the most stable configurations. Electronic band behaviours with the change of structures computed through band structure analysis. At first, BLG shows zero band gap at K point. Electric fields were applied by changing the voltage of the second metallic region for opening a band gap, and then cell size was set to cover hexagonal unit cell. Applied voltage was changed 4V/nm in z-direction which is just above the experimental data. Theoretical lattice constant of BLG was found 2.4612 Å and band gap energy at Fermi level was found 1.1682 eV. The band structure calculations of rhenium, tungsten and osmium metals inserted bilayer graphene structures showed band gap 0.04617 eV, 0.086524 eV ve 0.11472 eV, respectively. As a nitrogen doped system, the band gap of WNBLG was calculated as 0.076143 eV at Fermi level. Thus, the modifications of band gap tailoring by inserting metal atoms to the graphene layer enhances conductivity. Then, each nanostructure was investigated by electron density, electron difference density and electron localization function analyses to understand the behaviours of electrons. Finally, molecular orbital analyses were carried out to determine HOMO and LUMO energies. In the second part of the study, the optical properties of each structure were analyzed in terms of energy, absorption, reflectivity and dielectric properties.

The electronic and optical properties of metal inserted bilayer graphene structures are affected by the type of dopant and metal, the data presented in this study can be used for further nanotechnology research and guide the experimental studies.

6. REFERENCES

- Allen MJ, Tung, VC and Kaner, RB (2010). “Honeycomb Carbon: A Review of Graphene”, *Chemical Reviews*, 110(1): 132–145.
- Atomistix Toolkit version 2017.2 (2017). Synopsys Quantum ATK.
- Brandt RB (1988). “The Structure of Virtue”, *Midwest Studies In Philosophy*, 13(1): 64–82.
- Brinkley SR (1933). “Principles of General Chemistry”, *Journal of the American Chemical Society*, vol. 55(11): 4732.
- Bui VQ, Le HM, Kawazoe Y & Nguyen-Manh D (2013). “Graphene-Cr-Graphene Intercalation Nanostructures: Stability and Magnetic Properties from Density Functional Theory Investigations”, *The Journal of Physical Chemistry C*, 117(7): 3605–3614.
- Cappelluti E, Benfatto L and Kuzmenko AB (2010). “Phonon switching and combined Fano-Rice effect in optical spectra of bilayer graphene”, *Physical Review B*, 82(4): 041402.
- Cappelluti E, Benfatto L, Manzardo M and Kuzmenko AB (2012). “Charged-phonon theory and Fano effect in the optical spectroscopy of bilayer graphene”, *Physical Review B*, 86(11): 115439.
- Chung F and Lu L (2002). “The average distances in random graphs with given expected degrees”, *Proceedings of the National Academy of Sciences of the United States of America*, 99(25): 15879–82.
- Dasari BL, Nouri JM, Brabazon D and Naher S (2017). “Graphene and derivatives – Synthesis techniques, properties and their energy applications”, *Energy*, 140: 766–778.
- Fano U (1961). “Effects of Configuration Interaction on Intensities and Phase Shifts”, *Physical Review*, 124(6): 1866–1878.
- Geim AK and Novoselov KS (2007). “The rise of graphene”, *Nature Materials*, 6(3): 183–191.
- Greenwood NN and Earnshaw A (1997). *Chemistry of the Elements*, Second Edition, Elsevier.
- Hirsch A (2010). “The era of carbon allotropes”, *Nature Materials*, 9(11): 868–871.
- Hohenberg P and Kohn W (1964) “Inhomogeneous Electron Gas”, *Physical Review*, 136(3B): B864–B871.

- Ichinokura S, Sugawara K, Takayama A, Takahashi T and Hasegawa S (2016). “Superconducting Calcium-Intercalated Bilayer Graphene”, *ACS Nano*, 10(2): 2761–2765.
- Iijima S and Ichihashi T (1993). “Single-shell carbon nanotubes of 1-nm diameter”, *Nature*, 363(6430): 603–605.
- Katsnelson MI (2007). “Graphene: carbon in two dimensions”, *Materials Today*, 10(1-2): 20–27.
- Kohn W and Sham LJ (1965). “Self-Consistent Equations Including Exchange and Correlation Effects”, *Physical Review*, 140(4A): A1133–A1138.
- Kroto HW, Heath JR, O’Brien SC, Curl RF and Smalley RE (1985). “C₆₀: Buckminsterfullerene”, *Nature*, 318(6042): 162–163.
- Kuzmenko AB, Benfatto L, Cappelluti E, Crassee I, van der Marel D, Blake P, Novoselov KS and Geim AK (2009). “Gate Tunable Infrared Phonon Anomalies in Bilayer Graphene”, *Physical Review Letters*, 103(11): 116804.
- Li Z, Liu Z, Sun H and Gao C (2015). “Superstructured Assembly of Nanocarbons: Fullerenes, Nanotubes, and Graphene”, *Chemical Reviews*, 115(15): 7046–7117.
- Liao JH, Zhao YJ, Tang JJ, Yang XB and Xu H (2016). “High-coverage stable structures of 3d transition metal intercalated bilayer graphene”, *Physical Chemistry Chemical Physics*, 18(21): 14244–14251.
- Liu Z, Suenaga K, Harris PJF and Iijima S (2009). “Open and Closed Edges of Graphene Layers”, *Physical Review Letters*, 102(1): 015501.
- Lopes dos Santos JMB, Peres NMR and Castro Neto AH (2007). “Graphene Bilayer with a Twist: Electronic Structure”, *Physical Review Letters*, 99(25): 256802.
- Mak, KF, Lui, CH, Shan, J & Heinz, TF (2009). “Observation of an Electric-Field-Induced Band Gap in Bilayer Graphene by Infrared Spectroscopy”, *Physical Review Letters*, 102(25): 256405.
- Mccann, E & Koshino, M (2013). “The electronic properties of bilayer graphene”, 76(5): 056503.
- Nakada K, Torobu T and Ishii A (2012). “Investigation of Hf Adatom Adsorption on Graphene Using Density Functional Theory Calculations”, *e-Journal of Surface Science and Nanotechnology*, 10(0) 325–330.
- Novoselov KS, Geim AK, Morozov SV, Jiang D, Zhang Y, Dubonos S V, Grigorieva IV and Firsov AA (2004). “Electric field effect in atomically thin carbon films”, *Science*, 306(5696): 666–669.
- Pakhira S, Lucht KP and Mendoza-Cortes JL (2018). “Dirac cone in two dimensional

- bilayer graphene by intercalation with V, Nb, and Ta transition metals”, *The Journal of Chemical Physics*, 148(6): 064707.
- Rozhkov AV, Sboychakov AO, Rakhmanov AL and Nori F (2016). “Electronic properties of graphene-based bilayer systems”, *Physics Reports*, 648(1): 104.
- Soldano C, Mahmood A and Dujardin E (2010). “Production, properties and potential of graphene”, *Carbon*, 48(8): 2127–2150.
- Soukiassian PG and Rao MSR (2010). “Carbon-based nanoscience and nanotechnology: Where are we, where are we heading? ”, *Journal of Physics D: Applied Physics*, 43(37): 42–43.
- Sugawara K, Kanetani K, Sato T and Takahashi T (2011). “Fabrication of Li-intercalated bilayer graphene”, *AIP Advances*, 1(2): 022103.
- Tang TT, Zhang Y, Park CH, Geng B, Girit C, Hao Z, Martin MC, Zettl A, Crommie MF, Louie SG, Shen YR and Wang F (2010). “A tunable phonon–exciton Fano system in bilayer graphene”, *Nature Nanotechnology*, 5(1): 32–36.
- Terse-Thakoor T, Badhulika S and Mulchandani A (2017). “Graphene based biosensors for healthcare”, *Journal of Materials Research*, 32(15): 2905–2929.
- Wallace PR (1947). “The Band Theory of Graphite”, *Physical Review*, 71(9): 622–634.
- Wang Z, Selbach SM and Grande T (2014). “Van der Waals density functional study of the energetics of alkali metal intercalation in graphite”, *RSC Adv.*, 4(8): 3973–3983.
- Xia F, Farmer DB, Lin Y and Avouris P (2010). “Graphene Field-Effect Transistors with High On/Off Current Ratio and Large Transport Band Gap at Room Temperature”, *Nano Letters*, 10(2): 715–718.
- Xu Z and Buehler MJ (2010). “Interface structure and mechanics between graphene and metal substrates: a first-principles study”, *Journal of Physics: Condensed Matter*, 22(48): 485301.
- Zan R, Bangert U, Ramasse Q and Novoselov KS (2011). “Metal–Graphene Interaction Studied via Atomic Resolution Scanning Transmission Electron Microscopy”, *Nano Letters*, 11(3): 1087–1092.
- Zhang LM, Li ZQ, Basov DN, Fogler MM, Jiang Z, Hao Z, Martin MC, Henriksen EA, Kim P and Stormer HL (2008). “Determination of the electronic structure of bilayer graphene from infrared spectroscopy results” *Phys. Rev. B*, 78: 235408.
- Zhang X, Xu W, Dai J and Liu Y (2017). “Role of embedded 3d transition metal atoms on the electronic and magnetic properties of defective bilayer graphene”, *Carbon*, 118: 376–383.

Zhang Y, Tang TT, Girit C, Hao Z, Martin MC, Zettl A, Crommie MF, Shen YR and Wang F (2009). “Direct observation of a widely tunable bandgap in bilayer graphene”, *Nature*, 459(7248): 820–823.

Zhen Z and Zhu H (2018). *Graphene*, Elsevier, United Kingdom.



7. APPENDICES

Appendix A.1

Cartesian and Fractional Coordinates, and Z-matrix Tables of graphene structures before and after geometry optimizations are given in Tables from 7.1 to 7.41.

Table 7.1. Cartesian coordinates of BLG(2+2) before optimization.

	Element	x(Å)	y(Å)	z(Å)
0	Carbon	10.0000	10.7105	10.0000
1	Carbon	10.0000	10.7105	13.3545
2	Carbon	11.2306	11.4210	10.0000
3	Carbon	11.2326	10.0000	13.3545
4	Carbon	10.0000	10.7105	10.0000
5	Carbon	10.0000	10.7105	13.3545
6	Carbon	11.2306	11.4210	10.0000
7	Carbon	11.2306	10.0000	13.3545

Table 7.2. Fractional coordinates of BLG(2+2) before optimization.

	Element	a	b	c
0	Carbon	0.471018	0.5	0.428183
1	Carbon	0.471018	0.5	0.571817
2	Carbon	0.528982	0.533168	0.428183
3	Carbon	0.528982	0.533168	0.571817
4	Carbon	0.471018	0.5	0.428183
5	Carbon	0.471018	0.5	0.571817
6	Carbon	0.528982	0.533168	0.428183
7	Carbon	0.528982	0.466832	0.571817

Table 7.3. Cartesian coordinates of BLG(2+2) after geometry optimization.

	Element	x(Å)	y(Å)	z(Å)
0	Carbon	0.6153	0.0000	10.8228
1	Carbon	0.6153	0.0000	14.1772
2	Carbon	1.8459	0.7105	10.8228
3	Carbon	1.8459	-0.7105	14.1772

Table 7.4. Fractional coordinates of BLG(2+2) after geometry optimization.

	Element	a	b	c
0	Carbon	0.25	0.25	0.43291
1	Carbon	0.25	0.25	0.56709
2	Carbon	0.583333	0.916667	0.56709
3	Carbon	0.916667	0.583333	0.56709

Table 7.5. Z-matrix of BLG(2+2).

	Element	d (Å)	θ (°)	φ (°)
0	Carbon	3.3545		
1	Carbon	3.64305	22.9576	
2	Carbon	3.64305	22.4924	
3	Carbon			-117.996

Table 7.6. Cartesian coordinates of BLG(4+4) before geometry optimization.

	Element	x(Å)	y(Å)	z(Å)
0	Carbon	3.07829	4.73135	0.71709
1	Carbon	3.07851	7.57300	0.88824
2	Carbon	0.61717	4.71864	0.95762
3	Carbon	1.83685	2.60621	0.95809
4	Carbon	1.85879	6.86923	0.95812
5	Carbon	3.07853	3.31762	0.96846
6	Carbon	4.30248	5.43744	0.96992
7	Carbon	1.85480	5.43734	0.94285
8	Carbon	1.85127	4.01940	4.83534
9	Carbon	4.30584	4.01930	4.43758
10	Carbon	3.07844	6.14475	4.84106
11	Carbon	1.85667	2.59034	4.85175
12	Carbon	1.83883	6.85339	4.85227
13	Carbon	0.61708	4.73774	4.85298
14	Carbon	3.07858	1.88532	4.91462
15	Carbon	3.07828	4.72755	5.03784

Table 7.7. Fractional coordinates of BLG(4+4) before geometry optimization.

	Element	a	b	c
0	Carbon	0.625298	0.500232	0.124699
1	Carbon	0.625344	0.800671	0.154328
2	Carbon	0.125367	0.498888	0.166382
3	Carbon	0.373123	0.275547	0.166463
4	Carbon	0.377579	0.726264	0.166468
5	Carbon	0.625347	0.350762	0.168266
6	Carbon	0.873969	0.574885	0.168518
7	Carbon	0.376768	0.574874	0.169028
8	Carbon	0.376051	0.424959	0.840117
9	Carbon	0.874652	0.424949	0.840506
10	Carbon	0.625329	0.649667	0.841111
11	Carbon	0.377148	0.273869	0.842968
12	Carbon	0.373353	0.724588	0.84306
13	Carbon	0.125348	0.500908	0.843182
14	Carbon	0.625357	0.199329	0.853893
15	Carbon	0.625295	0.49983	0.875301

Table 7.8. Z-matrix of BLG(4+4).

	Element	d (Å)	θ (°)	ϕ (°)
0	Carbon			
1	Carbon	2.84676		
2	Carbon	3.76967	40.9938	
3	Carbon	2.43926	109.224	6.10421
4	Carbon	4.26308	30.2963	1.13255
5	Carbon	3.75524	19.2497	179.543
6	Carbon	2.44779	48.9558	179.729
7	Carbon	2.44768	59.9963	0.337981
8	Carbon	4.11453	90.1145	69.9206
9	Carbon	2.45457	90.0008	0.037231
10	Carbon	2.4544	59.9925	69.9206
11	Carbon	3.75855	48.9755	0.394018
12	Carbon	4.26308	19.2101	179.76
13	Carbon	2.44307	30.2455	179.53
14	Carbon	3.76818	109.199	1.02928
15	Carbon	2.84491	40.9195	4.56768

Table 7.9. Cartesian coordinates of BLG(4+4) after geometry optimization.

	Element	x(Å)	y(Å)	z(Å)
0	Carbon	3.08207	4.34892	0.227190
1	Carbon	3.09259	7.78396	0.353528
2	Carbon	0.65842	4.98026	0.246254
3	Carbon	2.03669	1.94827	0.356814
4	Carbon	2.36111	6.71641	0.335902
5	Carbon	2.73593	3.02711	0.268888
6	Carbon	4.41518	4.76203	0.236394
7	Carbon	2.01629	5.39280	0.241883
8	Carbon	2.01673	3.63138	3.266410
9	Carbon	4.41590	4.27429	3.292710
10	Carbon	2.73023	5.99986	3.228800
11	Carbon	2.36187	2.30853	3.152340
12	Carbon	2.05081	7.08721	3.128670
13	Carbon	0.68685	4.04117	3.297340
14	Carbon	3.09532	1.24290	3.155800
15	Carbon	3.08185	4.68130	3.278520

Table 7.10. Fractional coordinates of BLG(4+4) after geometry optimization.

	Element	a	b	c
0	Carbon	0.604171	0.481775	0.06446
1	Carbon	0.606233	0.862311	0.100305
2	Carbon	0.13436	0.551716	0.069869
3	Carbon	0.399249	0.215831	0.101237
4	Carbon	0.462843	0.744047	0.095304
5	Carbon	0.536318	0.335344	0.07629
6	Carbon	0.865498	0.52754	0.067071
7	Carbon	0.395249	0.597417	0.068628
8	Carbon	0.395335	0.402286	0.926766
9	Carbon	0.86564	0.473508	0.934226
10	Carbon	0.535202	0.664667	0.916094
11	Carbon	0.462992	0.25574	0.8944
12	Carbon	0.402016	0.785125	0.887686
13	Carbon	0.134641	0.447682	0.93554
14	Carbon	0.606769	0.137689	0.895381
15	Carbon	0.604128	0.518597	0.930202

Table 7.11. Z-matrix of BLG(4+4).

	Element	d (Å)	θ (°)	ϕ (°)
0	Carbon			
1	Carbon	3.43739		
2	Carbon	3.69685	40.4524	
3	Carbon	3.32131	115.243	4.19135
4	Carbon	4.7792	27.9567	0.322084
5	Carbon	3.7089	9.77793	-168.829
6	Carbon	2.41472	49.8975	-174.374
7	Carbon	2.48044	60.6672	-2.2912
8	Carbon	3.50006	82.7507	59.8068
9	Carbon	2.48396	83.051	26.2014
10	Carbon	2.41312	60.666	59.277
11	Carbon	3.71045	50.0964	-2.96722
12	Carbon	4.78885	9.53556	-174.193
13	Carbon	3.34174	27.955	-165.507
14	Carbon	3.69474	114.983	1.08063
15	Carbon	3.44062	40.4655	4.79641

Table 7.12. Cartesian coordinates of MBLG before geometry optimization.
(M; W, Re, Os.)

	Element	x(Å)	y(Å)	z(Å)
0	Carbon	0.61530	0.00000	10.822800
1	Carbon	1.84590	2.13146	10.822800
2	Carbon	1.84590	-2.13146	10.822800
3	Carbon	3.07650	0.00000	10.822800
4	Carbon	0.61530	0.00000	14.177200
5	Carbon	1.84590	2.13146	14.177200
6	Carbon	1.84590	-2.13146	14.177200
7	Carbon	3.07650	0.00000	14.177200
8	Carbon	1.84590	0.71049	10.822800
9	Carbon	3.07650	2.84195	10.822800
10	Carbon	3.07650	-1.42097	10.822800
11	Carbon	4.30710	0.71049	10.822800
12	Carbon	1.84590	-0.71049	14.177200
13	Carbon	3.07650	1.42097	14.177200
14	Carbon	3.07650	-2.84195	14.177200
15	Carbon	4.30710	-0.71049	14.177200
16	Metal	3.07650	0.00000	12.500000

Table 7.13. Fractional coordinates of MBLG before geometry optimization.
(M; W, Re, Os.)

	Element	a	b	c
0	Carbon	0.125	0.125	0.43291
1	Carbon	0.125	0.625	0.43291
2	Carbon	0.625	0.125	0.43291
3	Carbon	0.625	0.625	0.43291
4	Carbon	0.125	0.125	0.56709
5	Carbon	0.125	0.625	0.56709
6	Carbon	0.625	0.125	0.56709
7	Carbon	0.625	0.625	0.56709
8	Carbon	0.291667	0.458333	0.43291
9	Carbon	0.291667	0.958333	0.43291
10	Carbon	0.791667	0.458333	0.43291
11	Carbon	0.791667	0.958333	0.43291
12	Carbon	0.458333	0.291667	0.56709
13	Carbon	0.458333	0.791667	0.56709
14	Carbon	0.958333	0.291667	0.56709
15	Carbon	0.958333	0.791667	0.56709
16	Metal	0.625	0.625	0.5

Table 7.14. Cartesian coordinates of ReBLG after geometry optimization.

	Element	x(Å)	y(Å)	z(Å)
0	Carbon	0.61521	-0.01123	10.572300
1	Carbon	1.85609	2.13795	10.572400
2	Carbon	1.83557	-2.12501	10.572100
3	Carbon	3.07631	0.00051	10.367400
4	Carbon	0.61515	0.01056	14.429800
5	Carbon	1.83607	2.12533	14.430100
6	Carbon	1.85547	-2.13764	14.429700
7	Carbon	3.07628	-0.00051	14.619700
8	Carbon	1.85062	0.70796	10.594900
9	Carbon	3.07632	2.84219	10.505100
10	Carbon	3.07631	-1.41514	10.593000
11	Carbon	4.30213	0.70801	10.592900
12	Carbon	1.84962	-0.70849	14.409600
13	Carbon	3.07624	1.41621	14.411400
14	Carbon	3.07626	-2.84216	14.493500
15	Carbon	4.30305	-0.70857	14.411800
16	Rhenium	3.08024	-0.00014	12.491700

Table 7.15. Fractional coordinates of ReBLG after geometry optimization.

	Element	a	b	c
0	Carbon	0.126299	0.123665	0.422894
1	Carbon	0.126308	0.62783	0.422896
2	Carbon	0.622145	0.123658	0.422884
3	Carbon	0.624901	0.625022	0.414696
4	Carbon	0.123732	0.126208	0.577193
5	Carbon	0.123723	0.622284	0.577202
6	Carbon	0.62767	0.12622	0.577187
7	Carbon	0.625016	0.624897	0.584789
8	Carbon	0.292922	0.458996	0.423797
9	Carbon	0.291603	0.958326	0.420205
10	Carbon	0.790943	0.458978	0.42372
11	Carbon	0.790948	0.957034	0.423715
12	Carbon	0.458855	0.292658	0.576385
13	Carbon	0.45884	0.791056	0.576457
14	Carbon	0.958309	0.291593	0.579742
15	Carbon	0.957286	0.79107	0.576472
16	Rhenium	0.625776	0.625743	0.49967

Table 7.16. Z-matrix of ReBLG.

	Element	d (Å)	θ (°)	φ (°)
0	Carbon			
1	Carbon	2.48168		
2	Carbon	4.26301	29.7252	
3	Carbon	2.46965	30.3382	170.554
4	Carbon	4.74981	70.7684	53.458
5	Carbon	2.4419	75.0983	177.912
6	Carbon	4.26301	30.2599	-62.2596
7	Carbon	2.46857	30.2898	-171.231
8	Carbon	4.26653	85.9324	-62.9846
9	Carbon	2.46279	92.024	-177.714
10	Carbon	4.25823	29.8699	71.8725
11	Carbon	2.45162	30.0212	-175.823
12	Carbon	4.75279	58.9249	72.0076
13	Carbon	2.45335	58.9679	179.984
14	Carbon	4.25916	30.0188	-71.9389
15	Carbon	2.4625	29.8986	176.108
16	Rhenium	2.38407	91.6429	-54.7214

Table 7.17. Cartesian coordinates of WBLG after geometry optimization.

	Element	x(Å)	y(Å)	z(Å)
0	Carbon	0.61478	-0.01063	10.5589
1	Carbon	1.85640	2.13997	10.5594
2	Carbon	1.83446	-2.12306	10.5594
3	Carbon	3.07590	0.00209	10.3190
4	Carbon	0.61469	0.00848	14.4543
5	Carbon	1.83644	2.12412	14.4536
6	Carbon	1.85428	-2.13893	14.4530
7	Carbon	3.07589	-0.00171	14.6391
8	Carbon	1.85241	0.70807	10.5741
9	Carbon	3.07612	2.84373	10.4895
10	Carbon	3.07614	-1.41165	10.5697
11	Carbon	4.30009	0.70817	10.5712
12	Carbon	1.84888	-0.70987	14.4366
13	Carbon	3.07605	1.41549	14.4423
14	Carbon	3.07619	-2.84395	14.5159
15	Carbon	4.30345	-0.70997	14.4389
16	Tungsten	3.08163	-0.00074	12.4673

Table 7.18. Fractional coordinates of WBLG after geometry optimization.

	Element	a	b	c
0	Carbon	0.126141	0.123648	0.422375
1	Carbon	0.126136	0.628131	0.41276
2	Carbon	0.621691	0.123662	0.578171
3	Carbon	0.624633	0.625123	0.578142
4	Carbon	0.123882	0.12587	0.578121
5	Carbon	0.12394	0.622217	0.585565
6	Carbon	0.627578	0.125826	0.422966
7	Carbon	0.625076	0.624674	0.419581
8	Carbon	0.293273	0.459372	0.422966
9	Carbon	0.291381	0.958466	0.419581
10	Carbon	0.7905	0.459355	0.42279
11	Carbon	0.790513	0.956637	0.422848
12	Carbon	0.458866	0.292344	0.577465
13	Carbon	0.458866	0.790932	0.577694
14	Carbon	0.958506	0.291369	0.580636
15	Carbon	0.95753	0.790985	0.577555
16	Tungsten	0.626129	0.625955	0.498693

Table 7.19. Z-matrix of WBLG.

	Element	d (Å)	θ (°)	φ (°)
0	Carbon			
1	Carbon	2.48328		
2	Carbon	4.26308	29.7046	
3	Carbon	2.47289	30.4639	168.923
4	Carbon	4.81228	70.1754	52.3974
5	Carbon	2.44307	75.2344	177.561
6	Carbon	4.26308	30.2455	-62.6536
7	Carbon	2.46873	30.2717	-171.367
8	Carbon	4.30405	86.0382	-63.3394
9	Carbon	2.46286	91.9603	-177.873
10	Carbon	4.25613	29.8147	72.0665
11	Carbon	2.44779	30.0205	-175.987
12	Carbon	4.79174	59.2303	72.1355
13	Carbon	2.4542	59.3235	179.959
14	Carbon	4.26007	30.0236	-72.1475
15	Carbon	2.46292	29.9066	176.145
16	Tunsten	2.42545	91.5914	-55.4926

Table 7.20. Cartesian coordinates of MNBLG before geometry optimization. (M; W, Re, Os.)

	Element	x(Å)	y(Å)	z(Å)
0	Carbon	0.62911	4.82514	0.851517
1	Carbon	1.89579	7.01886	0.851679
2	Carbon	1.87780	2.66171	0.851757
3	Carbon	3.14471	4.83542	0.729906
4	Carbon	0.62910	4.84139	4.869200
5	Carbon	1.87778	7.00483	4.868950
6	Carbon	1.89579	2.64768	4.869030
7	Carbon	3.14471	4.83114	4.990980
8	Nitrogen	1.88726	5.56086	0.886771
9	Carbon	3.14462	7.73968	0.802885
10	Carbon	3.14464	3.38329	0.886470
11	Carbon	4.40179	5.56084	0.886734
12	Nitrogen	1.88727	4.10566	4.833970
13	Carbon	3.14465	6.28322	4.834270
14	Carbon	3.14464	1.92686	4.917830
15	Carbon	4.40181	4.10570	4.834010
16	Metal	3.14574	4.83327	2.860400

Table 7.21. Fractional coordinates of MNBLG before geometry optimization.
(M; W, Re, Os.)

	Element	a	b	c
0	Carbon	0.125049	0.499159	0.148844
1	Carbon	0.376829	0.726099	0.148872
2	Carbon	0.373253	0.275353	0.148885
3	Carbon	0.625079	0.500223	0.127586
4	Carbon	0.125046	0.50084	0.851127
5	Carbon	0.373249	0.724647	0.851084
6	Carbon	0.376828	0.273902	0.851098
7	Carbon	0.625078	0.49978	0.872414
8	Nitrogen	0.375133	0.575269	0.155006
9	Carbon	0.625061	0.800667	0.140343
10	Carbon	0.625064	0.35	0.154953
11	Carbon	0.87495	0.575267	0.154999
12	Nitrogen	0.375135	0.42473	0.84497
13	Carbon	0.625067	0.649997	0.845021
14	Carbon	0.625064	0.199333	0.859627
15	Carbon	0.874954	0.424733	0.844976
16	Metal	0.625283	0.5	0.499993

Table 7.22. Cartesian coordinates of ReNBLG after geometry optimization.

	Element	x(Å)	y(Å)	z(Å)
0	Carbon	4.30758	4.79562	4.740090
1	Carbon	3.06596	4.79512	2.589490
2	Carbon	3.08790	4.79515	6.852520
3	Carbon	1.84646	5.03553	4.727370
4	Carbon	4.30767	0.90026	4.720980
5	Carbon	3.08592	0.90097	2.605340
6	Carbon	3.06809	0.90149	6.868390
7	Carbon	1.84648	0.71540	4.731170
8	Nitrogen	3.06995	4.78039	4.021390
9	Carbon	1.84624	4.86500	1.885730
10	Carbon	1.84622	4.78478	6.141110
11	Carbon	0.62228	4.78332	4.021290
12	Nitrogen	3.07349	0.91790	5.439330
13	Carbon	1.84631	0.91218	3.313970
14	Carbon	1.84617	0.83861	7.573410
15	Carbon	0.61892	0.91566	5.439430
16	Rhenium	1.84074	2.88720	4.730200

Table 7.23. Fractional coordinates of ReNBLG after geometry optimization.

	Element	a	b	c
0	Carbon	0.874354	0.833887	0.501112
1	Carbon	0.622329	0.8338	0.273756
2	Carbon	0.626783	0.833806	0.724434
3	Carbon	0.374795	0.875603	0.499768
4	Carbon	0.874372	0.156541	0.499092
5	Carbon	0.626381	0.156664	0.275431
6	Carbon	0.62276	0.156756	0.726111
7	Carbon	0.374798	0.124397	0.50017
8	Nitrogen	0.62314	0.831238	0.425133
9	Carbon	0.37475	0.84595	0.199355
10	Carbon	0.374746	0.832001	0.649225
11	Carbon	0.12631	0.831748	0.425122
12	Nitrogen	0.623856	0.15961	0.575034
13	Carbon	0.374764	0.158615	0.350346
14	Carbon	0.374736	0.145823	0.800645
15	Carbon	0.125628	0.15922	0.575045
16	Rhenium	0.373633	0.502041	0.500067

Table 7.24. Z-matrix of ReNBLG.

	Element	d (Å)	θ (°)	ϕ (°)
0	Carbon			
1	Carbon	3.22011		
2	Carbon	2.53316	66.8572	
3	Carbon	4.35719	29.7661	42.7123
4	Carbon	2.51892	30.1144	174.46
5	Carbon	4.84377	72.453	57.0969
6	Carbon	2.49794	75.0109	178.872
7	Carbon	4.35719	30.2293	-62.1989
8	Nitrogen	2.51837	30.1223	-174.452
9	Carbon	4.3541	87.5034	-65.6801
10	Carbon	2.51699	91.8466	-178.228
11	Carbon	4.35719	29.9889	71.5943
12	Nitrogen	2.51439	30.0176	-176.168
13	Carbon	4.90113	59.0985	72.0374
14	Carbon	2.51451	59.0977	179.995
15	Carbon	4.35716	30.0217	-72.0405
16	Rhenium	2.51691	29.9846	176.17

Table 7.25. Cartesian coordinates of WNBLG after geometry optimization.

	Element	x(Å)	y(Å)	z(Å)
0	Carbon	1.36887	1.40802	1.285436
1	Carbon	1.24471	1.40797	1.070377
2	Carbon	1.24690	1.40798	1.496679
3	Carbon	1.12276	1.43201	1.284164
4	Carbon	1.36888	1.01849	1.283525
5	Carbon	1.24670	1.01856	1.071961
6	Carbon	1.24492	1.01861	1.498266
7	Carbon	1.12276	1.00000	1.284544
8	Nitrogen	1.24510	1.40650	1.213566
9	Carbon	1.12273	1.41496	1.000000
10	Carbon	1.12273	1.40694	1.425538
11	Carbon	1.00034	1.40679	1.213556
12	Nitrogen	1.24546	1.02025	1.355360
13	Carbon	1.12274	1.01968	1.142825
14	Carbon	1.12273	1.01232	1.568768
15	Carbon	1.00000	1.02003	1.355370
16	Tungsten	1.12218	1.21718	1.284447

Table 7.26. Cartesian coordinates of OsNBLG after geometry optimization.

	Element	x(Å)	y(Å)	z(Å)
0	Carbon	0.61618	4.70708	0.877624
1	Carbon	1.85624	6.85507	0.877792
2	Carbon	1.83722	2.59218	0.877799
3	Carbon	3.07731	4.71817	0.715932
4	Carbon	0.61618	4.72854	4.769200
5	Carbon	1.83740	6.84377	4.769030
6	Carbon	1.85605	2.58088	4.769040
7	Carbon	3.07731	4.71769	4.927720
8	Nitrogen	1.84878	5.42712	0.911720
9	Carbon	3.07739	7.55990	0.818531
10	Carbon	3.07729	3.29917	0.911160
11	Carbon	4.30588	5.42714	0.911754
12	Nitrogen	1.84854	4.00860	4.739020
13	Carbon	3.07729	6.13697	4.739430
14	Carbon	3.07738	1.87598	4.827160
15	Carbon	4.30612	4.00858	4.739020
16	Osmium	3.07774	4.71774	2.821900

Table 7.27. Fractional coordinates of OsNBLG after geometry optimization.

	Element	a	b	c
0	Carbon	0.125181	0.498849	0.155506
1	Carbon	0.377109	0.72649	0.155536
2	Carbon	0.373243	0.274715	0.155537
3	Carbon	0.625177	0.500024	0.126856
4	Carbon	0.125181	0.501123	0.845055
5	Carbon	0.373281	0.725292	0.845025
6	Carbon	0.37707	0.273518	0.845026
7	Carbon	0.625177	0.499973	0.873144
8	Nitrogen	0.375592	0.575157	0.161548
9	Carbon	0.625193	0.801186	0.145036
10	Carbon	0.625174	0.34964	0.161449
11	Carbon	0.87477	0.575159	0.161554
12	Nitrogen	0.375544	0.424826	0.839708
13	Carbon	0.625174	0.650386	0.83978
14	Carbon	0.625192	0.198814	0.855326
15	Carbon	0.874819	0.424823	0.839707
16	Osmium	0.625265	0.499978	0.500013

Table 7.28. Z-matrix of OsNBLG.

	Element	d (Å)	θ (°)	φ (°)
0	Carbon			
1	Carbon	2.48025		
2	Carbon	4.26293	29.7427	
3	Carbon	2.46655	30.2126	172.499
4	Carbon	4.74197	71.6302	55.2503
5	Carbon	2.44245	75.0682	178.392
6	Carbon	4.26293	30.2506	-62.198
7	Carbon	2.46629	30.2052	-172.645
8	Nitrogen	4.25921	86.6069	-64.1498
9	Carbon	2.46311	92.0645	-177.863
10	Carbon	4.26175	29.9435	71.8003
11	Carbon	2.45717	30.0228	-175.634
12	Nitrogen	4.76432	58.966	72.1758
13	Carbon	2.45759	58.9623	-179.997
14	Carbon	4.26189	30.0214	-72.0351
15	Carbon	2.46284	29.9507	175.878
16	Osmium	2.38477	91.6778	-54.683

Table 7.29. Cartesian coordinates of WOBLG before geometry optimization.

	Element	x(Å)	y(Å)	z(Å)
0	Carbon	10.88090	0.69479	0.58531
1	Carbon	15.14390	0.69479	3.04651
2	Carbon	6.61801	0.69479	3.04651
3	Carbon	10.88090	0.69479	5.50771
4	Carbon	13.00970	0.66369	1.81873
5	Carbon	17.26670	0.66369	4.27993
6	Carbon	8.74081	0.66369	4.27993
7	Carbon	13.00370	0.66369	6.74113
8	Carbon	8.76794	1.06778	1.79335
9	Carbon	13.03090	1.06778	4.25455
10	Carbon	4.50501	1.06778	4.25455
11	Carbon	8.76794	1.06778	6.71575
12	Carbon	10.89710	0.62420	3.02264
13	Carbon	15.16000	0.62420	5.48384
14	Carbon	6.63414	0.62420	5.48384
15	Carbon	10.89710	0.62420	7.94504
16	Carbon	8.96338	4.52520	0.63940
17	Carbon	13.22630	4.52520	3.10060
18	Carbon	4.70046	4.52520	3.10060
19	Carbon	8.96338	4.52520	5.56180
20	Carbon	11.07710	4.23606	1.86083
21	Carbon	15.34000	4.23606	4.32203
22	Carbon	6.81414	4.23606	4.32203
23	Carbon	11.07710	4.23606	6.78323
24	Carbon	6.83582	4.54244	1.87867
25	Carbon	11.09870	4.54244	4.33987
26	Carbon	2.57290	4.54244	4.33987
27	Carbon	6.83582	4.54244	6.80107
28	Carbon	8.93785	4.62583	3.07366
29	Carbon	13.20080	4.62583	5.53486
30	Carbon	4.67493	4.62583	5.53486

Table 7.30. (continued) Cartesian coordinates of WOBLG before geometry optimization.

	Element	x(Å)	y(Å)	z(Å)
31	Carbon	8.93785	4.62583	7.99606
32	Carbon	11.58580	0.66863	1.83371
33	Carbon	15.84870	0.66863	4.29491
34	Carbon	7.32288	0.66863	4.29491
35	Carbon	11.58580	0.66863	6.75611
36	Carbon	13.70480	0.59702	3.07946
37	Carbon	17.96780	0.59702	5.54066
38	Carbon	9.44191	0.59702	5.54066
39	Carbon	13.70480	0.59702	8.00186
40	Carbon	9.48952	1.04355	3.07517
41	Carbon	13.75240	1.04355	5.53637
42	Carbon	5.22659	1.04355	5.53637
43	Carbon	9.48952	1.04355	7.99757
44	Carbon	11.55580	1.03222	4.25565
45	Carbon	15.81870	1.03222	6.71685
46	Carbon	7.29286	1.03222	6.71685
47	Carbon	11.55580	1.03222	9.17805
48	Carbon	8.25588	4.55598	1.88626
49	Carbon	12.51880	4.55598	4.34746
50	Carbon	3.99296	4.55598	4.34746
51	Carbon	8.25588	4.55598	6.80866
52	Carbon	10.35090	4.24308	3.12161
53	Carbon	14.61380	4.24308	5.58281
54	Carbon	6.08794	4.24308	5.58281
55	Carbon	10.35090	4.24308	8.04401
56	Carbon	6.13459	4.60666	3.13228
57	Carbon	10.39750	4.60666	5.59348
58	Carbon	1.87167	4.60666	5.59348
59	Carbon	6.13459	4.60666	8.05468
60	Carbon	8.27676	4.23398	4.30744
61	Carbon	12.53970	4.23398	6.76864
62	Carbon	4.01383	4.23398	6.76864
63	Carbon	8.27676	4.23398	9.22984
64	Tungsten	8.54113	2.55928	6.62702
65	Tungsten	12.05850	3.23031	1.41897
66	Tungsten	11.35060	1.50066	4.55305
67	Oxygen	9.70851	3.79970	7.57524
68	Oxygen	13.22580	4.47073	2.36720
69	Oxygen	12.51800	2.74107	5.50128
70	Oxygen	11.33130	2.65785	3.06306
71	Oxygen	12.86130	0.62798	3.83483
72	Oxygen	13.37660	1.88717	1.55322
73	Oxygen	9.83994	2.37333	5.27127
74	Oxygen	11.36990	0.34346	6.04304
75	Oxygen	9.32463	1.11415	7.55288

Table 7.31. Fractional coordinates of WOBLG before geometry optimization.

	Element	a	b	c
0	Carbon	0.54845	0.139816	0.059634
1	Carbon	0.763321	0.139816	0.310389
2	Carbon	0.333579	0.139816	0.310389
3	Carbon	0.54845	0.139816	0.561144
4	Carbon	0.655449	0.133557	0.185299
5	Carbon	0.87032	0.133557	0.436054
6	Carbon	0.440577	0.133557	0.436054
7	Carbon	0.655449	0.133557	0.686809
8	Carbon	0.441945	0.214876	0.182712
9	Carbon	0.656816	0.214876	0.433468
10	Carbon	0.227074	0.214876	0.433468
11	Carbon	0.441945	0.214876	0.684223
12	Carbon	0.549263	0.125611	0.307957
13	Carbon	0.764134	0.125611	0.558712
14	Carbon	0.334392	0.125611	0.558712
15	Carbon	0.549263	0.125611	0.809467
16	Carbon	0.451796	0.910632	0.065144
17	Carbon	0.666668	0.910632	0.315899
18	Carbon	0.236925	0.910632	0.315899
19	Carbon	0.451796	0.910632	0.566654
20	Carbon	0.558336	0.852448	0.189587
21	Carbon	0.773207	0.852448	0.440342
22	Carbon	0.343465	0.852448	0.440342
23	Carbon	0.558336	0.852448	0.691098
24	Carbon	0.344557	0.914103	0.191405
25	Carbon	0.559429	0.914103	0.44216
26	Carbon	0.129686	0.914103	0.44216
27	Carbon	0.344557	0.914103	0.692915
28	Carbon	0.45051	0.930883	0.313154
29	Carbon	0.665381	0.930883	0.563909
30	Carbon	0.235638	0.930883	0.563909
31	Carbon	0.45051	0.930883	0.814664
32	Carbon	0.583979	0.134552	0.186824
33	Carbon	0.79885	0.134552	0.437579
34	Carbon	0.369107	0.134552	0.437579
35	Carbon	0.583979	0.134552	0.688334
36	Carbon	0.690788	0.120143	0.313745
37	Carbon	0.905659	0.120143	0.5645
38	Carbon	0.475917	0.120143	0.5645
39	Carbon	0.690788	0.120143	0.815256
40	Carbon	0.478316	0.209999	0.313308
41	Carbon	0.693187	0.209999	0.564063
42	Carbon	0.263445	0.209999	0.564063
43	Carbon	0.478316	0.209999	0.814819
44	Carbon	0.582465	0.20772	0.43358
45	Carbon	0.797337	0.20772	0.684434
46	Carbon	0.367594	0.20772	0.684434
47	Carbon	0.582465	0.20772	0.93509
48	Carbon	0.416135	0.916827	0.192179
49	Carbon	0.631006	0.916827	0.442934
50	Carbon	0.201264	0.916827	0.442934
51	Carbon	0.416135	0.916827	0.693689
52	Carbon	0.521732	0.853861	0.31804
53	Carbon	0.736603	0.853861	0.568795
54	Carbon	0.30686	0.853861	0.568795
55	Carbon	0.521732	0.853861	0.81955
56	Carbon	0.309212	0.927027	0.319127
57	Carbon	0.524083	0.927027	0.569889
58	Carbon	0.094341	0.927027	0.569889
59	Carbon	0.309212	0.927027	0.820638
60	Carbon	0.417187	0.852029	0.438856
61	Carbon	0.632059	0.852029	0.689611
62	Carbon	0.202316	0.852029	0.689611
63	Carbon	0.417187	0.852029	0.940366
64	Tungsten	0.430513	0.51502	0.675182
65	Tungsten	0.607803	0.650054	0.46388
66	Tungsten	0.572124	0.301986	0.46388
67	Oxygen	0.489354	0.764637	0.771791
68	Oxygen	0.666644	0.899671	0.241178
69	Oxygen	0.630965	0.551602	0.560488
70	Oxygen	0.57115	0.534855	0.312075
71	Oxygen	0.648269	0.126372	0.390705
72	Oxygen	0.674243	0.379766	0.158247
73	Oxygen	0.495979	0.4776	0.537055
74	Oxygen	0.573098	0.069117	0.615685
75	Oxygen	0.470005	0.224206	0.769513

Table 7.32. Cartesian coordinates of WOBLG after geometry optimization.

	Element	x(Å)	y(Å)	z(Å)
0	Carbon	0.58531	10.88090	0.62221
1	Carbon	3.04651	15.14390	0.62221
2	Carbon	3.04651	6.61801	0.62221
3	Carbon	5.50771	10.88090	0.59110
4	Carbon	1.81873	13.00370	0.59110
5	Carbon	4.27993	17.26670	0.59110
6	Carbon	4.27983	8.74081	0.59110
7	Carbon	6.74113	13.00370	0.99520
8	Carbon	1.79335	8.76794	0.99520
9	Carbon	4.25455	13.03090	0.99520
10	Carbon	4.36544	5.40401	0.99520
11	Carbon	6.71575	8.76794	0.55162
12	Carbon	3.02264	10.89710	0.55162
13	Carbon	5.48384	15.16000	0.55162
14	Carbon	5.69485	6.63414	0.55162
15	Carbon	7.94504	10.89710	4.45262
16	Carbon	0.63940	8.96338	4.45262
17	Carbon	3.10060	13.22630	4.45262
18	Carbon	3.19850	4.70046	4.45262
19	Carbon	5.56180	8.96338	4.16348
20	Carbon	1.86083	11.07710	4.16348
21	Carbon	4.32203	15.34000	4.16348
22	Carbon	4.26420	6.81414	4.16348
23	Carbon	6.78323	11.07710	4.16348
24	Carbon	1.87867	6.83582	4.46986
25	Carbon	4.33987	11.09870	4.46986
26	Carbon	4.33987	2.57290	4.46986
27	Carbon	6.80107	6.83582	4.46986
28	Carbon	3.07366	8.93785	4.55325
29	Carbon	5.53486	13.20080	4.55325
30	Carbon	5.53486	4.67493	4.55325
31	Carbon	7.99606	8.93785	4.55325
32	Carbon	1.83371	11.58580	0.59605
33	Carbon	4.29491	15.84870	0.59605
34	Carbon	4.29491	7.32288	0.59605
35	Carbon	6.75677	11.58580	0.59605
36	Carbon	3.07946	13.70480	0.52444
37	Carbon	5.54066	17.96780	0.52444
38	Carbon	5.54066	9.44191	0.52444
39	Carbon	8.00186	13.70480	0.52444
40	Carbon	3.07517	9.48952	0.97096
41	Carbon	5.53637	13.75240	0.97096
42	Carbon	5.53637	5.22659	0.97096
43	Carbon	7.99757	9.48952	0.97096
44	Carbon	4.25565	11.55580	0.95964
45	Carbon	6.71685	15.81870	0.95964
46	Carbon	6.71685	7.29286	0.95964
47	Carbon	9.17805	11.55880	0.95964
48	Carbon	1.88626	8.25588	4.48340
49	Carbon	4.34746	12.51880	4.48340
50	Carbon	4.34746	3.99296	4.48340
51	Carbon	6.80866	8.25588	4.48340
52	Carbon	3.12161	10.35090	4.17050
53	Carbon	5.58281	14.61380	4.17050
54	Carbon	5.58281	6.08794	4.17050
55	Carbon	8.04401	10.35090	4.17050
56	Carbon	3.13228	6.13459	4.53408
57	Carbon	5.59348	10.39750	4.53408
58	Carbon	5.59348	1.87167	4.53408
59	Carbon	8.05468	6.13459	4.53408
60	Carbon	4.30744	8.27676	4.16140
61	Carbon	6.76864	12.53970	4.16140
62	Carbon	6.76864	4.01383	4.16140
63	Carbon	9.22984	8.27676	4.16140
64	Tungsten	4.32203	6.81414	2.21398
65	Tungsten	4.32203	13.13440	2.21398
66	Tungsten	6.14653	9.97427	2.21398
67	Oxygen	4.32203	6.81414	4.16348
68	Oxygen	4.32203	13.13440	4.16348
69	Oxygen	6.14653	9.97427	4.16348
70	Oxygen	4.81829	9.97427	2.21398
71	Oxygen	7.47476	11.31420	2.21398
72	Oxygen	6.14653	13.61470	2.21398
73	Oxygen	4.81829	13.61470	2.21398
74	Oxygen	7.47476	8.63438	2.21398
75	Oxygen	6.14653	6.33380	2.21398

Table 7.33. Fractional coordinates of WOBLG after geometry optimization.

	Element	a	b	c
0	Carbon	0.059634	0.54845	0.122537
1	Carbon	0.310389	0.763321	0.122537
2	Carbon	0.310389	0.333579	0.122537
3	Carbon	0.561144	0.54845	0.122537
4	Carbon	0.185299	0.655449	0.116412
5	Carbon	0.436054	0.87032	0.116412
6	Carbon	0.436054	0.440577	0.116412
7	Carbon	0.686809	0.655449	0.116412
8	Carbon	0.182712	0.441945	0.195995
9	Carbon	0.433468	0.565816	0.195995
10	Carbon	0.433468	0.227074	0.195995
11	Carbon	0.684223	0.441945	0.195995
12	Carbon	0.307957	0.549263	0.108636
13	Carbon	0.558712	0.764134	0.108636
14	Carbon	0.558712	0.334392	0.108636
15	Carbon	0.809467	0.549263	0.108636
16	Carbon	0.065144	0.451796	0.876898
17	Carbon	0.315899	0.666668	0.876898
18	Carbon	0.315899	0.236925	0.876898
19	Carbon	0.566654	0.451796	0.876898
20	Carbon	0.189587	0.558336	0.819956
21	Carbon	0.440342	0.773207	0.819956
22	Carbon	0.440342	0.343465	0.819956
23	Carbon	0.691098	0.558336	0.819956
24	Carbon	0.191405	0.344557	0.880295
25	Carbon	0.44216	0.559429	0.880295
26	Carbon	0.44216	0.129686	0.880295
27	Carbon	0.692915	0.344557	0.880295
28	Carbon	0.313154	0.45051	0.896716
29	Carbon	0.563909	0.665381	0.896716
30	Carbon	0.563909	0.235638	0.896716
31	Carbon	0.814664	0.45051	0.896716
32	Carbon	0.186824	0.583979	0.117385
33	Carbon	0.437579	0.79885	0.117385
34	Carbon	0.437579	0.369107	0.117385
35	Carbon	0.688334	0.583989	0.117385
36	Carbon	0.313745	0.690788	0.103284
37	Carbon	0.5645	0.905659	0.103284
38	Carbon	0.5645	0.475917	0.103284
39	Carbon	0.815256	0.690788	0.103284
40	Carbon	0.313308	0.478316	0.191222
41	Carbon	0.564063	0.693187	0.191222
42	Carbon	0.564063	0.263445	0.191222
43	Carbon	0.814819	0.478316	0.191222
44	Carbon	0.43358	0.582465	0.188992
45	Carbon	0.684335	0.797337	0.188992
46	Carbon	0.684335	0.367594	0.188992
47	Carbon	0.93509	0.582465	0.882961
48	Carbon	0.192179	0.416135	0.882961
49	Carbon	0.442934	0.631006	0.882961
50	Carbon	0.442934	0.201264	0.882961
51	Carbon	0.693689	0.416135	0.821338
52	Carbon	0.31804	0.521732	0.821338
53	Carbon	0.568795	0.736603	0.821338
54	Carbon	0.568795	0.30686	0.821338
55	Carbon	0.81955	0.521732	0.892942
56	Carbon	0.319127	0.309212	0.892942
57	Carbon	0.569883	0.524083	0.892942
58	Carbon	0.569883	0.094341	0.892942
59	Carbon	0.820638	0.309212	0.819546
60	Carbon	0.438856	0.417187	0.819546
61	Carbon	0.689611	0.632059	0.819546
62	Carbon	0.689611	0.202316	0.819546
63	Carbon	0.940366	0.417187	0.819546
64	Tungsten	0.440342	0.343465	0.436022
65	Tungsten	0.440342	0.662035	0.436022
66	Tungsten	0.626229	0.50275	0.436022
67	Oxygen	0.440342	0.343465	0.819956
68	Oxygen	0.440342	0.662035	0.819956
69	Oxygen	0.626229	0.50275	0.819956
70	Oxygen	0.490903	0.570287	0.436022
71	Oxygen	0.761554	0.570287	0.436022
72	Oxygen	0.626229	0.686246	0.436022
73	Oxygen	0.490903	0.435213	0.436022
74	Oxygen	0.761554	0.435213	0.436022
75	Oxygen	0.626229	0.319253	0.436022

Table 7.34. Z-matrix of WOBLG.

	Element	d (Å)	θ (°)	ϕ (°)
0	Carbon			
1	Carbon	4.9224		
2	Carbon	8.52585	30	
3	Carbon	4.9224	30	-180
4	Carbon	4.25627	89.918	-0.41868
5	Carbon	4.9224	89.918	180
6	Carbon	8.52585	30	0.41868
7	Carbon	4.9224	30	180
8	Carbon	6.25278	19.7425	10.563
9	Carbon	4.9224	19.7425	-180
10	Carbon	8.52585	30	-10.563
11	Carbon	4.9224	30	-180
12	Carbon	4.28591	89.9642	-5.94064
13	Carbon	4.9224	89.9642	-180
14	Carbon	8.52585	30	5.94064
15	Carbon	4.9224	30	-180
16	Carbon	8.50466	51.214	36.0469
17	Carbon	4.9224	51.214	180
18	Carbon	8.52585	30	-36.0469
19	Carbon	4.9224	30	180
20	Carbon	4.27182	89.732	-3.881
21	Carbon	4.9224	89.732	180
22	Carbon	8.52585	30	3.881
23	Carbon	4.9224	30	-180
24	Carbon	6.49128	19.3313	8.19726
25	Carbon	4.9224	19.3313	-180
26	Carbon	8.52585	30	-8.19726
27	Carbon	4.9224	30	180
28	Carbon	4.28008	89.4204	1.11634
29	Carbon	4.9224	89.4204	-180
30	Carbon	8.52585	30	-1.11634
31	Carbon	4.9224	30	-180
32	Carbon	7.78753	84.1926	-30.7149
33	Carbon	4.9224	84.1926	-180
34	Carbon	8.52585	30	30.7149
35	Carbon	4.9224	30	-180
36	Carbon	4.24419	89.957	-0.96667
37	Carbon	4.9224	89.957	180
38	Carbon	8.52585	30	0.966661
39	Carbon	4.9224	30	-180
40	Carbon	6.49927	19.8292	11.6852
41	Carbon	4.9224	19.8292	180
42	Carbon	8.52585	30	-11.6852
43	Carbon	4.9224	30	180
44	Carbon	4.27452	88.9072	-0.15181
45	Carbon	4.9224	88.9072	-180
46	Carbon	8.52585	30	0.15181
47	Carbon	4.9224	30	-180
48	Carbon	8.74508	41.9527	37.0664
49	Carbon	4.9224	41.9527	-180
50	Carbon	8.52585	30	-37.0664
51	Carbon	4.9224	30	180
52	Carbon	4.2522	89.6063	-4.22003
53	Carbon	4.9224	89.6063	-180
54	Carbon	8.52585	30	4.22003
55	Carbon	4.9224	30	-180
56	Carbon	6.48338	19.612	9.6179
57	Carbon	4.9224	19.612	-180
58	Carbon	8.52585	30	-9.6179
59	Carbon	4.9224	30	180
60	Carbon	4.33239	89.756	-4.93486
61	Carbon	4.9224	89.756	180
62	Carbon	8.52585	30	4.93486
63	Carbon	4.9224	30	-180
64	Tungsten	5.4789	47.2288	-28.9603
65	Tungsten	6.32025	74.5169	165.45
66	Tungsten	3.649	30	21.6432
67	Oxygen	4.13712	116.168	-31.6707
68	Oxygen	6.32025	40.1955	-24.0011
69	Oxygen	3.649	30	-46.897
70	Oxygen	2.71295	47.7384	76.1585
71	Oxygen	2.65647	60.6862	105.342
72	Oxygen	2.65647	60	-124.501
73	Oxygen	5.15443	44.9329	0
74	Oxygen	2.65647	75.0671	0
75	Oxygen	2.65647	60	-180

Table 7.35. Cartesian coordinates of ReOBLG before geometry optimization.

	Element	x(Å)	y(Å)	z(Å)
0	Carbon	10.88090	0.62221	0.58531
1	Carbon	15.14390	0.62221	3.04651
2	Carbon	6.61801	0.62221	3.04651
3	Carbon	10.88090	0.62221	5.50771
4	Carbon	13.00370	0.59110	1.81873
5	Carbon	17.26670	0.59110	4.27993
6	Carbon	8.74081	0.59110	4.27993
7	Carbon	13.00370	0.59110	6.74113
8	Carbon	8.76794	0.99520	1.79335
9	Carbon	13.03090	0.99520	4.25455
10	Carbon	4.50501	0.99520	4.25455
11	Carbon	8.76794	0.99520	6.71575
12	Carbon	10.89710	0.55162	3.02264
13	Carbon	15.16000	0.55162	5.48384
14	Carbon	6.63414	0.55162	5.48384
15	Carbon	10.89710	0.55162	7.94504
16	Carbon	8.96338	4.45262	0.63940
17	Carbon	13.22630	4.45262	3.10060
18	Carbon	4.70046	4.45262	3.10060
19	Carbon	8.96338	4.45262	5.56180
20	Carbon	11.07710	4.16348	1.86083
21	Carbon	15.34000	4.16348	4.32203
22	Carbon	6.81414	4.16348	4.32203
23	Carbon	11.07710	4.16348	6.78323
24	Carbon	6.83582	4.46986	1.87867
25	Carbon	11.09870	4.46986	4.33987
26	Carbon	2.57290	4.46986	4.33987
27	Carbon	6.83582	4.46986	6.80107
28	Carbon	8.93785	4.55325	3.07366
29	Carbon	13.20080	4.55325	5.53486
30	Carbon	4.67493	4.55325	5.53486
31	Carbon	8.93785	4.55325	7.99606
32	Carbon	11.58580	0.59605	1.83371
33	Carbon	15.84870	0.59605	4.29491
34	Carbon	7.32288	0.59605	4.29491
35	Carbon	11.58580	0.59605	6.75611
36	Carbon	13.70480	0.52444	3.07946
37	Carbon	17.96780	0.52444	5.54066
38	Carbon	9.44191	0.52444	5.54066
39	Carbon	13.70480	0.52444	8.00186
40	Carbon	9.48952	0.97096	3.07517
41	Carbon	13.75240	0.97096	5.53637
42	Carbon	5.22659	0.97096	5.53637
43	Carbon	9.48952	0.97096	7.99757
44	Carbon	11.55580	0.95964	4.25565
45	Carbon	15.81870	0.95964	6.71685
46	Carbon	7.29286	0.95964	6.71685
47	Carbon	11.55580	0.95964	9.17805
48	Carbon	8.25588	4.48340	1.88626
49	Carbon	12.51880	4.48340	4.34746
50	Carbon	3.99296	4.48340	4.34746
51	Carbon	8.25588	4.48340	6.80866
52	Carbon	10.35090	4.17050	3.12161
53	Carbon	14.61380	4.17050	5.58281
54	Carbon	6.08794	4.17050	5.58281
55	Carbon	10.35090	4.17050	8.04401
56	Carbon	6.13459	4.53408	3.13228
57	Carbon	10.39750	4.53408	5.59348
58	Carbon	1.87167	4.53408	5.59348
59	Carbon	6.13459	4.53408	8.05468
60	Carbon	8.27676	4.16140	4.30744
61	Carbon	12.53970	4.16140	6.76864
62	Carbon	4.01383	4.16140	6.76864
63	Carbon	8.27676	4.16140	9.22984
64	Rhenium	10.08720	2.49320	4.75135
65	Oxygen	11.95420	2.49320	4.75135
66	Oxygen	10.08720	2.49320	6.61835
67	Oxygen	10.08720	4.36020	4.75135

Table 7.36. Fractional coordinates of ReOBLG before geometry optimization.

	Element	a	b	c
0	Carbon	0.54845	0.139816	0.059634
1	Carbon	0.763321	0.139816	0.310389
2	Carbon	0.333579	0.139816	0.310389
3	Carbon	0.54845	0.139816	0.561144
4	Carbon	0.655449	0.133557	0.185299
5	Carbon	0.87032	0.133557	0.436054
6	Carbon	0.440577	0.133557	0.436054
7	Carbon	0.655449	0.133557	0.686809
8	Carbon	0.441945	0.214876	0.182712
9	Carbon	0.656816	0.214876	0.433468
10	Carbon	0.227074	0.214876	0.433468
11	Carbon	0.441945	0.214876	0.684223
12	Carbon	0.549263	0.125611	0.307957
13	Carbon	0.764134	0.125611	0.558712
14	Carbon	0.334392	0.125611	0.558712
15	Carbon	0.549263	0.125611	0.809467
16	Carbon	0.451796	0.910632	0.065144
17	Carbon	0.666668	0.910632	0.315899
18	Carbon	0.236925	0.910632	0.315899
19	Carbon	0.451796	0.910632	0.566654
20	Carbon	0.558336	0.852448	0.189587
21	Carbon	0.773207	0.852448	0.440342
22	Carbon	0.343465	0.852448	0.440342
23	Carbon	0.558336	0.852448	0.691098
24	Carbon	0.344557	0.914103	0.191405
25	Carbon	0.559429	0.914103	0.44216
26	Carbon	0.129686	0.914103	0.44216
27	Carbon	0.344557	0.914103	0.692915
28	Carbon	0.45051	0.930883	0.313154
29	Carbon	0.665381	0.930883	0.563909
30	Carbon	0.235638	0.930883	0.563909
31	Carbon	0.45051	0.930883	0.814664
32	Carbon	0.583979	0.134552	0.186824
33	Carbon	0.79885	0.134552	0.437579
34	Carbon	0.369107	0.134552	0.437579
35	Carbon	0.583979	0.134552	0.688334
36	Carbon	0.690788	0.120143	0.313745
37	Carbon	0.905659	0.120143	0.5645
38	Carbon	0.475917	0.120143	0.5645
39	Carbon	0.690788	0.120143	0.815256
40	Carbon	0.478316	0.209999	0.313308
41	Carbon	0.693187	0.209999	0.564063
42	Carbon	0.263445	0.209999	0.564063
43	Carbon	0.478316	0.209999	0.814819
44	Carbon	0.582465	0.20772	0.43358
45	Carbon	0.797337	0.20772	0.684335
46	Carbon	0.367594	0.20772	0.684335
47	Carbon	0.582465	0.20772	0.93509
48	Carbon	0.416135	0.916827	0.192179
49	Carbon	0.631006	0.916827	0.442934
50	Carbon	0.201264	0.916827	0.442934
51	Carbon	0.416135	0.916827	0.693689
52	Carbon	0.521732	0.853861	0.31804
53	Carbon	0.736603	0.853861	0.568795
54	Carbon	0.30686	0.853861	0.568795
55	Carbon	0.521732	0.853861	0.81955
56	Carbon	0.309212	0.927027	0.319127
57	Carbon	0.524083	0.927027	0.569883
58	Carbon	0.094341	0.927027	0.569883
59	Carbon	0.309212	0.927027	0.820638
60	Carbon	0.417187	0.852029	0.438856
61	Carbon	0.632059	0.852029	0.689611
62	Carbon	0.202316	0.852029	0.689611
63	Carbon	0.417187	0.852029	0.940366
64	Rhenium	0.430513	0.51502	0.675182
65	Oxygen	0.954985	0.488522	0.268114
66	Oxygen	0.465098	0.457985	0.523487
67	Oxygen	0.445211	0.632451	0.503004

Table 7.37. Cartesian coordinates of ReOBLG after geometry optimization.

	Element	x(Å)	y(Å)	z(Å)
0	Carbon	0.30774	9.91726	1.42642
1	Carbon	22.38527	14.71210	1.34912
2	Carbon	2.89131	5.68680	1.43423
3	Carbon	4.76561	10.44500	0.69628
4	Carbon	1.13464	12.48780	1.25974
5	Carbon	4.11940	16.72180	1.75813
6	Carbon	3.51915	8.23180	0.93735
7	Carbon	6.01491	12.59420	0.95695
8	Carbon	0.90045	8.78312	1.33465
9	Carbon	3.55380	12.65090	0.77878
10	Carbon	3.19868	4.35448	1.75959
11	Carbon	6.06506	8.38394	1.22998
12	Carbon	2.38506	10.49370	0.92909
13	Carbon	4.78537	14.73010	1.18433
14	Carbon	5.00036	6.17587	1.42808
15	Carbon	7.20794	10.57410	1.25845
16	Carbon	0.47036	9.07708	5.58441
17	Carbon	2.89165	13.06900	5.90581
18	Carbon	2.46772	4.24979	5.57688
19	Carbon	4.88244	8.43874	6.32325
20	Carbon	1.05607	10.15800	5.91233
21	Carbon	3.10246	14.39990	5.50110
22	Carbon	3.69618	6.30719	5.89129
23	Carbon	6.15743	10.55660	6.17511
24	Carbon	1.29415	6.51488	5.57721
25	Carbon	3.62613	10.59020	6.40106
26	Carbon	4.11300	2.12524	5.40662
27	Carbon	6.12749	6.34921	5.66243
28	Carbon	2.48287	8.40045	6.32131
29	Carbon	5.02119	12.73220	5.99433
30	Carbon	4.86727	4.18746	5.41580
31	Carbon	7.35635	8.40954	5.82916
32	Carbon	1.08902	11.12500	1.20260
33	Carbon	3.45905	15.46280	1.43396
34	Carbon	3.63171	6.83634	1.18104
35	Carbon	5.96340	11.15110	0.85188
36	Carbon	2.28842	13.30210	1.09792
37	Carbon	5.38937	17.16430	1.77988
38	Carbon	4.78344	9.00158	0.92517
39	Carbon	7.36876	12.82250	1.42681
40	Carbon	2.30227	9.00339	1.02589
41	Carbon	4.83222	13.34750	0.91655
42	Carbon	4.44879	4.86375	1.68318
43	Carbon	7.34247	9.14716	1.48406
44	Carbon	3.55409	11.22740	0.62923
45	Carbon	5.60234	15.81040	1.43742
46	Carbon	6.02373	7.00702	1.42844
47	Carbon	8.02225	11.74150	1.51566
48	Carbon	1.21732	7.84000	5.82697
49	Carbon	3.69845	11.99680	6.24821
50	Carbon	3.51473	3.46096	5.47758
51	Carbon	6.04561	7.75918	5.99418
52	Carbon	2.42430	9.85110	6.32865
53	Carbon	4.37534	13.97010	5.58487
54	Carbon	4.94852	5.58714	5.65693
55	Carbon	7.28536	9.74637	5.99008
56	Carbon	2.39456	5.66272	5.66444
57	Carbon	4.88279	9.85651	6.39732
58	Carbon	5.36708	1.63607	5.31910
59	Carbon	7.53200	6.17493	5.33011
60	Carbon	3.67682	7.67286	6.27169
61	Carbon	6.08016	11.95780	6.00003
62	Carbon	5.61693	3.02923	5.33699
63	Carbon	8.18614	7.25514	5.49377
64	Rhenium	3.70378	9.97745	2.74605
65	Oxygen	8.35788	8.58240	1.91933
66	Oxygen	3.70108	8.58598	3.75764
67	Oxygen	3.86879	11.50260	3.53493

Table 7.38. Fractional coordinates of ReOBLG after geometry optimization.

	Element	a	b	c
0	Carbon	0.035513	0.527505	0.202897
1	Carbon	0.275256	0.782547	0.1919
2	Carbon	0.333653	0.308484	0.204007
3	Carbon	0.549944	0.555578	0.099039
4	Carbon	0.130935	0.664236	0.179188
5	Carbon	0.475372	0.889444	0.250079
6	Carbon	0.406105	0.437854	0.13333
7	Carbon	0.694112	0.669893	0.136118
8	Carbon	0.10391	0.467179	0.189843
9	Carbon	0.410104	0.67291	0.110775
10	Carbon	0.369123	0.231617	0.250287
11	Carbon	0.699899	0.445946	0.174955
12	Carbon	0.275232	0.558165	0.132155
13	Carbon	0.552224	0.783503	0.168461
14	Carbon	0.577034	0.328498	0.203133
15	Carbon	0.831786	0.562444	0.179004
16	Carbon	0.054278	0.482815	0.794335
17	Carbon	0.333692	0.695146	0.840051
18	Carbon	0.284771	0.226049	0.793264
19	Carbon	0.563427	0.448862	0.899429
20	Carbon	0.121869	0.54031	0.840978
21	Carbon	0.358019	0.76594	0.782486
22	Carbon	0.426534	0.335483	0.837986
23	Carbon	0.710558	0.34653	0.878357
24	Carbon	0.149343	0.563301	0.793311
25	Carbon	0.41845	0.113043	0.910497
26	Carbon	0.474634	0.337718	0.769046
27	Carbon	0.707104	0.446825	0.805432
28	Carbon	0.28652	0.677235	0.899152
29	Carbon	0.579519	0.222733	0.852643
30	Carbon	0.561676	0.447308	0.770352
31	Carbon	0.848911	0.591746	0.829148
32	Carbon	0.125671	0.822473	0.17106
33	Carbon	0.399169	0.363629	0.203969
34	Carbon	0.419094	0.363132	0.167993
35	Carbon	0.688168	0.593132	0.121173
36	Carbon	0.26408	0.707549	0.15617
37	Carbon	0.621925	0.912977	0.253173
38	Carbon	0.552002	0.478799	0.131597
39	Carbon	0.850344	0.682036	0.202952
40	Carbon	0.265679	0.478895	0.145924
41	Carbon	0.557631	0.70996	0.130371
42	Carbon	0.513384	0.258705	0.239417
43	Carbon	0.84731	0.486543	0.211095
44	Carbon	0.410136	0.59719	0.089503
45	Carbon	0.646501	0.840964	0.204461
46	Carbon	0.695129	0.372707	0.203183
47	Carbon	0.925756	0.624537	0.21559
48	Carbon	0.140477	0.417014	0.828838
49	Carbon	0.426796	0.638116	0.888755
50	Carbon	0.405595	0.184091	0.779139
51	Carbon	0.697654	0.412715	0.852622
52	Carbon	0.279761	0.523986	0.900197
53	Carbon	0.504907	0.743078	0.7944
54	Carbon	0.571052	0.297183	0.804651
55	Carbon	0.84072	0.518415	0.852038
56	Carbon	0.276329	0.301203	0.805719
57	Carbon	0.563466	0.524273	0.909965
58	Carbon	0.619353	0.087023	0.756597
59	Carbon	0.869182	0.328448	0.758163
60	Carbon	0.424299	0.408124	0.892094
61	Carbon	0.701642	0.636043	0.853453
62	Carbon	0.648185	0.161127	0.759142
63	Carbon	0.944668	0.385905	0.781442
64	Rhenium	0.427411	0.530706	0.390602
65	Oxygen	0.964487	0.456503	0.273008
66	Oxygen	0.427099	0.456693	0.534493
67	Oxygen	0.446453	0.611832	0.502815

Table 7.39. Z-matrix of ReOBLG.

	Element	d (Å)	θ (°)	ϕ (°)
0	Carbon			
1	Carbon	5.22617		
2	Carbon	9.03991	26.6351	
3	Carbon	5.16705	25.7847	162.825
4	Carbon	4.20411	96.6055	-7.2685
5	Carbon	5.20421	84.9983	164.501
6	Carbon	8.55071	30.9909	-6.70171
7	Carbon	5.02591	26.2261	167.722
8	Carbon	6.38943	23.7967	-3.1442
9	Carbon	4.72326	19.0801	-160.802
10	Carbon	8.36176	31.7721	7.34747
11	Carbon	4.97324	32.7682	-178.869
12	Carbon	4.25252	84.8787	-1.69263
13	Carbon	4.8587	90.0769	170.467
14	Carbon	8.56041	31.3088	-4.04184
15	Carbon	4.92411	28.0807	170.376
16	Carbon	8.14556	56.4074	37.7212
17	Carbon	4.67986	56.7529	171.044
18	Carbon	8.83548	28.5022	-45.7575
19	Carbon	4.89237	27.871	-169.485
20	Carbon	4.21495	83.4718	7.51787
21	Carbon	4.72765	88.9409	-166.655
22	Carbon	8.12385	29.9613	8.85884
23	Carbon	4.91892	34.7908	-164.968
24	Carbon	6.35172	20.2403	2.99306
25	Carbon	4.76712	20.8048	161.02
26	Carbon	8.53711	32.8701	-14.1853
27	Carbon	4.68675	28.2967	166.336
28	Carbon	4.23379	94.3088	0.567724
29	Carbon	5.03169	88.4298	-173.979
30	Carbon	8.56579	30.2866	5.35159
31	Carbon	4.91857	29.4125	-162.866
32	Carbon	8.24974	84.4291	-33.1469
33	Carbon	4.94838	84.1722	-179.259
34	Carbon	8.63184	29.7922	32.7241
35	Carbon	4.91549	30.0282	166.902
36	Carbon	4.26534	91.7257	-6.63504
37	Carbon	4.99968	82.1287	167.662
38	Carbon	8.22963	34.3082	-5.36733
39	Carbon	4.64057	29.667	176.899
40	Carbon	6.35733	19.0134	5.78437
41	Carbon	5.02829	23.2767	-159.77
42	Carbon	8.52693	27.855	3.43047
43	Carbon	5.17307	31.5218	177.073
44	Carbon	4.40566	85.2638	-5.14755
45	Carbon	5.08454	92.7716	166.911
46	Carbon	8.81345	28.2085	-5.53226
47	Carbon	5.13975	25.6411	162.591
48	Carbon	8.95077	46.4522	44.7962
49	Carbon	4.85926	44.0028	167.953
50	Carbon	8.57252	29.4817	-50.1333
51	Carbon	5.01467	29.1275	-178.09
52	Carbon	4.19546	89.998	4.60851
53	Carbon	4.618	93.8549	-164.435
54	Carbon	8.40284	30.4133	9.84392
55	Carbon	4.78237	33.5177	-154.332
56	Carbon	6.37983	20.7988	9.22794
57	Carbon	4.93115	20.1516	166.528
58	Carbon	8.30499	33.7281	-14.4045
59	Carbon	5.02875	29.7065	162.761
60	Carbon	4.24179	85.8683	-2.09173
61	Carbon	4.92043	81.4512	-177.609
62	Carbon	8.96514	27.3207	3.06667
63	Carbon	4.9481	28.3895	-168.719
64	Rhenium	5.92051	89.1342	-33.2044
65	Oxygen	4.92851	39.8935	-111.177
66	Oxygen	5.00652	19.9228	31.068
67	Oxygen	2.92995	85.386	-31.1768

Table 7.40. Cartesian coordinates of OsOBLG after geometry optimization.

	Element	x(Å)	y(Å)	z(Å)
0	Carbon	10.52500	9.81040	10.27210
1	Carbon	15.27820	10.15730	12.42640
2	Carbon	5.25378	10.75880	13.02980
3	Carbon	11.03500	9.48103	14.77260
4	Carbon	13.03590	10.07640	11.21230
5	Carbon	17.38100	10.18010	14.08840
6	Carbon	8.89250	9.15238	13.50530
7	Carbon	13.19220	0.82114	16.11420
8	Carbon	9.46454	9.47773	10.88950
9	Carbon	13.21180	9.88728	13.64400
10	Carbon	4.83297	10.24510	14.13940
11	Carbon	8.92244	9.59217	15.99350
12	Carbon	11.11990	9.46859	12.42260
13	Carbon	15.35070	9.98719	14.83520
14	Carbon	6.22832	9.65026	15.70730
15	Carbon	10.99100	9.95906	17.31200
16	Carbon	9.38713	14.39250	10.44010
17	Carbon	13.63670	13.78860	13.20520
18	Carbon	4.60571	14.46090	12.54650
19	Carbon	8.89188	14.28180	14.98710
20	Carbon	10.52210	14.20910	10.97020
21	Carbon	15.01000	13.69160	13.53410
22	Carbon	6.69145	14.42310	13.77030
23	Carbon	10.96000	14.11640	16.31450
24	Carbon	6.81976	14.55890	11.30280
25	Carbon	11.06060	13.96300	13.74830
26	Carbon	2.52953	14.05410	14.19440
27	Carbon	6.68724	14.35690	16.23630
28	Carbon	8.79676	14.30180	12.58620
29	Carbon	13.18270	14.12580	15.27980
30	Carbon	4.55222	14.38020	14.93400
31	Carbon	8.80010	14.46380	17.60980
32	Carbon	11.71520	9.81186	11.12550
33	Carbon	16.05820	10.08890	13.48200
34	Carbon	6.66459	10.95780	12.67150
35	Carbon	11.69310	10.07320	15.93680
36	Carbon	13.86940	10.07400	12.34940
37	Carbon	17.86080	10.16430	15.35540
38	Carbon	9.66767	9.30175	14.75370
39	Carbon	13.29900	9.72899	17.51920
40	Carbon	9.66871	9.29235	12.33100
41	Carbon	13.95110	9.90056	14.92140
42	Carbon	4.90850	9.64210	15.36310
43	Carbon	9.58075	10.08450	17.17540
44	Carbon	11.82870	9.55601	13.60930
45	Carbon	16.48660	10.07330	15.61430
46	Carbon	7.56709	9.56314	15.69660
47	Carbon	12.15460	9.73528	18.12140
48	Carbon	8.19083	14.47440	11.30160
49	Carbon	12.50450	14.12510	13.87760
50	Carbon	3.82215	14.38460	13.59940
51	Carbon	8.15121	13.86650	16.19670
52	Carbon	10.26390	13.95450	12.43380
53	Carbon	14.18880	13.78600	14.76000
54	Carbon	5.95199	14.38590	15.01440
55	Carbon	10.10030	13.94560	17.51450
56	Carbon	6.02563	14.50680	12.46170
57	Carbon	10.26680	14.21160	15.00710
58	Carbon	2.07492	13.78660	15.44610
59	Carbon	6.55113	14.90210	17.50780
60	Carbon	8.11323	14.37240	13.78970
61	Carbon	12.37410	14.14290	16.32420
62	Carbon	3.44039	14.03740	15.69820
63	Carbon	7.67533	14.90520	18.20910
64	Osmium	6.89986	9.30222	13.80100
65	Osmium	10.15810	12.07340	16.90140
66	Oxygen	7.31703	11.69600	11.98410
67	Oxygen	10.61740	12.71910	13.06570
68	Oxygen	11.61490	11.54230	15.78490
69	Oxygen	8.30700	12.47070	16.42370

Table 7.41. Fractional coordinates of OsOBLG after geometry optimization.

	Element	a	b	c
0	Carbon	0.530507	0.408277	0.358605
1	Carbon	0.770092	0.422714	0.433813
2	Carbon	0.264815	0.447745	0.45488
3	Carbon	0.556214	0.39457	0.515723
4	Carbon	0.657068	0.419346	0.39143
5	Carbon	0.876082	0.423662	0.491835
6	Carbon	0.448223	0.380892	0.471479
7	Carbon	0.664949	0.408724	0.562556
8	Carbon	0.477057	0.394414	0.380159
9	Carbon	0.665937	0.411476	0.47632
10	Carbon	0.243604	0.426366	0.493616
11	Carbon	0.449733	0.399195	0.558346
12	Carbon	0.560493	0.394052	0.43368
13	Carbon	0.773747	0.415634	0.517907
14	Carbon	0.131936	0.401612	0.548351
15	Carbon	0.553997	0.414463	0.604374
16	Carbon	0.473155	0.59897	0.364469
17	Carbon	0.687353	0.573837	0.461002
18	Carbon	0.232149	0.601814	0.438007
19	Carbon	0.448192	0.59436	0.52321
20	Carbon	0.530362	0.591335	0.382976
21	Carbon	0.756574	0.569799	0.472484
22	Carbon	0.33728	0.600243	0.480731
23	Carbon	0.552435	0.58748	0.569551
24	Carbon	0.343748	0.605895	0.394589
25	Carbon	0.557504	0.581095	0.479961
26	Carbon	0.1275	0.584884	0.495536
27	Carbon	0.337068	0.597487	0.566819
28	Carbon	0.443398	0.595196	0.439394
29	Carbon	0.66447	0.587869	0.533427
30	Carbon	0.229453	0.598458	0.521357
31	Carbon	0.443566	0.601937	0.61477
32	Carbon	0.590501	0.408337	0.3884
33	Carbon	0.809408	0.419869	0.470665
34	Carbon	0.335926	0.456026	0.442369
35	Carbon	0.589386	0.419215	0.556364
36	Carbon	0.699083	0.419246	0.431127
37	Carbon	0.900267	0.423004	0.536068
38	Carbon	0.487296	0.387108	0.515062
39	Carbon	0.67033	0.404889	0.611608
40	Carbon	0.481348	0.386717	0.430483
41	Carbon	0.7032	0.412029	0.520916
42	Carbon	0.247412	0.401273	0.536338
43	Carbon	0.482915	0.419683	0.599606
44	Carbon	0.596221	0.39769	0.475108
45	Carbon	0.830999	0.419216	0.545106
46	Carbon	0.381417	0.397987	0.54798
47	Carbon	0.612647	0.40515	0.632629
48	Carbon	0.412856	0.602378	0.394547
49	Carbon	0.630287	0.58784	0.484476
50	Carbon	0.192654	0.598641	0.47478
51	Carbon	0.410859	0.57708	0.565438
52	Carbon	0.517349	0.58074	0.434072
53	Carbon	0.730304	0.573728	0.515281
54	Carbon	0.300001	0.598695	0.524163
55	Carbon	0.509104	0.58037	0.611444
56	Carbon	0.30372	0.603726	0.435048
57	Carbon	0.517494	0.591442	0.52391
58	Carbon	0.104586	0.573752	0.539234
59	Carbon	0.330208	0.620178	0.611208
60	Carbon	0.408945	0.598132	0.481409
61	Carbon	0.62371	0.58858	0.569889
62	Carbon	0.173412	0.584191	0.548036
63	Carbon	0.386873	0.620307	0.635691
64	Osmium	0.347785	0.387128	0.481802
65	Osmium	0.512015	0.502455	0.590041
66	Oxygen	0.761554	0.570287	0.940366
67	Oxygen	0.490903	0.686246	0.484083
68	Oxygen	0.761554	0.435213	0.674299
69	Oxygen	0.626229	0.319253	0.484083

Table 7.42. Z-matrix of OsOBLG.

	Element	d (Å)	θ (°)	ϕ (°)
0	Carbon			
1	Carbon	5.23014		
2	Carbon	10.0605	28.7324	
3	Carbon	6.17189	21.7559	141.5
4	Carbon	4.12719	100.408	-10.5492
5	Carbon	5.21176	86.0444	164.411
6	Carbon	8.57032	30.0393	3.4447
7	Carbon	5.07354	27.1049	-167.102
8	Carbon	6.42737	23.5732	9.44956
9	Carbon	4.66877	18.2349	-174.838
10	Carbon	8.4011	40.3621	-15.2787
11	Carbon	4.53739	28.8459	156.286
12	Carbon	4.19476	97.3831	-10.9941
13	Carbon	4.89793	91.7218	165.74
14	Carbon	9.17016	35.2794	-3.08177
15	Carbon	5.03523	24.0927	176.351
16	Carbon	8.33377	65.6564	40.4996
17	Carbon	5.10583	47.9582	179.094
18	Carbon	9.07989	28.8535	-34.3418
19	Carbon	4.9224	89.732	180.7652
20	Carbon	8.52585	30.1256	3.881
21	Carbon	5.1945	82.4856	-176.33
22	Carbon	8.35399	31.2319	1.46614
23	Carbon	4.97871	32.3637	-175.925
24	Carbon	6.51571	19.6046	5.50514
25	Carbon	4.9315	20.6013	-170.205
26	Carbon	8.54318	33.4765	16.9096
27	Carbon	4.64193	29.4544	-159.573
28	Carbon	4.21613	93.8123	6.90129
29	Carbon	5.15001	88.497	-174.222
30	Carbon	8.64115	29.2472	0.845167
31	Carbon	5.02108	30.0262	-174.17
32	Carbon	8.49614	82.7869	-28.3291
33	Carbon	4.94885	84.6662	176.052
34	Carbon	9.46845	25.0066	13.3294
35	Carbon	6.06056	28.0349	152.719
36	Carbon	4.19589	88.263	-4.81798
37	Carbon	4.99752	84.2606	170.563
38	Carbon	8.26034	33.0838	9.30061
39	Carbon	4.568443	32.9313	-172.065
40	Carbon	6.34722	17.7235	1.00486
41	Carbon	5.04172	23.9246	177.02
42	Carbon	9.05705	34.2678	-13.228
43	Carbon	5.0309	24.1936	178.761
44	Carbon	4.24853	100.258	-0.94268
45	Carbon	5.0974	98.0879	179.517
46	Carbon	8.93441	23.8786	3.00804
47	Carbon	5.19171	28.3907	170.937
48	Carbon	9.20216	44.793	46.519
49	Carbon	5.03645	38.3994	-177.581
50	Carbon	8.6907	29.0618	-44.3824
51	Carbon	5.07472	29.3491	176.179
52	Carbon	4.31633	88.2439	-5.97148
53	Carbon	4.8259	90.4344	176.182
54	Carbon	8.56166	30.5658	-5.69897
55	Carbon	4.86345	32.6952	173.768
56	Carbon	6.51526	19.9624	-0.47696
57	Carbon	4.95516	20.1487	174.829
58	Carbon	5.05286	34.6134	5.1957
59	Carbon	4.06749	29.1856	-148.489
60	Carbon	4.96749	86.4742	10.363
61	Carbon	4.96294	82.4689	-163.891
62	Carbon	8.95619	26.9356	14.6379
63	Carbon	4.99923	28.0988	-152.527
64	Osmium	2.68477	91.6778	-54.683
65	Osmium	2.38477	91.6778	-54.683
66	Oxygen	4.92658	89.1342	-111.177
67	Oxygen	5.00964	39.8935	31.068
68	Oxygen	2.94995	85.386	-31.1768
69	Oxygen	5.10003	18.8945	-32.2085

Appendix A.2

The angular distributions of graphene structures are given in Figures from 7.1 to 7.11.

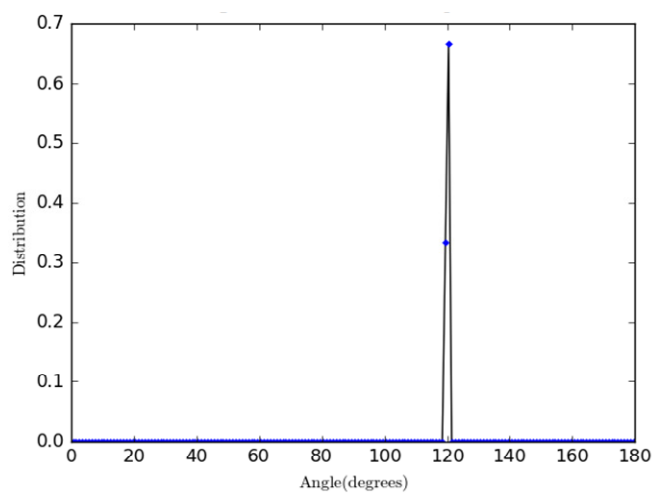


Figure 7.1. Angular distribution of graphene.

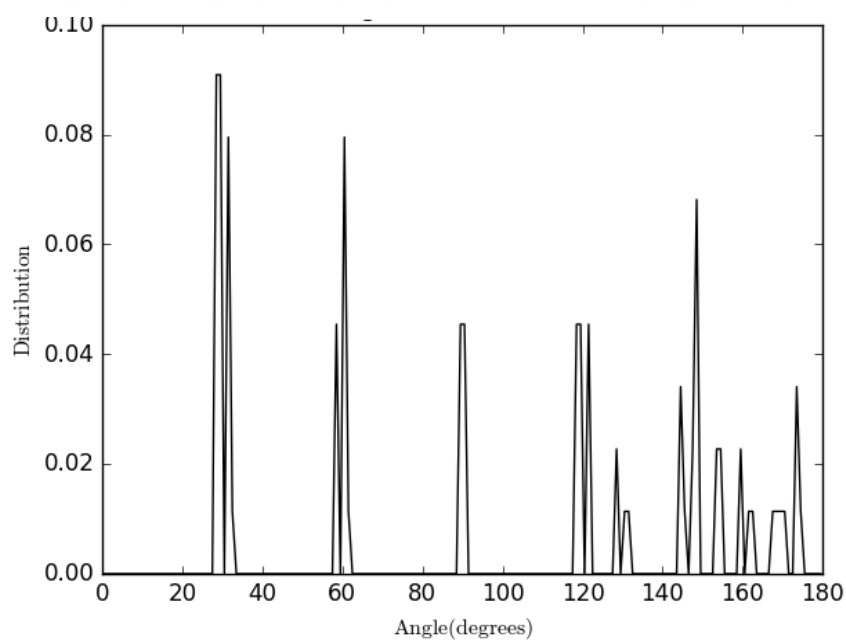


Figure 7.2. Angular distribution of BLG.

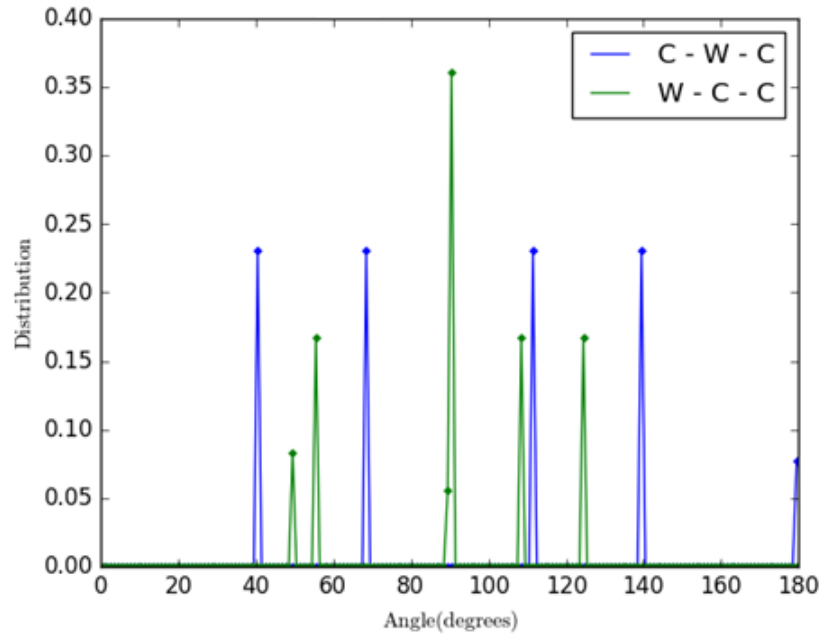


Figure 7.3. Angular distribution of WBLG.

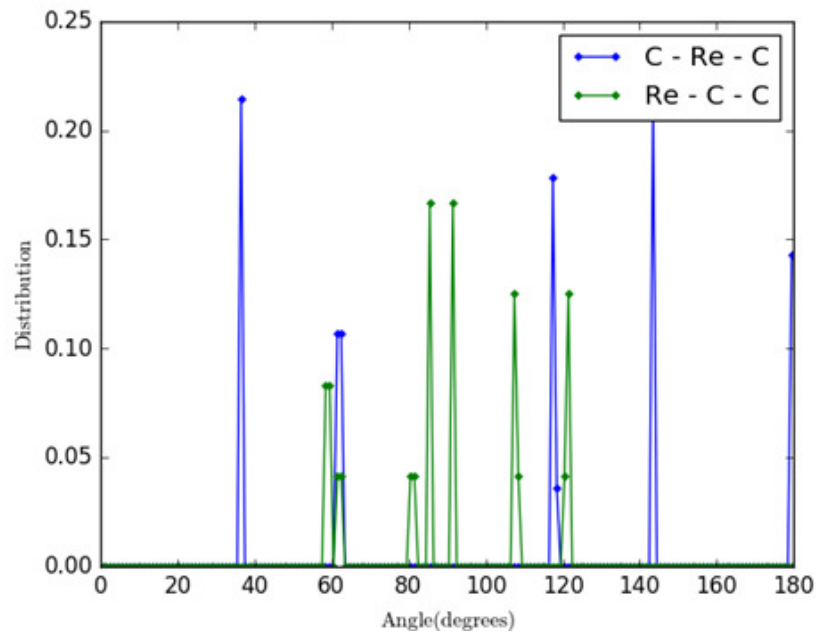


Figure 7.4. Angular distribution of ReBLG.

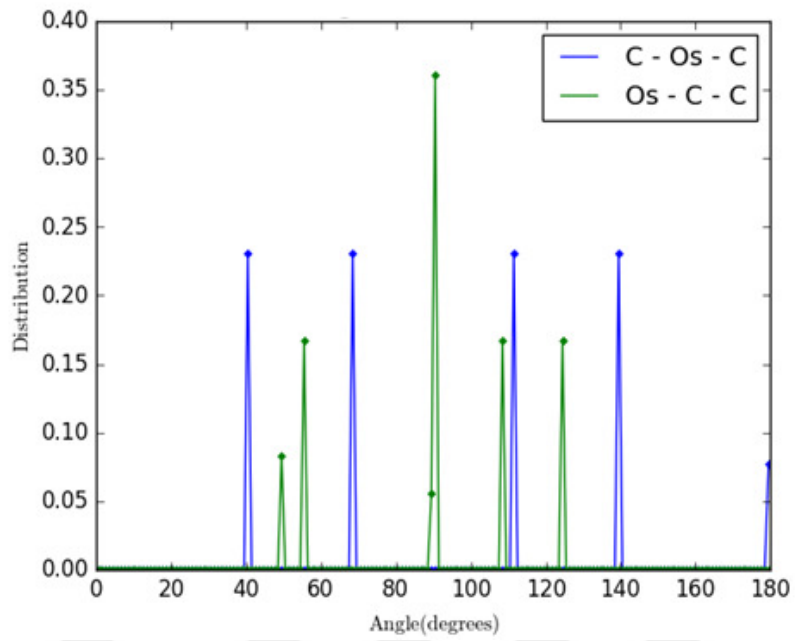


Figure 7.5. Angular distribution of OsBLG.

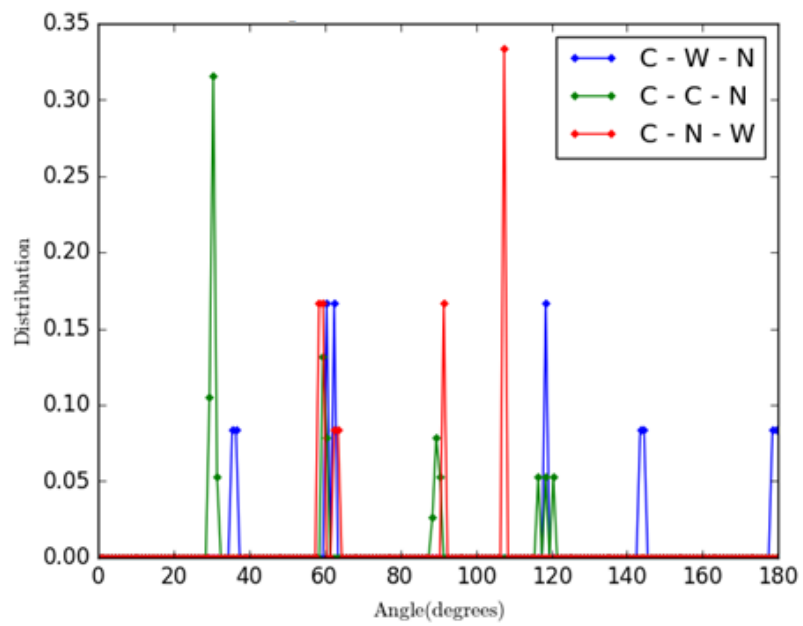


Figure 7.6. Angular distribution of WNBLG.

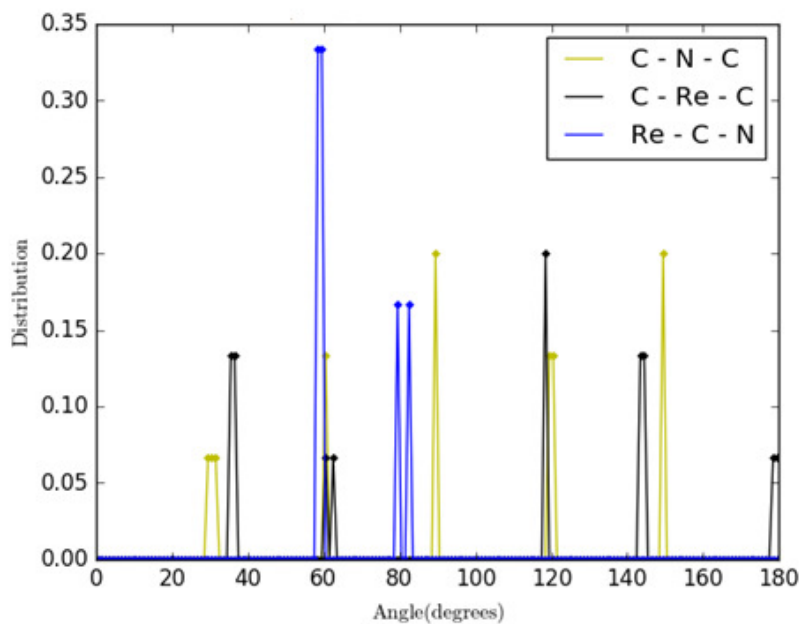


Figure 7.7. Angular distribution of ReNBLG.

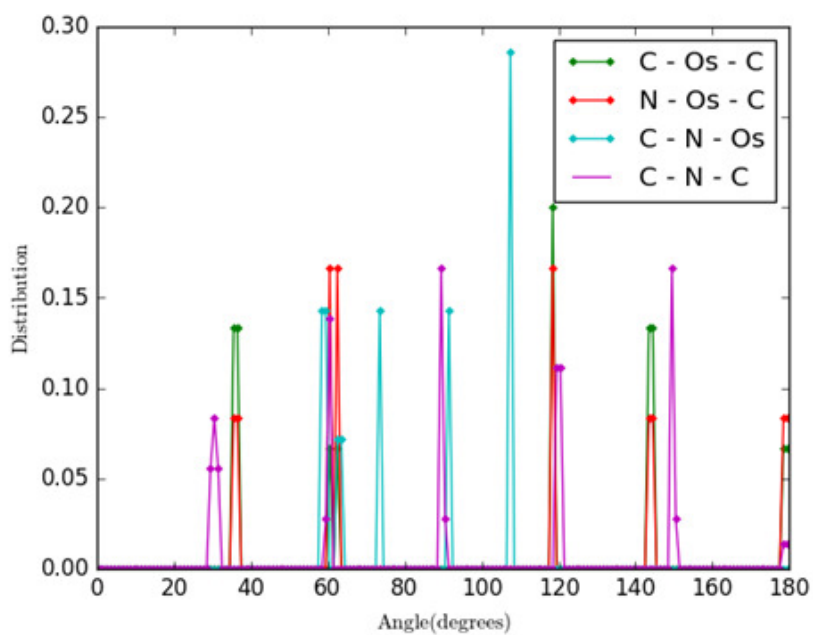


Figure 7.8. Angular distribution of OsNBLG.

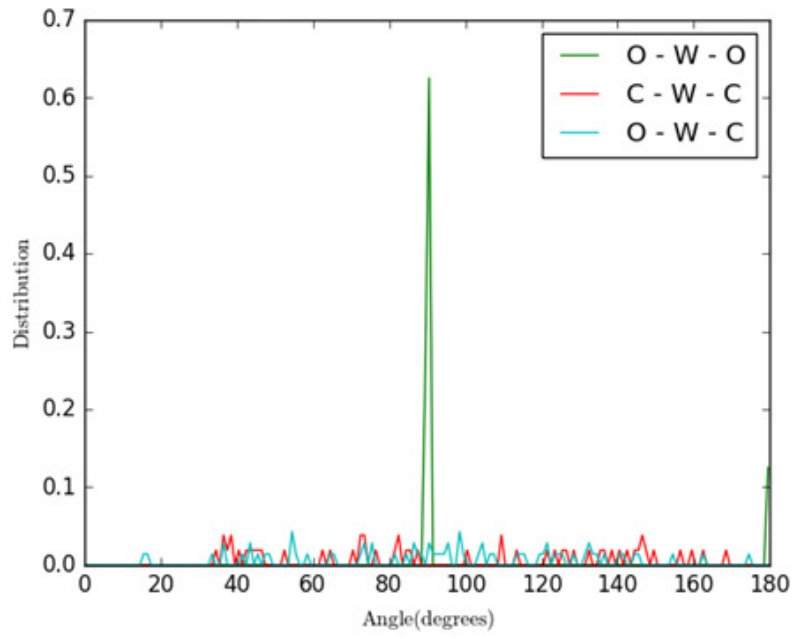


Figure 7.9. Angular distribution of WOBLG.

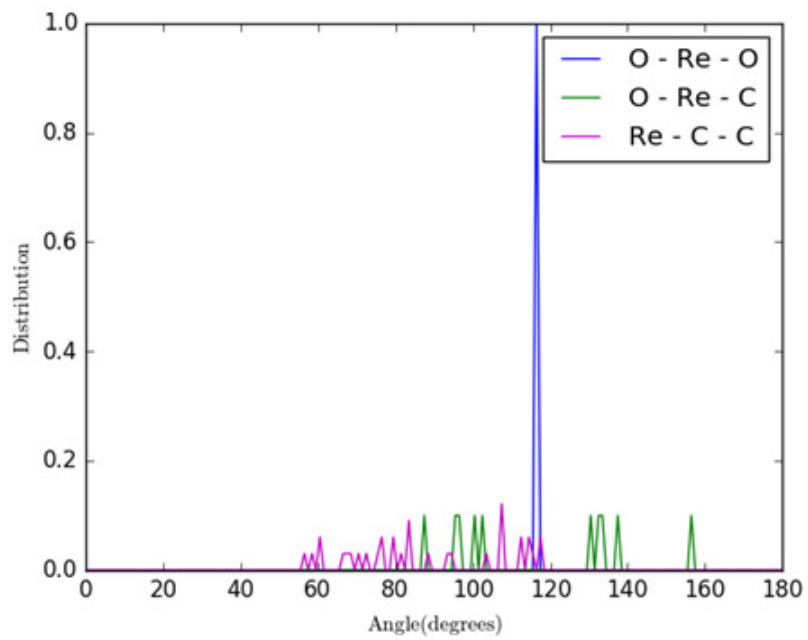


Figure 7.10. Angular distribution of ReOBLG.

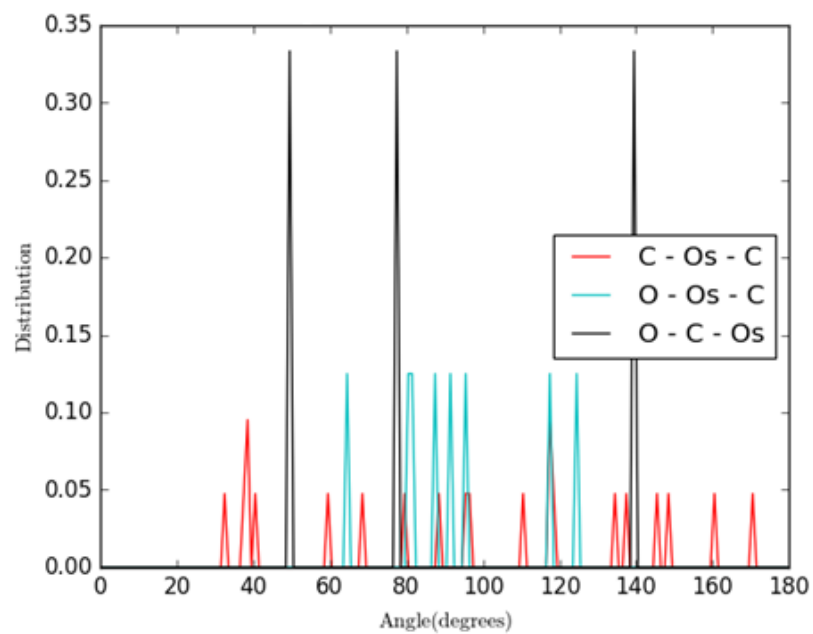


Figure 7.11. Angular distribution of OsOBLG.

Appendix A.3

The radial distributions of graphene structures are given in Figures from 7.12 to 7.22.

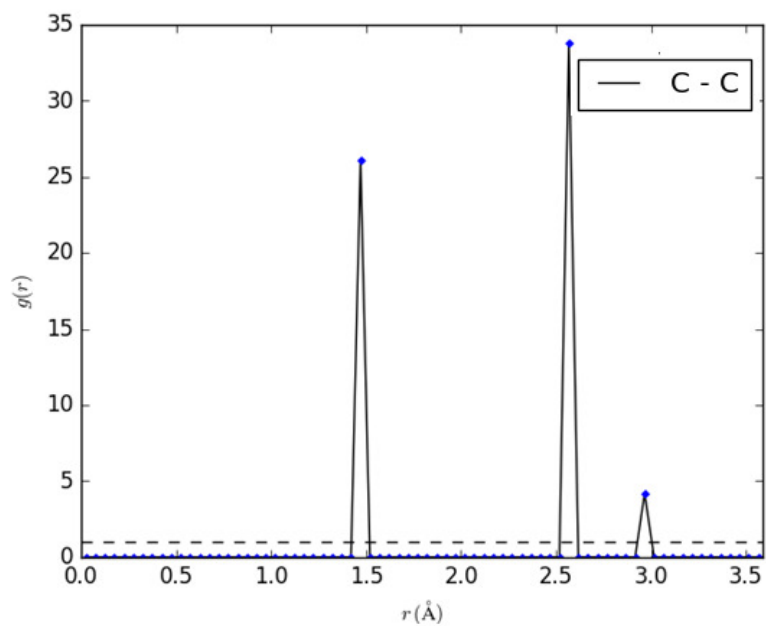


Figure 7.12. Radial distribution of graphene.

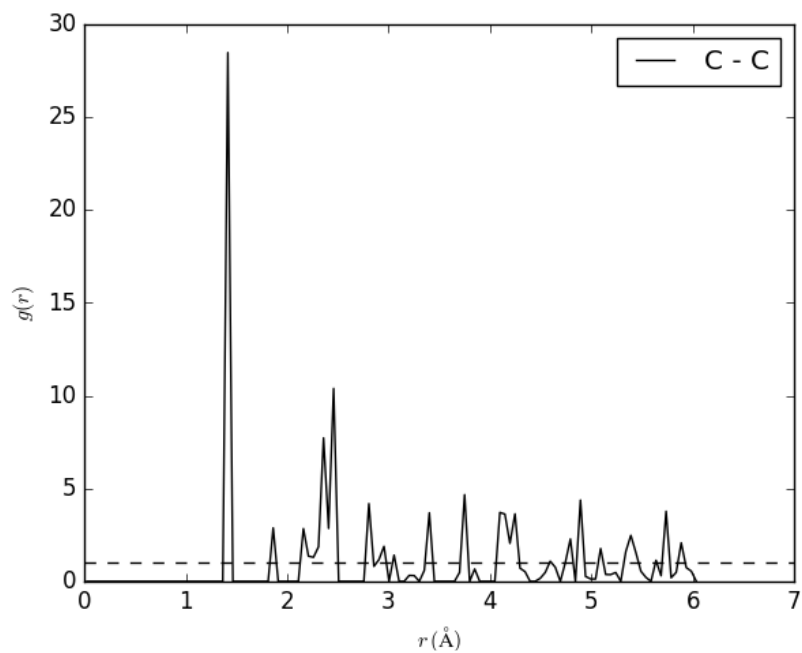


Figure 7.13. Radial distribution of BLG.

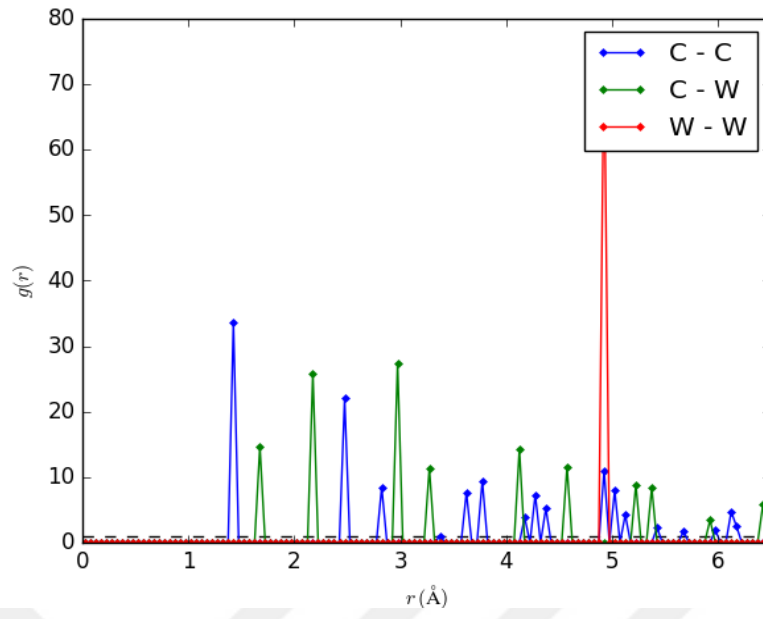


Figure 7.14. Radial distribution of WBLG.

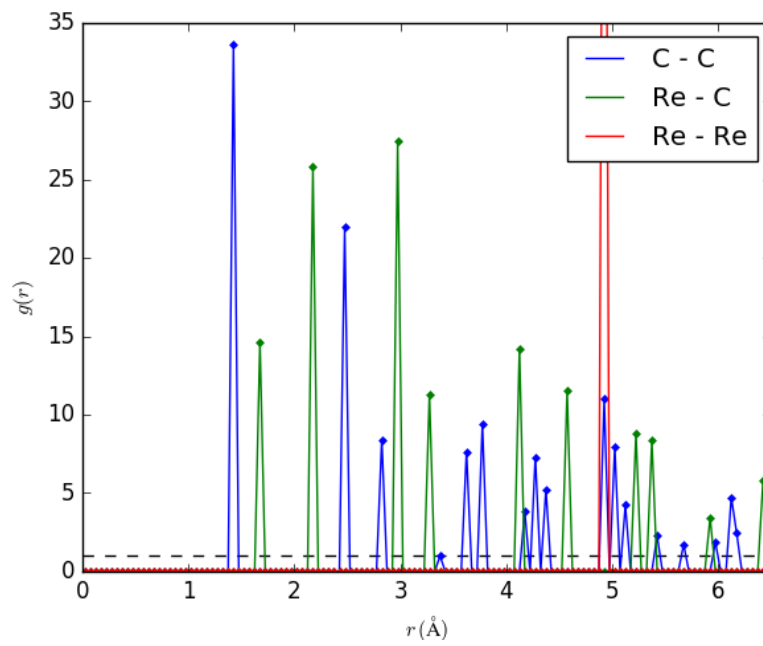


Figure 7.15. Radial distribution of ReBLG.

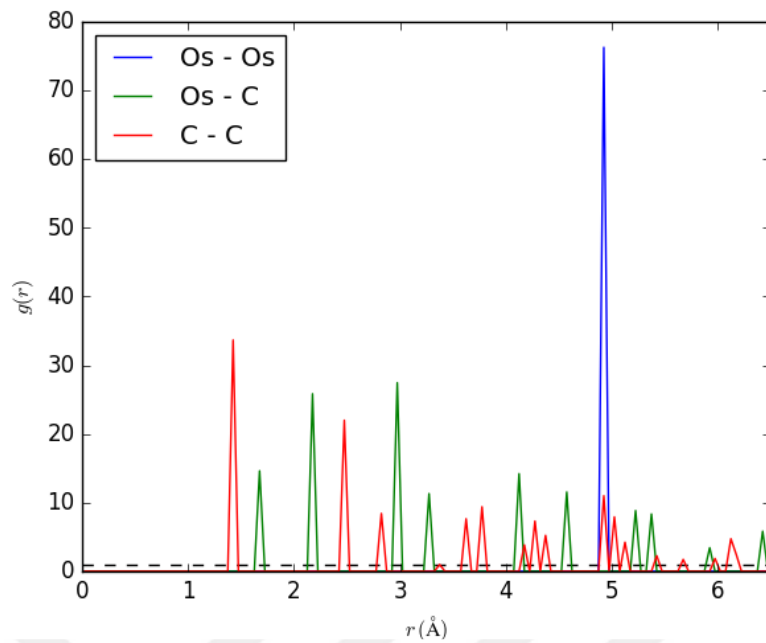


Figure 7.16. Radial distribution of OSBLG.

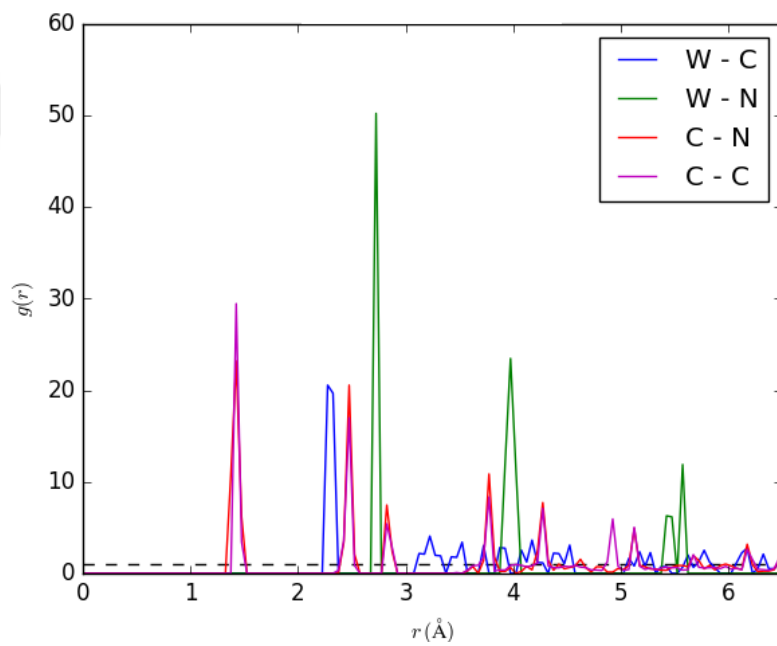


Figure 7.17. Radial distribution of WNBLG.

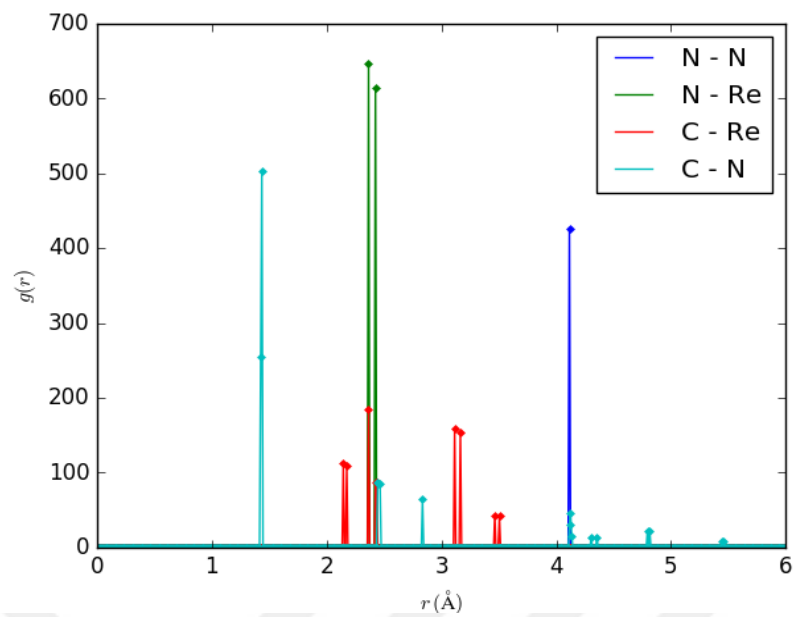


Figure 7.18. Radial distribution of ReNBLG.

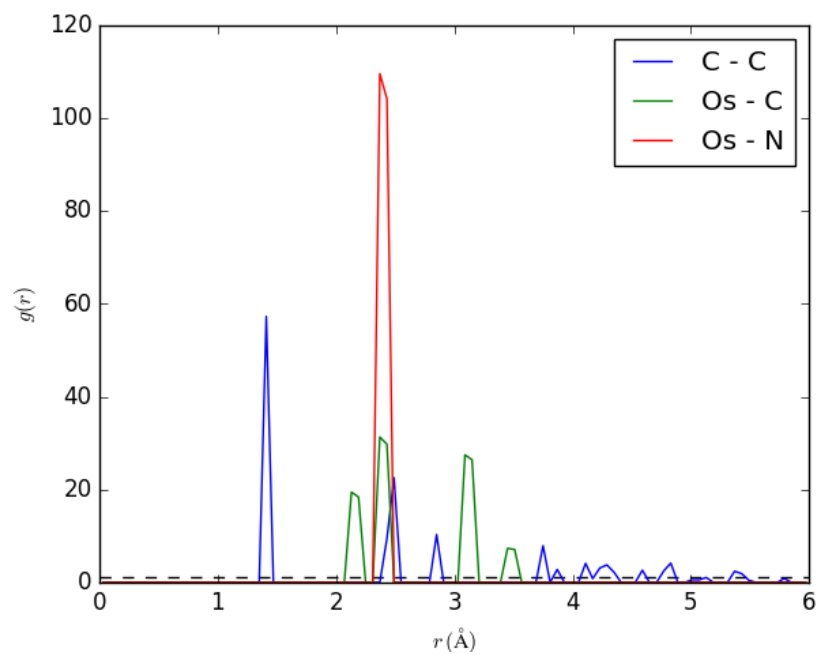


Figure 7.19. Radial distribution of OsNBLG.

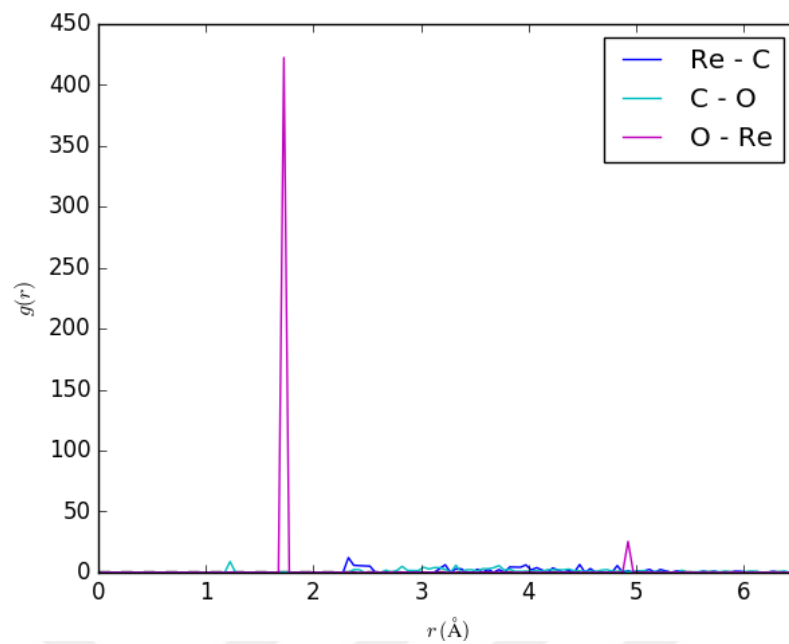


Figure 7.20. Radial distribution of ReOBLG.

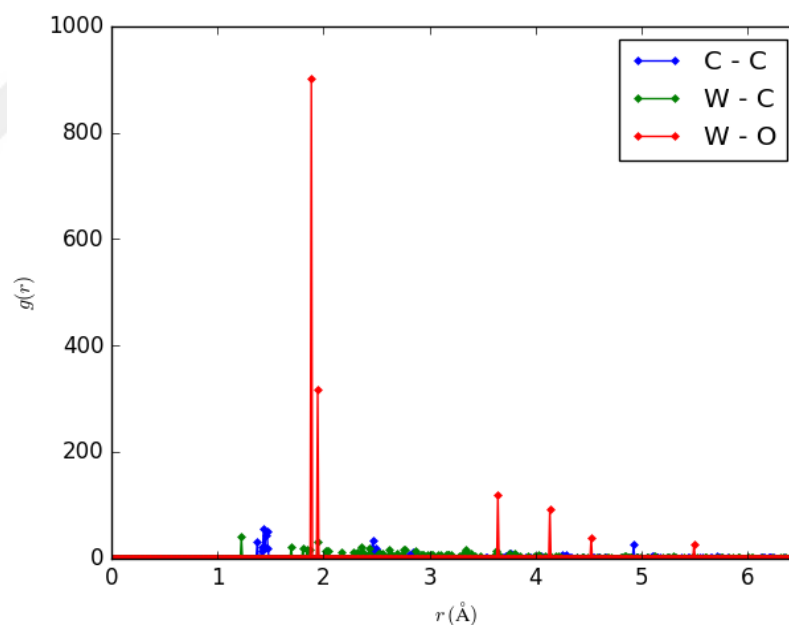


Figure 7.21. Radial distribution of WOBLG.

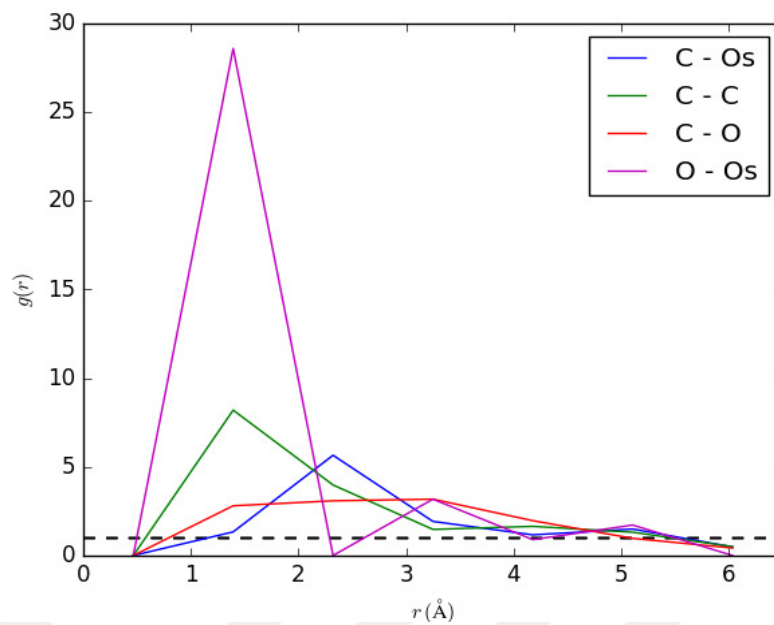


Figure 7.22. Radial distribution of OsOBLG.

Appendix A.4

Bader charge volumes and distances were calculated by Bader charge analysis to examine electron densities and presented in Tables from 7.42 to 7.52.

Table 7.43. Bader charge volumes of MLG with total number of electrons are 33 and identified 24 maxima.

#	Atom	Charge	Distance
0	5	1.2842	1.0981
1	0	1.3118	0.1417
2	4	1.3524	0.1398
3	4	1.2247	0.1137
4	1	1.4105	0.1137
5	1	1.411	0.1137
6	5	1.2285	0.1137
7	5	1.3679	0.1398
8	4	1.411	0.1137
9	5	1.2453	0.1137
10	5	1.411	1.1764
11	3	1.1975	0.1137
12	2	1.3524	0.1398
13	6	1.2842	0.1417
14	3	1.3679	0.1398
15	3	1.2746	0.1137
16	7	1.411	0.1137
17	7	1.4105	1.1764
18	6	1.314	0.1417
19	7	1.2247	0.1137
20	6	1.3991	0.1417
21	7	1.3524	0.1398
22	7	1.4012	1.0981
23	6	1.3524	1.0963

Table 7.44. Bader charge volumes of BLG with total number of electrons are 64 and identified 45 maxima.

#	Atom	Charge	Distance
0	14	2.3076	0.105
1	1	2.3098	0.1055
2	3	2.3175	0.1244
3	9	2.3814	0.1405
4	2	2.238	0.1377
5	2	1.8214	0.1443
6	13	2.2478	0.1389
7	6	2.3976	0.1425
8	12	2.3557	0.1215
9	11	0.9423	0.1023
10	11	1.3669	0.1792
11	4	1.343	0.1789
12	4	0.6689	0.1069
13	7	1.3458	0.1279
14	4	0.1377	0.1243
15	4	1.9566	0.1233
16	11	1.8222	0.1266
17	8	1.3668	0.1262
18	14	1.6162	0.1693
19	1	1.6192	0.1722
20	8	1.2311	0.1685
21	7	1.2192	0.1706
22	13	1.8089	0.1453
23	3	1.6715	0.1576
24	12	1.64	0.1587
25	10	1.6875	0.1196
26	5	1.6533	0.1182
27	15	1.1373	0.131
28	0	1.1531	0.1308
29	7	1.3272	0.1304
30	8	1.3155	0.1361
31	0	1.012	0.1238

Table 7.45. (continued) Bader charge volumes of BLG with total number of electrons are 64 and identified 45 maxima.

#	Atom	Charge	Distance
32	15	1.0456	0.1234
33	5	1.195	0.1457
34	0	0.5914	0.1409
35	15	0.721	0.1409
36	10	1.1424	0.1513
37	5	0.9043	0.0904
38	10	0.2525	0.1008
39	10	0.9232	0.0997
40	5	0.2462	0.1027
41	15	1.1791	0.1162
42	9	1.603	0.152
43	0	1.1856	0.116
44	6	1.5919	0.1463



Table 7.46. Bader charge volumes of ReBLG with total number of electrons are 151 and identified 116 maxima.

#	Atom	Charge	Distance
0	0	1.4164	57.9301
1	0	1.4163	12.7385
2	0	1.4327	12.7993
3	0	1.1943	13.6879
4	0	1.2251	57.9152
5	3	1.3445	57.4521
6	1	1.2529	13.6697
7	3	1.49	57.4606
8	1	1.2248	57.9084
9	1	1.3743	57.9302
10	1	1.4121	12.7907
11	1	1.4255	12.7464
12	9	1.4383	57.6312
13	1	1.3814	13.5738
14	9	1.3652	56.9041
15	9	1.1641	56.8667
16	9	1.39	13.8278
17	9	1.3116	57.7253
18	9	1.3317	59.3695
19	9	1.1521	14.666
20	9	1.2649	16.3254
21	9	1.4092	17.8104
22	9	1.4138	59.7166
23	9	1.3626	61.2186
24	0	1.1941	58.8221
25	0	1.4305	57.9596
26	9	1.3702	21.7481
27	3	0.8633	27.7068
28	0	1.2228	12.7236
29	1	1.2205	12.7246
30	3	0.8776	30.6085
31	0	1.3442	13.5175
32	1	1.3195	13.517
33	9	1.3739	14.6813
34	3	1.0671	33.5413
35	3	1.3318	12.255
36	3	1.3359	55.7553
37	3	1.3357	12.2367
38	9	1.4695	13.7437
39	9	1.3846	13.5356
40	2	1.49	13.4956
41	3	1.2882	10.4811
42	3	1.4371	10.4895
43	9	1.2941	56.882
44	9	1.3361	13.8409
45	9	1.326	15.5003
46	2	1.2528	58.7965
47	9	1.2226	13.6281
48	9	1.4096	13.6655
49	2	1.2247	12.7133
50	2	1.3744	12.7364
51	2	1.4122	57.9456
52	2	1.2219	57.9127
53	3	1.2867	56.9014
54	3	1.4442	56.9113
55	3	1.4482	56.9197
56	9	1.4334	57.6678
57	3	0.9525	27.7312
58	3	1.4212	57.5156
59	3	1.3265	55.7767
60	3	1.098	24.8383
61	3	0.0945	34.9536
62	3	0.0943	23.3481
63	11	1.2208	59.1396
64	9	1.3798	59.6325
65	2	1.4252	57.9358
66	2	1.3802	58.7755
67	3	1.3185	57.4818
68	3	1.3441	55.5607
69	9	1.2786	61.1389
70	3	1.4481	10.4994
71	2	1.4383	12.8071
72	3	0.9372	30.633
73	11	1.4255	14.1999
74	2	1.164	13.7089
75	3	1.3442	12.0421

Table 7.47. (continued) Bader charge volumes of ReBLG with total number of electrons are 151 and identified 116 maxima.

#	Atom	Charge	Distance
76	11	1.1685	14.4324
77	10	1.294	14.4214
78	3	1.4813	14.0069
79	11	1.3531	16.1362
80	2	1.3655	15.4129
81	2	1.3899	60.8203
82	3	1.4698	57.5001
83	10	1.4335	14.2117
84	3	1.421	13.9984
85	3	1.4815	57.5254
86	11	1.4492	14.219
87	11	1.2896	14.4404
88	2	1.3294	18.5464
89	2	1.3151	16.9013
90	10	1.2201	14.48
91	11	1.2166	14.4712
92	2	1.1521	60.3307
93	2	1.3779	62.0117
94	10	1.2227	59.1614
95	11	1.2168	59.1603
96	11	1.4058	60.864
97	10	1.3324	62.6924
98	10	1.3804	64.0462
99	10	1.4095	60.8579
100	3	1.4254	60.7719
101	3	1.4491	60.7887
102	11	1.2956	62.7088
103	2	1.4124	68.8028
104	2	1.2649	63.6568
105	3	1.2895	61.9984
106	3	1.1685	61.9913
107	2	1.4124	20.8926
108	10	1.3805	16.1765
109	11	1.4059	16.175
110	2	1.3624	24.0606
111	10	1.2773	18.6783
112	11	1.2989	18.6783
113	10	1.3298	66.011
114	3	1.3532	65.3407
115	2	1.37	74.7404

Table 7.48. Bader charge volumes of WBLG with total number of electrons are 80 and identified 54 maxima.

#	Atom	Charge	Distance
0	0	1.268	0.1887
1	2	1.3279	3.1233
2	16	1.2644	0.3116
3	16	1.2462	0.3116
4	5	1.3279	3.1235
5	4	1.268	0.1887
6	4	1.4356	0.2049
7	0	1.3428	0.1466
8	4	1.3263	1.05
9	8	1.3327	0.1595
10	8	1.3443	0.1804
11	5	1.3488	0.9849
12	1	1.3754	0.2181
13	1	1.2463	0.1883
14	10	1.3621	0.2102
15	16	1.1664	0.285
16	5	1.3633	0.1752
17	5	1.3363	0.2195
18	15	1.357	0.1587
19	5	1.3116	1.0808
20	1	1.5186	0.2288
21	0	1.3263	1.0499
22	0	1.4356	0.2048
23	9	1.2453	0.1559
24	4	1.3427	0.1466
25	5	1.3543	0.1451
26	16	1.2176	0.3724
27	12	1.3327	0.1595
28	16	1.2336	0.3725
29	13	1.3513	0.1594
30	16	1.1705	0.2852
31	8	1.3311	0.2093
32	12	1.3311	0.2093
33	7	1.3002	0.1848
34	13	1.3283	0.1794
35	2	1.3488	0.9849
36	12	1.3444	0.1803
37	7	1.3907	0.2151
38	13	1.3621	0.2102
39	6	1.3754	0.2182
40	6	1.2462	0.1883
41	2	1.3543	0.1452
42	2	1.3632	0.1752
43	3	1.3002	0.1849
44	3	1.3906	0.2151
45	3	1.4535	0.1427
46	10	1.3281	0.1795
47	2	1.3364	0.2194
48	10	1.3514	0.1594
49	11	1.357	0.1586
50	2	1.3116	1.0807
51	6	1.5186	0.2288
52	7	1.4517	0.1427
53	14	1.2453	0.156

Table 7.49. Bader charge volumes of OsBLG with total number of electrons are 72 and identified 54 maxima.

#	Atom	Charge	Distance
0	0	1.3344	0.1802
1	2	1.3348	2.9391
2	16	1.2074	0.3121
3	16	1.2063	0.3148
4	5	1.3317	2.9387
5	4	1.3298	0.1801
6	4	1.4588	0.2054
7	0	1.2451	0.1584
8	4	1.2702	1.0538
9	8	1.4626	0.2116
10	8	1.4055	0.1987
11	5	1.1504	1.0823
12	1	1.2615	0.1709
13	1	1.3047	0.1816
14	10	1.3128	0.1864
15	16	1.1587	0.3279
16	5	1.4238	0.219
17	10	1.3176	0.1505
18	5	1.3185	0.1681
19	15	1.3569	0.1622
20	5	1.418	0.972
21	1	1.4509	0.1934
22	9	1.3767	0.1608
23	0	1.4638	0.2052
24	0	1.2741	1.0533
25	4	1.2376	0.1583
26	5	1.2564	0.1569
27	16	1.2295	0.3416
28	12	1.461	0.2112
29	13	1.4478	0.2121
30	16	1.2395	0.3388
31	16	1.1668	0.3257
32	8	1.3227	0.2353
33	12	1.3262	0.2353
34	7	1.4471	0.2257
35	13	1.3174	0.1504
36	7	1.4388	0.213
37	13	1.3096	0.1861
38	2	1.1531	1.0819
39	12	1.4033	0.1983
40	6	1.3011	0.1815
41	6	1.2614	0.1708
42	2	1.4306	0.2188
43	2	1.2655	0.157
44	3	1.4167	0.2258
45	3	1.4885	0.213
46	3	1.2764	0.1997
47	2	1.3172	0.1681
48	11	1.354	0.1623
49	2	1.4227	0.9721
50	10	1.4545	0.2125
51	6	1.4403	0.1936
52	7	1.2666	0.1996
53	14	1.3727	0.1606

Table 7.50. Bader charge volumes of ReNBLG with total number of electrons are 81 and identified 49 maxima.

#	Atom	Charge	Distance
0	14	2.3311	0.0905
1	9	2.3311	0.0905
2	2	2.3221	0.1156
3	15	2.4042	0.1539
4	15	1.7449	0.1581
5	16	2.2934	0.1711
6	0	1.7387	0.1064
7	10	1.0729	0.0942
8	10	1.1985	0.1257
9	3	1.4582	0.1102
10	0	1.3765	0.1693
11	11	2.3755	0.154
12	4	1.3805	0.1695
13	16	2.3173	0.1711
14	4	1.7502	0.1063
15	11	1.775	0.159
16	7	1.4676	0.1102
17	13	1.2209	0.1248
18	13	1.0476	0.0954
19	5	2.333	0.1159
20	1	1.7183	0.0993
21	6	1.7305	0.0994
22	12	1.2981	0.076
23	8	3.9258	0.078
24	1	1.7568	0.1406
25	6	1.7623	0.1404
26	9	1.6311	0.1593
27	14	1.6304	0.1594
28	6	0.1809	0.1632
29	1	0.1846	0.163
30	12	2.3288	0.0689
31	0	0.5839	0.168
32	12	2.4355	0.0746
33	8	2.1347	0.0781
34	4	0.5784	0.1681
35	16	2.0524	0.1726
36	16	2.0273	0.1726
37	2	1.6744	0.138
38	5	1.6728	0.1387
39	16	2.6	0.1735
40	16	2.5819	0.1738
41	3	0.5682	0.1652
42	7	0.5684	0.1652
43	10	1.7974	0.1672
44	13	1.803	0.166
45	3	1.6352	0.1125
46	7	1.6279	0.1125
47	7	0.3453	0.149
48	3	0.2265	0.149

Table 7.51. Bader charge volumes of WNBLG with total number of electrons are 82 and identified 48 maxima.

#	Atom	Charge	Distance
0	6	2.5745	2.6853
1	0	2.6242	4.4844
2	12	3.5114	2.0745
3	12	4.7545	1.4847
4	5	1.4374	4.7878
5	6	1.4629	1.7494
6	6	1.8542	1.7832
7	6	2.3618	3.405
8	12	0.9389	2.3107
9	5	1.8623	2.6867
10	8	2.3471	0.6601
11	2	0.2066	1.6899
12	2	0.2882	1.2114
13	2	1.4458	2.7998
14	5	1.405	0.6783
15	5	0.3732	1.034
16	5	0.2153	1.0667
17	2	2.2882	1.3397
18	13	2.2712	0.9605
19	6	1.4606	3.192
20	2	1.6105	1.6092
21	13	1.6038	0.427
22	10	2.3382	1.5918
23	13	2.3378	1.2607
24	5	1.445	1.3331
25	8	1.6223	0.4035
26	6	1.613	2.1677
27	12	2.3265	1.0243
28	16	2.2697	1.5669
29	14	1.9814	0.9832
30	8	2.0024	1.2022
31	14	1.7861	0.7412
32	16	1.5593	1.8869
33	14	1.3771	0.148
34	6	0.6367	1.6976
35	16	1.6557	1.701
36	5	0.6087	2.8454
37	14	2.9045	0.7744
38	16	2.9976	1.6706
39	14	0.1543	0.3068
40	10	0	10.9064
41	14	0.1557	0.1672
42	11	0.1441	2.5872
43	14	2.6067	4.7193
44	14	1.5786	1.012
45	11	1.573	1.2596
46	14	0.8998	2.0532
47	16	0.9119	2.5071
48	13	2.6162	3.8487

Table 7.52. Bader charge volumes of OsNBLG with total number of electrons are 83 and identified 48 maxima.

#	Atom	Charge	Distance
0	14	2.3323	0.1045
1	9	2.3325	0.1047
2	2	2.3303	0.1201
3	16	2.6433	0.1794
4	15	2.4878	0.1418
5	0	1.6903	0.111
6	10	1.2282	0.0992
7	15	1.6163	0.1517
8	0	1.4976	0.1648
9	11	2.4833	0.1427
10	4	1.4939	0.1651
11	11	1.6215	0.1523
12	16	2.67	0.1795
13	4	1.7002	0.1111
14	13	1.1393	0.1552
15	13	1.2188	0.1008
16	5	2.3307	0.1206
17	6	1.7281	0.104
18	1	1.7304	0.1037
19	12	3.5801	0.0954
20	8	3.5513	0.0998
21	1	1.7751	0.1241
22	9	1.5934	0.172
23	6	1.7715	0.1241
24	14	1.5999	0.1722
25	12	2.3963	0.0873
26	8	2.4234	0.0846
27	6	0.2102	0.1798
28	1	0.2106	0.18
29	16	2.5445	0.194
30	4	0.5376	0.1449
31	0	0.5394	0.1452
32	16	2.4932	0.1941
33	5	1.6493	0.1607
34	2	1.6491	0.1609
35	10	1.7568	0.1462
36	10	1.1419	0.1558
37	16	2.4165	0.1864
38	16	2.4395	0.1868
39	13	1.7687	0.1454
40	3	0.5408	0.1308
41	7	0.542	0.1308
42	3	1.555	0.1238
43	7	1.5504	0.1238
44	7	0.3315	0.1408
45	3	0.2297	0.1408
46	7	1.4663	0.1167
47	3	1.4611	0.1167

Table 7.53. The atomic charge volumes of ReOBLG structure, total number of electron is 289.

Atom	#	x	y	z	Charge
C	0	10.382	18.5087	9.9357	4.168
C	1	12.4595	23.3036	9.8584	3.9254
C	2	12.9655	14.2783	9.9435	4.0201
C	3	14.8398	19.0365	9.2056	4.1438
C	4	11.2089	21.0793	9.769	4.0106
C	5	14.1936	25.3133	10.2674	4.0596
C	6	13.5934	16.8233	9.4466	3.9959
C	7	16.0891	21.1857	9.4662	3.9222
C	8	10.9747	17.3746	9.8439	3.9903
C	9	13.628	21.2424	9.2881	3.9574
C	10	13.2729	12.9459	10.2689	4.0034
C	11	16.1393	16.9754	9.7393	3.9997
C	12	12.4593	19.0851	9.4384	4.1257
C	13	14.8596	23.3216	9.6936	3.9872
C	14	15.0746	14.7673	9.9374	4.0446
C	15	17.2822	19.1656	9.7677	3.8962
C	16	10.5446	17.6685	14.0937	4.1904
C	17	12.9659	21.6604	14.4151	3.9975
C	18	12.542	12.8413	14.0862	3.9925
C	19	14.9567	17.0302	14.8325	3.9719
C	20	11.1303	18.7495	14.4216	4.0381
C	21	13.1767	22.9914	14.0104	3.9739
C	22	13.7704	14.8987	14.4006	3.9747
C	23	16.2317	19.1481	14.6844	3.9365
C	24	11.3684	15.1063	14.0865	4.0204
C	25	13.7004	19.1817	14.9103	3.9399
C	26	14.1872	10.7167	13.9159	4.0357
C	27	16.2017	14.9407	14.1717	3.9553
C	28	12.5571	16.9919	14.8306	3.9165
C	29	15.0961	21.3237	14.5036	4.0796
C	30	14.9415	12.7789	13.9251	3.96
C	31	17.4306	17.001	14.3384	3.8507
C	32	11.1633	19.7165	9.7119	3.9938
C	33	13.5333	24.0542	9.9432	4.08
C	34	13.7059	15.4278	9.6903	4.0058
C	35	16.0376	19.7425	9.3612	3.9247
C	36	12.3627	21.8936	9.6072	3.9775
C	37	15.4636	25.7557	10.2892	3.983
C	38	14.8577	17.593	9.4344	4.0862
C	39	17.443	21.414	9.9361	4.0922
C	40	12.3765	17.5949	9.5352	3.9672
C	41	14.9065	21.9389	9.4258	3.9295
C	42	14.523	13.4552	10.1925	4.0521
C	43	17.4167	17.7386	9.9933	2.2756
C	44	13.6283	19.8188	9.1385	4.0323
C	45	15.6766	24.4018	9.9467	3.9984
C	46	16.098	15.5985	9.9377	3.9531
C	47	18.0965	20.333	10.0249	4.1328
C	48	11.2916	16.4315	14.3362	3.9433
C	49	13.7727	20.5883	14.7575	3.9567
C	50	13.589	12.0524	13.9869	4.0812
C	51	16.1198	16.3506	14.5035	3.8949
C	52	12.4985	18.4426	14.8379	3.9088
C	53	14.4496	22.5616	14.0941	4.0473
C	54	15.0228	14.1786	14.1662	3.9333
C	55	17.3596	18.3378	14.4994	4.1361
C	56	12.4688	14.2542	14.1737	3.9283
C	57	14.957	18.448	14.9066	4.0058
C	58	15.4413	10.2275	13.8284	3.9745
C	59	17.6062	14.7664	13.8394	4.0596
C	60	13.7511	16.2643	14.781	3.9836
C	61	16.1544	20.5493	14.5093	3.9831
C	62	15.6912	11.6207	13.8463	4.0242
C	63	18.2604	15.8466	14.003	4.1035
Re	64	13.778	18.5689	11.2553	13.0503
O	65	18.4321	17.1739	10.4286	7.8383
O	66	13.7753	17.1774	12.2669	6.7988
O	67	13.943	20.0941	12.0442	6.7804

Table 7.54. The atomic charge volumes of WOBLG structure, total number of electron is 352.

Atom	#	x	y	z	Charge
C	0	10	19.0093	10.0978	3.9063
C	1	12.4612	23.2722	10.0978	3.9923
C	2	12.4612	14.7463	10.0978	4.2186
C	3	14.9224	19.0093	10.0978	4.1467
C	4	11.2334	21.1321	10.0667	4.0298
C	5	13.6946	25.395	10.0667	4.0906
C	6	13.6946	16.8691	10.0667	3.9018
C	7	16.1558	21.1321	10.0667	4.0261
C	8	11.208	16.8963	10.4708	4.0265
C	9	13.6692	21.1592	10.4708	0
C	10	13.6692	12.6333	10.4708	4.1034
C	11	16.1304	16.8963	10.4708	3.78
N	12	12.4373	19.0254	10.0272	4.0153
C	13	14.8985	23.2883	10.0272	4.0524
C	14	14.8985	14.7625	10.0272	3.981
C	15	17.3597	19.0254	10.0272	3.9351
C	16	10.0541	17.0917	13.9282	3.9035
N	17	12.5153	21.3546	13.9282	3.9648
C	18	12.5153	12.8288	13.9282	3.9548
C	19	14.9765	17.0917	13.9282	3.6556
C	20	11.2755	19.2054	13.639	3.9968
C	21	13.7367	23.4683	13.639	4.1499
C	22	13.7367	14.9425	13.639	8.5443
C	23	16.1979	19.2054	13.639	3.9186
C	24	11.2934	14.9642	13.9454	3.9961
N	25	13.7546	19.2271	13.9454	3.9622
C	26	13.7546	10.7012	13.9454	4.2224
C	27	16.2158	14.9642	13.9454	4.0479
C	28	12.4883	17.0662	14.0288	3.9468
C	29	14.9495	21.3291	14.0288	3.8711
C	30	14.9495	12.8033	14.0288	4.0141
C	31	17.4107	17.0662	14.0288	4.0883
C	32	11.2484	19.7141	10.0716	4.0247
C	33	13.7096	23.9771	10.0716	3.9738
N	34	13.7096	15.4512	10.0716	4.1871
N	35	16.1708	19.7141	10.0716	3.8625
C	36	12.4941	21.8332	10	4.0982
C	37	14.9553	26.0961	10	4.0108
N	38	14.9553	17.5702	10	4.0831
C	39	17.4165	21.8332	10	4.003
C	40	12.4899	17.6178	10.4465	4.0746
N	41	14.9511	21.8808	10.4465	3.6392
N	42	14.9511	13.3549	10.4465	4.0367
C	43	17.4123	17.6178	10.4465	3.8804
N	44	13.6703	19.6841	10.4352	3.5261
C	45	16.1315	23.947	10.4352	3.923
C	46	16.1315	15.4212	10.4352	3.908
C	47	18.5927	19.6841	10.4352	3.8399
C	48	11.301	16.3842	13.959	4.0511
C	49	13.7622	20.6471	13.959	1.3456
C	50	13.7622	12.1213	13.959	3.8693
C	51	16.2234	16.3842	13.959	3.9726
C	52	12.5363	18.4792	13.6461	4.0679
C	53	14.9975	22.7421	13.6461	4.0984
N	54	14.9975	14.2163	13.6461	4.5303
C	55	17.4587	18.4792	13.6461	3.9384
C	56	12.547	14.2629	14.0096	4.5764
C	57	15.0082	18.5258	14.0096	1.6219
C	58	15.0082	10	14.0096	3.9939
C	59	17.4694	14.2629	14.0096	4.0208
N	60	13.7221	16.4051	13.637	4.4316
N	61	16.1833	20.668	13.637	3.7773
C	62	16.1833	12.1422	13.637	3.9236
C	63	18.6445	16.4051	13.637	3.8971
W	64	13.7367	14.9425	11.6895	12.3902
W	65	13.7367	21.2627	11.6895	17.0041
W	66	15.5612	18.1026	11.6895	11.8993
O	67	13.7367	14.9425	13.639	0
O	68	13.7367	21.2627	13.639	9.1271
O	69	15.5612	18.1026	13.639	9.1324
O	70	14.233	19.4425	11.6895	7.0245
O	71	16.8895	19.4425	11.6895	6.6816
O	72	15.5612	21.7431	11.6895	6.7523
O	73	14.233	16.7627	11.6895	6.9788
O	74	16.8895	16.7627	11.6895	6.7185
O	75	15.5612	14.4621	11.6895	6.6612

Table 7.55. The atomic charge volumes of OsOBLG structure, total number of electron is 312.

Atom	#	x	y	z	Charge
C	0	10	19.0093	10.0978	3.9063
C	1	12.4612	23.2722	10.0978	3.9923
C	2	12.4612	14.7463	10.0978	4.2186
C	3	14.9224	19.0093	10.0978	4.1467
C	4	11.2334	21.1321	10.0667	4.0298
C	5	13.6946	25.395	10.0667	4.0906
C	6	13.6946	16.8691	10.0667	3.9018
C	7	16.1558	21.1321	10.0667	4.0261
C	8	11.208	16.8963	10.4708	4.0265
C	9	13.6692	21.1592	10.4708	0
C	10	13.6692	12.6333	10.4708	4.1034
C	11	16.1304	16.8963	10.4708	3.78
N	12	12.4373	19.0254	10.0272	4.0153
C	13	14.8985	23.2883	10.0272	4.0524
C	14	14.8985	14.7625	10.0272	3.981
C	15	17.3597	19.0254	10.0272	3.9351
C	16	10.0541	17.0917	13.9282	3.9035
N	17	12.5153	21.3546	13.9282	3.9648
C	18	12.5153	12.8288	13.9282	3.9548
C	19	14.9765	17.0917	13.9282	3.6556
C	20	11.2755	19.2054	13.639	3.9968
C	21	13.7367	23.4683	13.639	4.1499
C	22	13.7367	14.9425	13.639	8.5443
C	23	16.1979	19.2054	13.639	3.9186
C	24	11.2934	14.9642	13.9454	3.9961
N	25	13.7546	19.2271	13.9454	3.9622
C	26	13.7546	10.7012	13.9454	4.2224
C	27	16.2158	14.9642	13.9454	4.0479
C	28	12.4883	17.0662	14.0288	3.9468
C	29	14.9495	21.3291	14.0288	3.8711
C	30	14.9495	12.8033	14.0288	4.0141
C	31	17.4107	17.0662	14.0288	4.0883
C	32	11.2484	19.7141	10.0716	4.0247
C	33	13.7096	23.9771	10.0716	3.9738
N	34	13.7096	15.4512	10.0716	4.1871
N	35	16.1708	19.7141	10.0716	3.8625
C	36	12.4941	21.8332	10	4.0982
C	37	14.9553	26.0961	10	4.0108
N	38	14.9553	17.5702	10	4.0831
C	39	17.4165	21.8332	10	4.003
C	40	12.4899	17.6178	10.4465	4.0746
N	41	14.9511	21.8808	10.4465	3.6392
N	42	14.9511	13.3549	10.4465	4.0367
C	43	17.4123	17.6178	10.4465	3.8804
N	44	13.6703	19.6841	10.4352	3.5261
C	45	16.1315	23.947	10.4352	3.923
C	46	16.1315	15.4212	10.4352	3.908
C	47	18.5927	19.6841	10.4352	3.8399
C	48	11.301	16.3842	13.959	4.0511
C	49	13.7622	20.6471	13.959	1.3456
C	50	13.7622	12.1213	13.959	3.8693
C	51	16.2234	16.3842	13.959	3.9726
C	52	12.5363	18.4792	13.6461	4.0679
C	53	14.9975	22.7421	13.6461	4.0984
N	54	14.9975	14.2163	13.6461	4.5303
C	55	17.4587	18.4792	13.6461	3.9384
C	56	12.547	14.2629	14.0096	4.5764
C	57	15.0082	18.5258	14.0096	1.6219
C	58	15.0082	10	14.0096	3.9939
C	59	17.4694	14.2629	14.0096	4.0208
N	60	13.7221	16.4051	13.637	4.4316
N	61	16.1833	20.668	13.637	3.7773
C	62	16.1833	12.1422	13.637	3.9236
C	63	18.6445	16.4051	13.637	3.8971
W	64	13.7367	14.9425	11.6895	12.3902
W	65	13.7367	21.2627	11.6895	17.0041
W	66	15.5612	18.1026	11.6895	11.8993
O	67	13.7367	14.9425	13.639	0
O	68	13.7367	21.2627	13.639	9.1271
O	69	15.5612	18.1026	13.639	9.1324
O	70	14.233	19.4425	11.6895	7.0245
O	71	16.8895	19.4425	11.6895	6.6816
O	72	15.5612	21.7431	11.6895	6.7523
O	73	14.233	16.7627	11.6895	6.9788
O	74	16.8895	16.7627	11.6895	6.7185
O	75	15.5612	14.4621	11.6895	6.6612

8. CURRICULUM VITAE

Name SURNAME : Özlem ÜNLÜ

Place and Date of Birth : Düzce 20.10.1985

Universities

Bachelor's Degree : Abant İzzet Baysal University

MSc Degree : Abant İzzet Baysal University

e-mail : ozlemilkin@gmail.com

Address : Kılıçarslan Mah. Dr. Akın Çakmakçı Blv.
Rönesans Apartmanı 22/5 Bolu

List of Publications :

- İlkın Özlem, Morkan İzzet (2013). Synthesis, characterization and applications of Antimicrobial textile products by sonochemical Nanomolecular coating. V. ULUSLARARASI AR-GE PROJE PAZARI, Bursa
- Tanyıldızı Seda, Morkan İzzet, Morkan Ayşe, İlkın Özlem (2012). Grup 6 B Elementlerinin Metal-Karbonil-2-Merkaptopirimidin Totomerlerinin Yoğunluk Fonksiyon Teorisi (DFT) ile Yapısal Analizi. III. FİZİKSEL KİMYA GÜNLERİ, Balıkesir
- İlkın Özlem, Morkan İzzet (2011). Metal Pirimidintiyol Bileşiklerinin Sentezi ve DFT Hesaplamaları. III. Ulusal Anorganik Kimya Kongresi, Çanakkale
- İlkın Özlem, Morkan İzzet (2010). Grup VI-B Elementlerinin Merkaptopirimidin Bileşiklerinin Sentezi, Termal Davranışları,

Spektroskopik Yapısının İncelenmesi. 24. ULUSAL KİMYA KONGRESİ,
Zonguldak

